Summer 2021

Effect of radiation damage on organic phase change materials thermal storage properties

Ryan Phillip Steere

Department: Nuclear Engineering and Radiation Science

EFFECT OF RADIATION DAMAGE ON ORGANIC PHASE CHANGE MATERIALS THERMAL STORAGE PROPERTIES

by

RYAN PHILLIP STEERE

A DISSERTATION

Presented to the Graduate Faculty of the

MISSOURI UNIVERSITY OF SCIENCE AND TECHNOLOGY

In Partial Fulfillment of the Requirements for the Degree

DOCTOR OF PHILOSOPHY

in

NUCLEAR ENGINEERING

2021

Approved by:

Dr. Joshua Schlegel, Advisor
Dr. Ayodeji Alajo
Dr. Carlos Castano
Dr. William Fahrenholtz
Dr. Joseph Graham
Dr. Haiming Wen

PUBLICATION DISSERTATION OPTION

This dissertation consists of the following three articles, formatted in the style used by the Missouri University of Science and Technology:

Paper I, found on pages 8-37, is intended for submission to *Nuclear Engineering and Technology*.

Paper II, found on pages 38-62, is intended for submission to *Advances in Space Research*.

Paper III, found on pages 63-90, is intended for submission to *Journal of Nuclear Materials*.

ABSTRACT

This work discusses the effects of radiation damage on organic phase change materials for use in nuclear reactor containments and space craft. The effects of radiation on the latent heat of polyethylene wax (PEW) and a eutectic of methyl palmitate and lauric acid (EMPaLA) are evaluated. These PCMs were irradiated in three locations: the Missouri University of Science and Technology research reactor (MSTR), the University of Missouri research reactor (MURR) and cyclotron (MUC) up to a total dose of 2826, 2895 and 662 Gy, respectively. The samples irradiated at the MSTR showed latent heat changes up to 15.5% lower than the starting values however the error bars are so close that the there is no conclusive evidence for a statistically significant change. The MUC irradiation did not yield any statistically significant change in the latent heat. The irradiation at MURR showed a drop of 18.8% which could indicate a dose rate effect. Raman spectra were also taken of the irradiated samples. PEW was found to have a a new peak at about 150 cm^{-1} when irradiated at MUC but no other observable changes were found. A statistical model was developed to calculate chain length distribution after irradiation by utilizing a displacements per atom (DPA) approach. This model was intended to extrapolate the change in latent heat from the change in molecular chain length. The current model only accounts for scissions and neglects any crosslinking that could occur. The model was found to have an absolute error of under 0.15 at the starting chain length when compared to a similar model developed by Charlesby. It was found that the current model predicts that there will be minimal change in the starting chain lengths which indicates no significant change in the latent heat. This agrees with the data found.

ACKNOWLEDGMENTS

I would like to thank all the people who have helped me get this far. First my wife, Haley Steere, for all the encouragement and support over these years and for the proofreading. My family for all their support and sacrifices. Special thanks goes to my parents, Donald Steere, Mary Steere and Duffy Steere, for being the driving force to getting me interested in science and engineering since I was just a kid. My advisor, Dr. Joshua Schlegel, for all of the guidance and instruction on being a good researcher, holding me and my research to high standards, and for having the best open-door policy ever. My committee Dr. Ayodeji Alajo, Dr. Carlos Castano, Dr. William Fahrenholtz, Dr. Joseph Graham, and Dr. Hiaming Wen, for all of their suggestions and assistance in my research. The reactor staff for all the work and assistance they gave me while completing irradiations for this project. The undergraduate students that helped with Flux analysis and DSC measurements. Finally, I would like to thank my friends who spent countless hours letting me bounce research ideas back and forth with them; I would never have made it this far without them.

TABLE OF CONTENTS

LIST OF ILLUSTRATIONS

SECTION Page

PAPER II

PAPER III

LIST OF TABLES

NOMENCLATURE

Symbol	Description
C	Counts Under 1099 keV Gamma Peak for Fe-59
ϵ	Detector Efficiency
υ	Branching Ratio per Decay for 1099 keV Gammas
ω	Natural Abundance of Fe-58
λ	Fe-59 Decay Constant
t	Time
D	Dose Rate
Φ	Neutron Flux
N	Atom Density
σ	Cross Section
Q	Average Neutron Scattering Energy Loss
ρ	Density
m	Mass
E	Neutron Energy
CI	Confidence Interval
ε	DSC Measurement Error
S	Number of Data Points
s	Standard Deviation
x	A latent heat measurement
P	Probability Distribution

Z	Number of initial units in the chain
p	Probability of a C-C break for one unit of radiation at Harwell B.E.P.O. pile reactor
R	the number of 1E17 units of radiation at the Harwell B.E.P.O. pile reactor
H	Damage Per Atom Per Second
k	number of Breakes in a Chain
G	Damage per Chain
H	Damage per atom
l	Chain Length
z	Hydrogen Bonds Broken
nc	Probability of a free radical on not forming a cross link
LH	Latent Heat

Subscript	Description
f	Foil
a	Absorption Cross Section
I	Irradiation
b	Between Irradiation and Counting
c	Counting
s	Scattering Cross Section
n	Neutron
T	Target
l	Chain Length Distribution

k	Number of Carbons in a Chain Length
0	A virtual unit of radiation
d	Displacement
m	Energy Needed to Break A C-C Bond
sc	Scissions per Chain
cl	Chain Length Distribution
st	Starting Chain Length
FP	Free Radical Production
t	Total Probability of not Forming a Crosslink
m	Mass Distribution
ν0	carbons per chain prior to irradiation
Δ	largest mass change between irradiated and unirradiated

1. INTRODUCTION

Phase Change materials (PCMs) have become a useful tool in many applications for their ability to store large amounts of thermal energy over a small temperature range. This property is due to their latent heat while transitioning from one phase to another. The most common applications of PCMs are enhancement of building insulation, temperature regulation in textiles, and energy storage systems [1-4]. Some less common applications of PCMs are neurons in neural networks, as a passive safety system in nuclear reactors, and as an environmental control system in space craft and space suits [5-8]. One issue that is unique to the nuclear reactor and space applications is the radiation environment that the PCMs would be exposed to during normal operation. The research presented here measures the change in latent heat associated with radiation dose from neutrons and associated gamma photons in nuclear reactor environments. A model to predict the change in latent heat at the desired operating temperature is then developed.

Table 1.1 shows the melting temperature range and latent heat necessary for PCMs to be used in nuclear reactor and spacecraft applications. It can be seen that a latent heat of >200 J/g is necessary nuclear applications and >170 J/g is necessary for space applications. This is important so that the overall system size can be minimized. The melting temperature must be between 70-90 °C for nuclear reactor applications. This is a requirement so that the PCMs do not melt during normal operation but will still effectively remove the heat from steam to condense it. The spacecraft application requires a PCM that melts close to room temperature for the comfort of the astronauts on the craft. Due to these requirements,

it has been found that organic PCMs are the ideal solution for these appliceations. Unfortunately, the radiation resistance of the organic materials is not well documented.

Table 1.1 – Thermal Properties for Nuclear Reactor and Space Applications

Property	Nuclear Reactor Applications	Spacecraft Applications
Latent Heat	>200 J/g	>2170 J/g
Melting Temperature	70-90 °C	20-25 °C

Radiation damage in organic materials comes in three main forms: scission, cross linking, and oxidation [9,10]. Scission and oxidation cause the chain lengths in the organic material to shorten while cross linking causes the the material to lengthen and to branch [9,10]. Figure 1.1 shows the melting temperature and latent heat of paraffins with different chain lengths [11]. It can be seen from Figure 1.1 that melting temperature decreases with shorter chain lengths and that latent heat in general decreases with shorter chain lengths. It should be noted that there is significant variation in the latent heat, namely that even chain lengths typically have higher latent heat than odd chain lengths, which could cause large changes in latent heat with radiation damage.

The first paper in this dissertation experimentally determines the effect of radiation damage on the latent heat of polyethylene wax with the necessary properties for nuclear reactor containment. The second paper experimentally determines the effects of radiation on the latent heat of a eutectic of methyl palmitate and lauric acid which has the necessary properties for space applications. Finally, the third paper presents a model that predicts the

change in the molecular chain lengths of organic materials due to the scission of chains, which can then be used to evaluate changes in latent heat at the desired temperature.

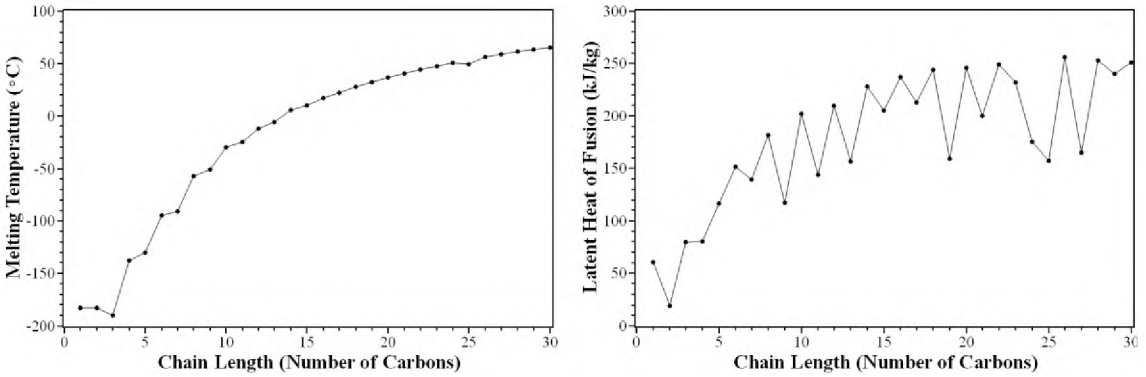

Figure 1.1 – Melting temperature (Left) and Latent heat (Right) of Paraffins with Different Chain Lengths [11]

2. BACKGROUND

2.1. DIFFERENTIAL SCANNING CALORIMETRY THEORY

Differential Scanning Calorimetry (DSC) is a useful tool that can be used to determine different properties that deal with thermal energy. The first two papers in this dissertation use DSC to obtain the the melting temperature and latent heat of several samples. A measurement is performed by placing one pan that is empty, called the blank, and another that is filled with the sample that you are obtaining data from on two separate heaters. These heaters are in a well-insulated container and are controlled by a computer which raises the temperature of both sample pans at the same rate while measuring the heat flux into each pan. The heat flux from the blank pan is subtracted from the sample pan's heat flux to provide the amount of heat that is put into the sample per temperature. Figure 2.1 shows a diagram for this system [12].

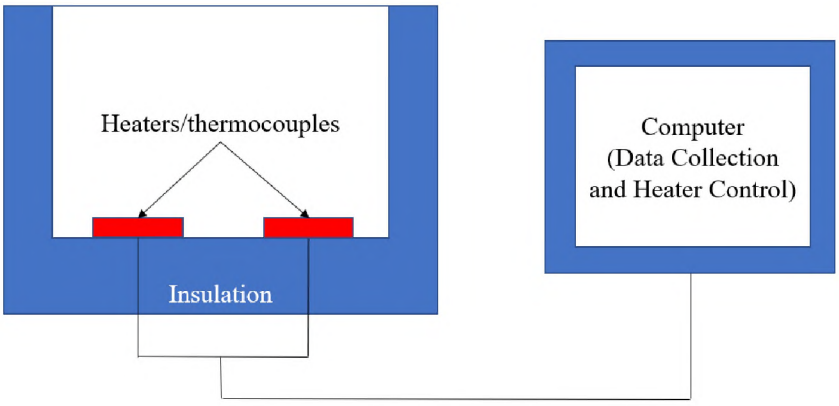

Figure 2.1 – Example DSC Layout and Control

Figure 2.2 shows a typical DSC output in the form of a thermograph as well as some basic analysis of the curve. In Figure 2.2, the green line is the output from the DSC

and follows the green axis on the left. The flat portion of the line from about 17 °C back is the region where the sample is solid. The flat portion of the green line from about 30 °C forward is where the sample is solid. The peak in between the 17 and 30 °C temperatures is the melt peak. The latent heat is obtained by numerical integration of the melt peak under a line that extends from the solid plateau to the liquid plateau shown as the red line in Figure 2.2. The melting temperature is found by following the leading edge of the melt peak back to the red line and can be seen as the intersection of the red and black lines in Figure 2.2. Above the red line is the melting temperature in °C and latent heat in J/g. The purple line is the running integral under the red line and shows the development of the latent heat with temperature and follows the purple axis to the left.

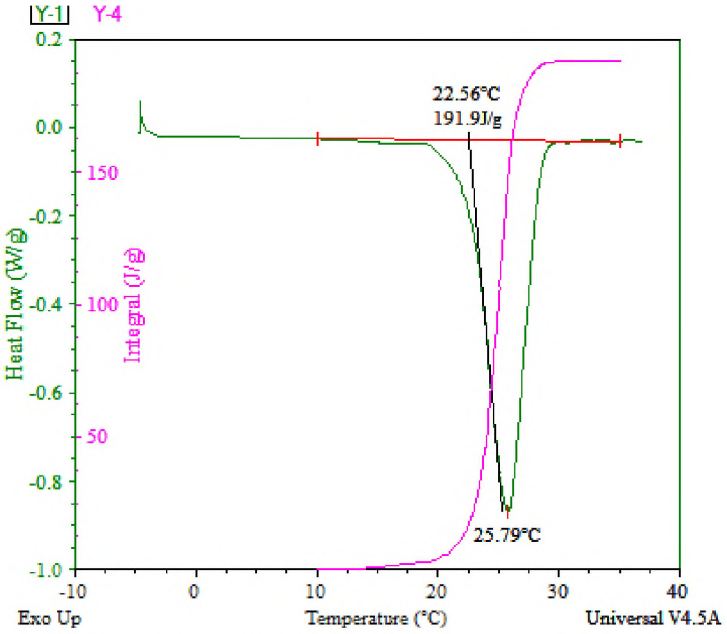

Figure 2.2 – Typical DSC Measurement

2.2. RAMAN SPECTROSCOPY THEORY

Raman spectroscopy is used as a method of determining the molecular structure and bonds of a substance. The first and second papers presented in this dissertation use Raman spectroscopy to further evaluate the damage done to the irradiated samples. Raman spectroscopy works by shining a laser onto the surface of a sample and measuring the shift in photon energy due to inelastic scattering. This inelastic scattering is caused by the shift in energy associated with various forms of molecular vibration or rotation that the photon can excite in the molecule. The Raman shift for many types of bonds in various molecules are already determined [13]. Figure 2.3 shows an example Raman spectrum for polyethylene.

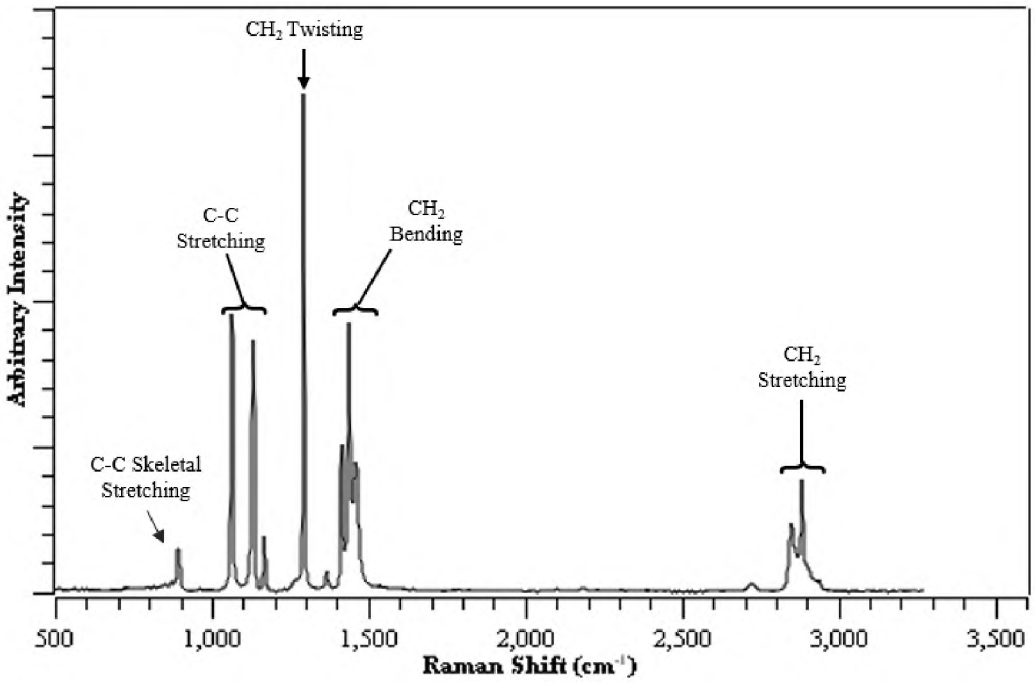

Figure 2.3 – Example Raman Spectrum of Polyethylene

As can be seen in Figure 2.3 there are 9 main peaks in polyethylene. These particular peaks are associated with the carbon skeleton stretching at the 890 cm^{-1} peak; individual C-C bonds stretching at the 1060 cm^{-1} and 1130 cm^{-1} peaks; CH_2 Twisting at the 1290 cm^{-1} peak; the CH_2 bending at the 1410 cm^{-1}, 1430, and 1460 cm^{-1} peaks; and finally CH_2 stretching at the 2850 cm^{-1} and 2880 cm^{-1} peaks [14]. These peaks can shift a few cm^{-1} but otherwise will stay at the same Raman shift for the same material.

While polyethylene irradiated with thermal neutrons has shown no changes in Raman spectra, fast neutron irradiated polyethylene has been shown to have several affect [14]. The changes from fast neutrons were a new peak at 854 cm^{-1}, the two C-C stretching peaks merged at 1065 cm^{-1}, a new peak formed at 1655 cm^{-1}, and the relative intensities of all the peaks decreased [14]. These changes took place after a fast neutron fluence of 2.42×10^{16} n/cm^2 and there were no measurements other than at that dose.

It has also been found that low Raman shift peaks (<500 cm^{-1}) in the Raman spectra of paraffins and fatty acids can be used to determine the approximate chain length of organic compounds [15]. This is due to the accordion motion molecules with a long carbon backbone can have. The Raman shift that the molecules accordion at is lower with longer carbon chains. This effect will be looked for in the current work, but it is unlikely to yield many results as the chain lengths for Polyethylene are very large.

The raw data from a Raman Spectrum can be difficult to interpret without processing the data first by removing the noise and background readings as well as normalizing the spectrum. Typically, software is used to do this as well as fit peaks to the data to obtain things like peak intensity, center, and full width at half the maximum (FWHM).

PAPER

I. NEUTRON AND GAMMA RADIATION EFFECTS ON THERMAL STORAGE PROPERTIES OF POLYETHYLENE WAX

ABSTRACT

Several nuclear reactors use ice condensers to condense steam in the case of a loss of coolant accident. These ice condensers have many problems that could be alleviated by using another material. The effects of low-dose neutron and gamma radiation on the thermal properties of polyethylene wax (PEW) were investigated for this purpose. PEW was irradiated in the Missouri University of Science and Technology Research Reactor (MSTR), the University of Missouri Cyclotron (MUC) and the University of Missouri Research Reactor (MURR) up to doses equivalent to 10 months in a nuclear power reactor's containment structure. The melting temperature and latent heat of fusion were determined using differential scanning calorimetry (DSC). Changes in the molecular bonds was determined using Raman spectroscopy. It was found that there was not a significant change in the thermal properties nor bonding over the investigated doses. This suggests that organic PCMs could be reliable alternatives to ice in nuclear reactor containment applications. The measured melting peak was found to be significantly wider expected by the suppliers' description. The ramifications of wide melting peaks are discussed in the context of reactor accident analysis and further experiments are suggested.

1. INTRODUCTION

Phase change materials (PCMs) are materials that can store and release large amounts of thermal energy at a nearly constant temperature. They do so by utilizing the latent heat of a phase transition, typically a solid-liquid transition. PCMs have many applications and are currently being used to enhance building insulation, to regulate temperature in textiles, and for energy storage [1-4]. PCMs also have potential for advanced computing methods by using small pockets of PCM as neurons in a neural network [5]. Several nuclear power reactors, such as D.C. Cook, use PCMs in the form of large ice condensers. These ice condensers contain approximately 2.6 million pounds of borated ice which cools steam produced during a loss of coolant accident (LOCA) and thereby helps reduce the temperature and pressure in the containment structure. Such condenser systems help reduce containment size and construction costs.

Several drawbacks of the ice condenser systems include requiring separate refrigeration systems to keep the ice cold; keeping the flow channels clean from foreign material; and replenishing ice lost due to sublimation. D.C. Cook was forced to shut down for 2 years starting in 1997 due to a flaw discovered in the ice condenser system. During this outage it was found that the ice condenser had accumulated approximately 2000 pounds of foreign material and was displacing ice in the system [6]. By replacing ice with a PCM that melts at a higher temperature, many of the problems associated with the current ice condenser systems in these plants can be mitigated. Moreover, doing so would turn an active safety system into a passive safety system. In addition to improving the current ice

condensers in some nuclear reactors, it is possible that other reactors could be retrofitted or constructed with such organic PCM systems to increase the response time for an accident

The ideal melting temperature range and latent heat of fusion for nuclear reactor applications is 70-90 °C and >200 J/g respectively. These values have been determined by considering the condensation point of water, the internal temperature of the containment building, and the containment volume constraints. The melting temperature range is based on the requirement that PCMs do not melt during normal operation, which is up to about 50 °C [7] but are still effective in removing the heat from steam to condense it during a LOCA when temperatures reach upwards of 150 °C [8]. In a nuclear reactor, PCMs would need to be able to withstand high radiation environments with little change in thermal properties. As will be discussed in the background, the ideal class of PCMs for this application is Organic PCMs. The effect that radiation has on the latent heat of organic materials is not well documented and significant degradation from radiation damage could reduce the ability of the PCM to properly remove the heat from the steam. The goal of this paper is to evaluate the effect that radiation has on the latent heat of Polyethylene Wax (PEW) which has thermal properties well suited for steam condensation applications.

2. BACKGROUND

2.1. REACTOR CONTAINMENT

In the containment structures of nuclear reactors there are elevated levels of gamma and neutron radiation. Materials within containment must be able to withstand accumulated radiation damage over their lifetime. In many cases, materials will need to be replaced after

a certain amount of time within the containment [9]. While the effects of radiation on the properties of structural materials found in containment structure is well documented, little research has been conducted on the change in latent heat of organic materials with irradiation.

It is important to be able to determine the amount of dose that a material is expected to be exposed to during normal operation. Ideally, using the dose that materials would experience in the ice condensers in D.C. Cook would give the closest estimate of how much dose the PCMs would be exposed to. Unfortunately, those dose rates are not readily available. In an attempt to compare the dose obtained in these experiments with some form of real-world data a study of Tihange-1 Pressurized Water Reactor will be used. It was found that the total neutron flux of Tihange-1 was approximately 1×10^{9} n/cm^2-s at the concrete basemat under the pressure vessel [10].

2.2. PHASE CHANGE MATERIALS

PCMs are materials that have a large latent heat that allows them to absorb a significant amount of energy at a phase transition temperature. Most PCMs that are currently used have a solid-liquid phase transition. This is driven by the need for a higher latent heat than solid-solid phase transitions can provide. Solid-vapor or liquid vapor phase transitions are not viable as they undergo larger volume changes than can be accommodated by a reactor containment structure. Solid-liquid PCMs can categorized into three groups: organic, inorganic, and eutectic (Figure 1) [11-12]. Figure 2 shows the typical melting temperatures and volumetric melting enthalpies of various types of PCMs [13]. As can be seen in Figure 2, paraffins, salt hydrates, and sugar alcohols are the ideal candidates

for a melting range of 70 to 90°C. Salt hydrate have favorable volumetric melting enthalpies but suffer from phase separation. This means that, over time, the salt hydrate will form precipitates that change the melting temperature and reduce the latent heat[14]. Sugar alcohols have the next highest latent heat but they tend to oxidize quickly after melting [15]. This leaves paraffins. Paraffins are a family of organic molecules with the chemical formula C_nH_{n+2}. Unlike salt hydrates, paraffins maintain their latent heat and melting temperatures over time and don't oxidize as easily as sugar alcohols. The largest draw-back of paraffins is that they have relatively low thermal conductivities, around 0.01 W/cm-K [16-17]. Low thermal conductivity causes an effect where the outside of the PCM will melt quickly but the bulk of the material will take a long time to melt. This can make paraffins less effective PCMs overall. Finally, there are two other types of PCMs that are not present in Figure 2 and that is non-paraffin polymers and eutectics. Polymers have similar properties to Paraffins but do not strictly follow the same chemical formula and can have branches or functional groups attached to their main chain. Eutectics are combinations of two or more PCMs that, when mixed in a particular ratio, have a single melting point and latent heat of fusion [11-12]. Since they are a combination of any other PCM this gives them the widest ranges of melting temperature and latent heat as they can fit into any of the categories of Figure 2 and beyond. Eutectics are distinct in that they have a lower melting temperature than their constituent parts and have the largest melting range and latent heat range.

In general, the melting temperature of Paraffins increases with carbon chain length however odd carbon chain lengths have lower latent heats than their even chain length neighbors. Figure 3 shows the melting temperature and latent heat of Paraffins from carbon

chain lengths of 1-30 [18]. This indicates that as radiation damage affects the materials that the latent heat could significantly change as the chain lengths change size and even minor chain length changes could lead to large changes in latent heat.

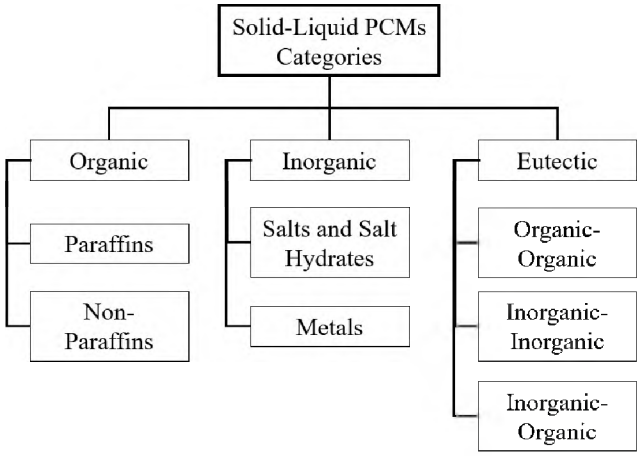

Figure 1 – Classification of Solid-Liquid PCMs

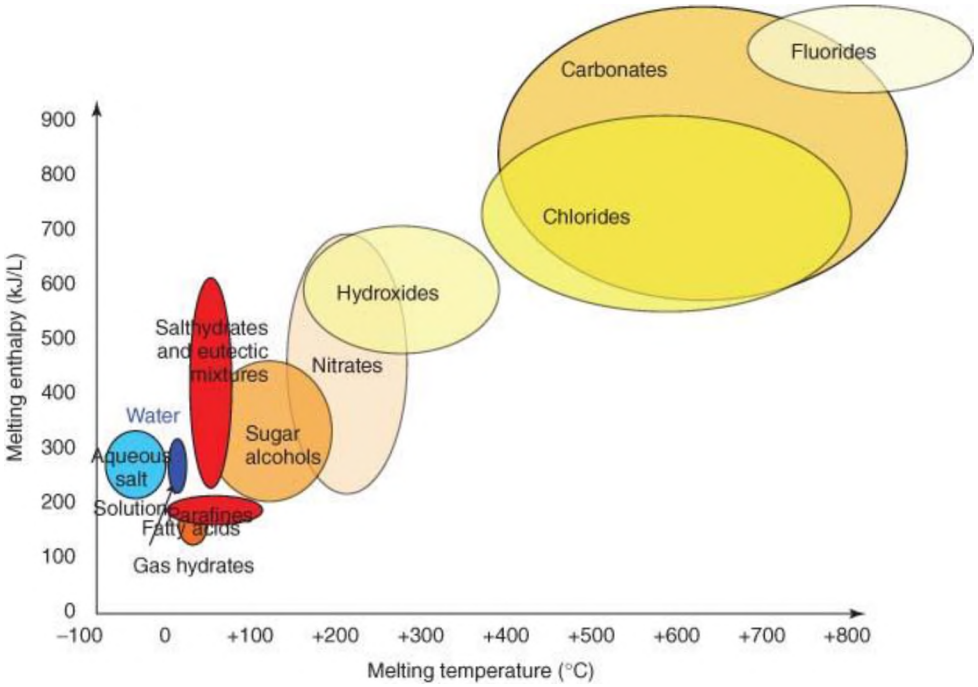

Figure 2 – PCMs Typical Melting Temperatures in °C and Latent Heat in kJ/L [12]

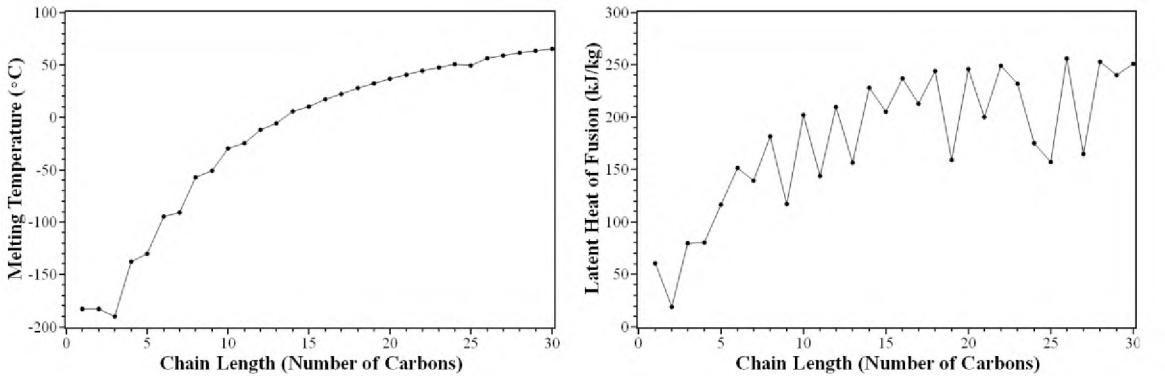

Figure 3 – Melting Temperature (Left) and Latent Heat (Right) of Paraffins with Different Chain Lengths [18]

2.3. RADIATION DAMAGE IN ORGANIC MATERIALS

2.3.1. Radiation Damage Mechanisms. The three main radiation effects in organic materials include scission, crosslinking, and oxidation. Scission occurs when radiation causes a C-C bond to break creating two separate chains each with a free radical. A crosslink occurs when two carbon free radicals from separate chains bond to each other. Oxidation occurs when a carbon free radical bonds with oxygen in the air [19]. Figure 4 illustrates each mechanism.

Radiation can also result in unsaturation of a molecule. For unsaturation to occur, two free radicals formed adjacent to one another form a double bond (Figure 5). The unsaturation of a molecule due to radiation damage is rare due to the unlikely scenario of two adjacent free radicals of carbon occurring on the same chain [20].

Scissions occur throughout the material wherever energetic radiation can penetrate. Oxidation and crosslinking are competing effects as they both require free radicals to occur. Typically, oxidation occurs near the surface of the material and decreases with depth due to need for oxygen to diffuse in the material. Crosslinking occurs more in the center of the material as it does not have to compete with oxygen for the free radicals. If the dose rate is

lower, oxidation occurs deeper in the material as oxygen has a longer time to diffuse into the material [19].

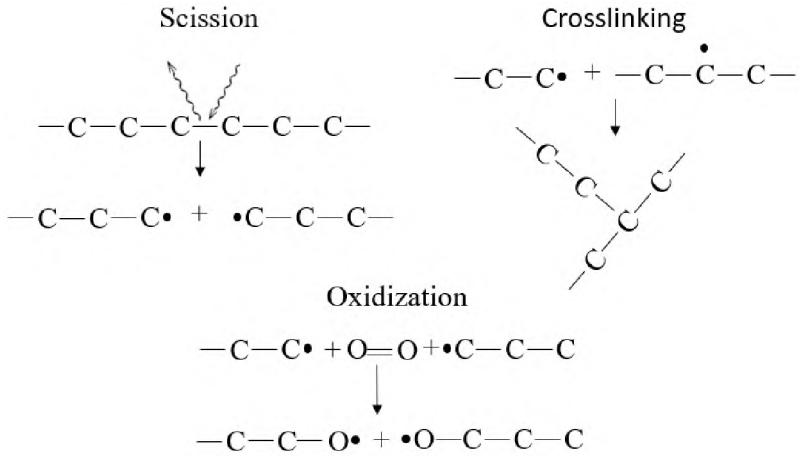

Figure 4 – Radiation Damage Mechanisms in Polyethylene

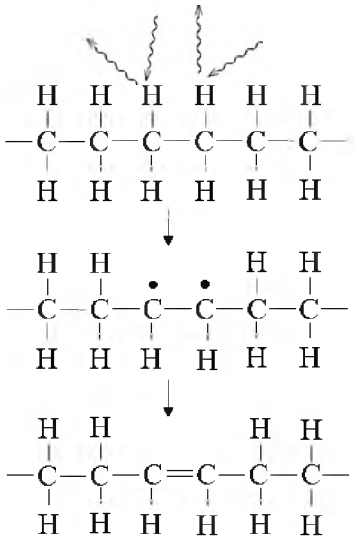

Figure 5 – Unsaturation of a Molecule

There has been some research done on the effects of temperature and mechanical stress during irradiation in organic materials. In general, it has been found that increased mechanical stresses cause more scissions to occur and this increases the number of free

radicals in the material [20]. Increased temperature has the effect of increasing the amount of crosslinking that occurs. However, at elevated temperatures gas formation competes with crosslinking [20].

2.3.2. Property Changes Due to Irradiation Damage. Scissions decrease the average molecular weight of a polymer. This decrease in molecular weight has a significant impact on the physical properties of the material. First, it can create gases in the form of small chain hydrocarbons and diatomic hydrogen. Mechanical properties such as the Young's modulus, tensile strength, hardness, and elasticity can also decrease. It can also increase the solubility and elongation of the material. With a decreased molecular weight melting temperature can also decrease [20].

Crosslinking increases the molecular weight of the material and therefore has somewhat opposite effects as scission. The Young's modulus, tensile strength, hardness, and elasticity all increase while the elongation and solubility decrease. Crosslinking has been shown to cause an increase in melting temperatures and to create a gel-like substance that does not melt [19-20]. Charlesby found that with increasing radiation dose, the melting temperature initially decreases but eventually increases sharply once cross linking becomes the dominant damage mechanism. Figure 6 shows this decrease and sudden increase with radiation dose. In Figure 6, each dose unit is estimated to be 44 MRads and is due to both gammas and neutrons.

Oxidation in general yields the same effects that scissions create. This is due to the fact that the free radicals created by the scissions are taken by oxygen instead of by crosslinking. In materials where oxidation is more prevalent than crosslinking the mechanical properties decrease significantly [20].

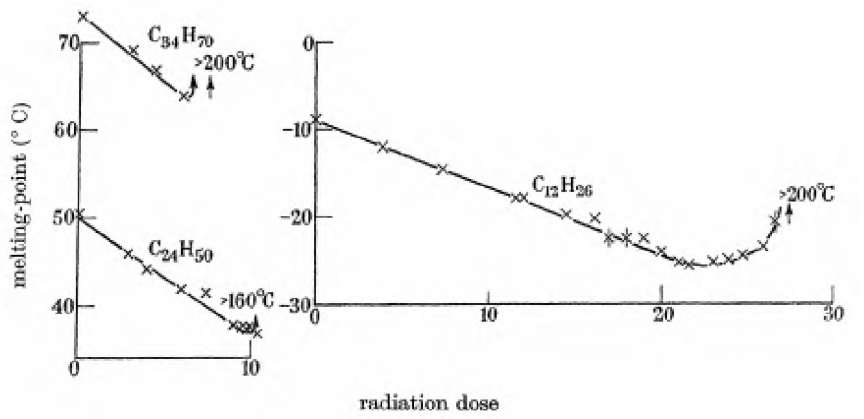

Figure 6 – Melting Temperature of Paraffins with Radiation Doses[20]

There is a significant gap in the current literature about the effects of radiation on the latent heat of fusion of organic materials. Since latent heat is one of the most important properties of a PCM, it is imperative to understand how radiation damage modifies latent heat. Polyethylene Wax was chosen with a melting temperature of 88 °C and latent heat of fusion around 220 J/g. This wax was chosen because of its ideal properties, affordability, and simple chemical structure.

2.4. MEASUREMENT TECHNIQUES

Differential Scanning Calorimetry (DSC) is a useful tool that can be used to measure thermal properties. It will be used to evaluate the change in the latent heat as well as the change in the melting temperature of the PEW with irradiation [21].

Raman spectroscopy is used as a method of determining the molecular structure and bonds of a substance by measuring the wavelength shift of a laser as it inelastically scatters off a sample. By measuring the wavelength shift it is possible to determine the types of bonds present in a material due to molecular movement [22].

There are 9 main first-order Raman active peaks in polyethylene. These particular peaks are associated with the carbon skeleton stretching at the 890 cm^{-1} peak; individual C-C bonds stretching at the 1060 cm^{-1} and 1130 cm^{-1} peaks; CH_2 Twisting at the 1290 cm^{-1} peak; the CH_2 bending at the 1410 cm^{-1}, 1430, and 1460 cm^{-1} peaks; and finally CH_2 stretching at the 2850 cm^{-1} and 2880 cm^{-1} peaks [22]. These peaks can shift a few cm^{-1} but otherwise are characteristic of the material.

It has been found that there are a few changes in the Raman spectrum of Polyethylene as when it is irradiated with fast neutrons [23]. These changes include; a new peak at 854 cm^{-1}, the two C-C stretching peaks merge at 1065 cm^{-1}, a new peak forms at 1655 cm^{-1}, and the relative intensities of all the peaks decreased [23].

Low frequency peaks (<500 cm^{-1}) in the Raman spectra of paraffins and fatty acids can be used to determine the approximate chain length of organic compounds [24]. This is due to the accordion modes whose frequencies depend on chain length.

The Raman spectra of the PEW will be evaluated to determine if there was any significant change in the bond structure after irradiation. In particular, what will be looked for in the spectra are changes similar to irradiated Polyethylene and changes in the low frequency accordion modes.

3. MATERIALS AND METHODS

3.1. POLYETHYLENE WAX

For this study, Polyethylene Wax was supplied by Baker Hughes. The PEW blend that was used is POLYWAX 500 polyethylene which has an advertised melting

temperature of 88 °C, latent heat of fusion of 220 J/g, and sharp melting peak. These properties should be ideal in a reactor system because the PCM should be fully solid during normal reactor operations and melt in an accident scenario as steam comes in contact with it [25].

3.2. DIFFERENTIAL SCANNING CALORIMETER

DSC measurements were performed using a TA Instruments DSC 2010 Differential Scanning Calorimeter (DSC). The instrument was calibrated using tin, lead, and indium standards. The temperature accuracy, temperature reproducibility, maximum sensitivity and calorimetric precision are ±0.1 °C, ±0.05 °C, 1 μW, and ±0.1% respectively. The samples were measured in aluminum pans with lids from DSC Consumables. The heating rate for the measurements was 2 °C/min. It was necessary to reduce the temperature of the samples to below 0 °C prior to starting a measurement. This was accomplished using a liquid nitrogen cryostat. The DSC thermographs were analyzed with TA Universal analysis software.

3.3. RAMAN SPECTROSCOPY

Raman spectra were collected using a Horiba XploRA Plus with a 785 nm laser. The instrument has an approximate resolution of <1.2 cm^{-1} FWHM with an 1800 mm^{-1} grating in the spectral range of interest. Calibration was performed with a (111) Si standard. For the measurements in this work, the grating was set to 1200 mm^{-1}. This lowers the measurement resolution but was necessary to achieve higher light throughput. For each measurement, the spectrum was averaged over five 60-second acquisition times. Post

processing of the data was performed using the acquisition software, Labspec6, and spectrum analysis tool Fityk. Noise was reduced using a moving average filter in the Labspec6 software. Background estimation, background removal, spectrum normalization, and peak fitting were performed using the Fityk software. Background estimation was done using a piecewise interpolation function where the points for the estimation were chosen for each spectrum individually to get the best results. The normalization was performed so that the total count area under the spectrum after background removal was one. Peak fitting was performed using a Pearson VII function.

3.4. RADIATION SOURCES

3.4.1. MSTR. At the MSTR sample irradiations were performed using the core access element (CAE). Figures 7 and 8 show cross sections of the CAE testing area. As can be seen in Figures 7 and 8, the CAE is lined with graphite. The graphite helps thermalize many of the neutrons that will interact with the samples. All samples were lowered through the guide and suspended in the center of the CAE testing area using a premeasured string and vial holder. Figure 9 shows the layout of the MSTR core with the CAE in place.

The neutron flux at the experiment location was experimentally determined using Fe flux foils. The foils were irradiated for 30 seconds in the CAE. Activity was measured using a high purity germanium (HPGe) detector to determine the foils' gamma spectra. Each foil was measured on the detector for 1 hour. Flux was measured three times at each power using a different foil.

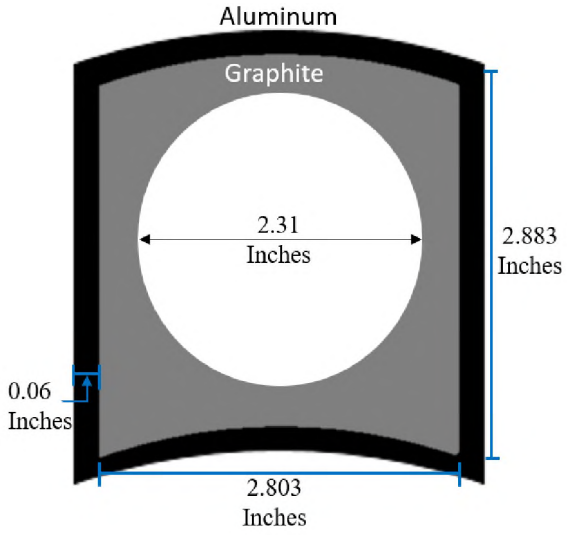

Figure 7 – Horizontal Cross Section of Core Access Element

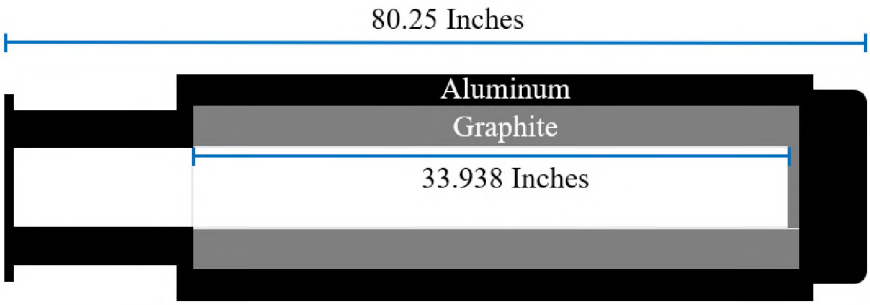

Figure 8 – Vertical Cross Section of Core Access Element

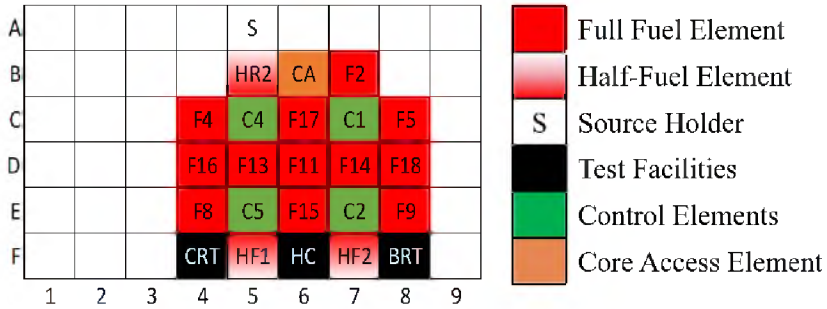

Figure 9 – MSTR Reactor Core Layout

Equation 1 was used to calculate the flux. In Equation 1 ϕ is the neutron flux, C is the number of counts under the 1099 keV gamma energy peak for Fe-59, ϵ is the detector efficiency at 1099 keV which was found to be 0.021 at the measurement location, υ is is branching ratio per decay for the 1099 keV gamma energy, ω is the natural abundance of Fe-58, m_f is the mass of the foil, σ_a is the absorption cross section of Fe-58, λ is the decay constant of Fe-59, t_i is amount of time the foil was irradiated for, t_b is the amount of time between the end of the irradiation to the start of the spectrum, t_c is the amount of time the sample was being counted on the detector,. Figure 10 shows the average neutron flux that was measured at each power. The uncertainty was calculated using Student's t-distribution with a 90% confidence interval.

$$\phi = \frac{C}{\epsilon \upsilon \omega m_f \sigma_a (1 - e^{-\lambda t_i}) e^{-\lambda t_b} \frac{1 - e^{-\lambda t_c}}{\lambda}} \tag{1}$$

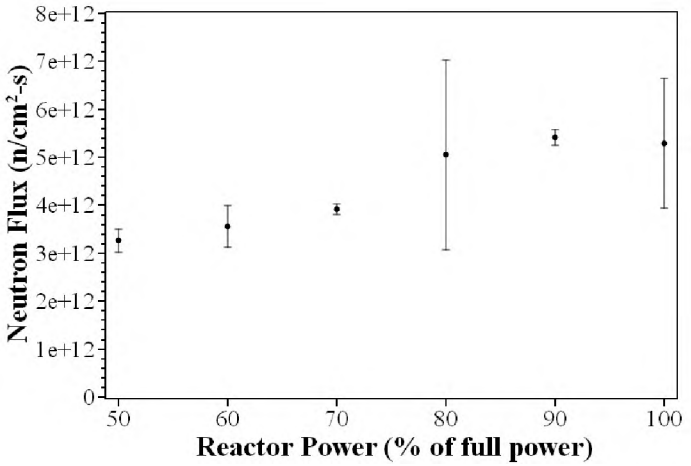

Figure 10 – Neutron Flux vs. Power of MSTR at 50-100% Power

As can be seen in Figure 10, there is significant error in the flux measurement at 80% power and 100% power. Possible causes for these large errors are human error in the

time recording or foil masses being skewed due to the presence of rust on some foils. Due to this the experiments were carried out at 50% and 90% reactor power to determine if any dose rate effects are present. MCNP [26] was used to calculate the flux spectrum at the center of the CAE. The flux spectrum was determined using an energy deposition tally and had an error of less than 0.01%. Figure 11 shows the energy dependent flux from the MCNP run at 100 kW and 180 kW. Table 1 shows the average experimental flux and the MCNP flux. The values from MCNP are well within the 90% confidence interval for the experimental fluxes obtained from the irradiated iron foils at both powers.

Table 1 – Reactor Flux at Experiment Powers

Power (kW [%])	**Experimental Flux (n/cm2-s)**	**MCNP Flux (n/cm^2-s)**
100 [50]	3.26×10^{12}	3.05×10^{12}
180 [90]	5.42×10^{12}	5.49×10^{12}

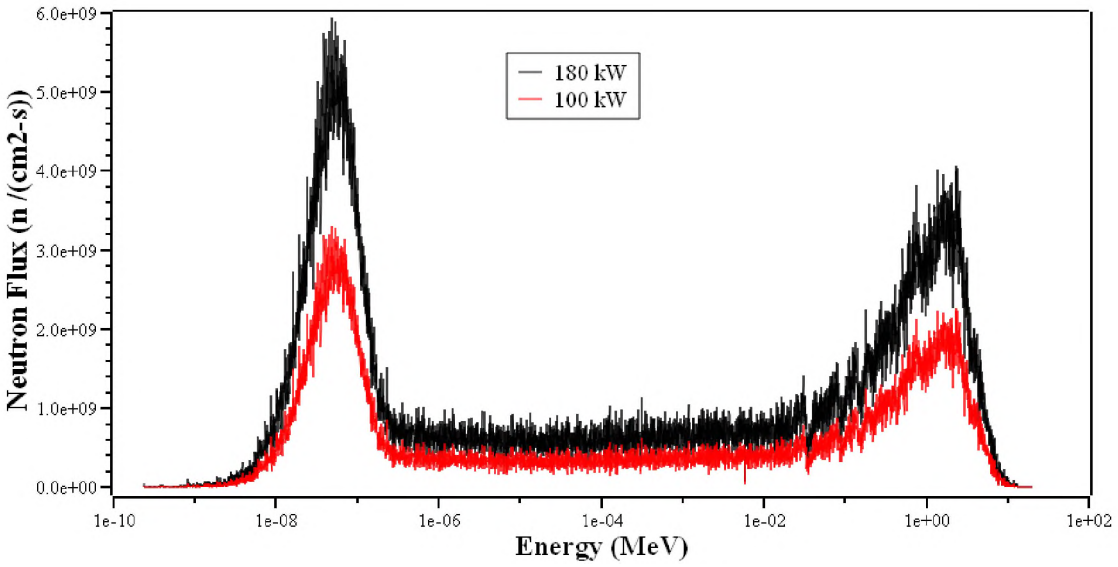

Figure 11 – MSTR Flux Spectrum at the Center of the CAE at 100 and 180 kW

The experiments were carried out with four batches of PEW. Two batches were irradiated at 50% power and the remaining two batches were irradiated at 90% power. Each batch was irradiated six times over six weeks and was irradiated for an amount of time so that the total neutron fluence would be approximately equal. The times chosen were 6 min for 90% power and 10 min for 50% power. Table 2 shows the irradiation times, accumulated irradiation time, accumulated fluence and total dose of the samples irradiated at 180 kW and 100 kW. As can be seen the fluence and neutron dose per irradiation for each of the flux power levels is comparable to one another. The dose rate was calculated using Equations 2 and 3 and multiplying by time In Equation 2, $\dot{D}$ is dose rate, Φ is neutron flux, N is atom density, σ_s is the scattering cross section, Q is the average energy that the neutrons lose, and ρ is target density. In Equation 3, Q is the average energy, m_n is the mass of a neutron, m_T is the mass of the impacted atom, and E is the neutron energy.

$$\dot{D} = \frac{\Phi N \sigma_s Q}{\rho} \tag{2}$$

$$Q = \frac{4 m_n m_t}{(m_n + m_T)^2} \frac{E}{2} \tag{3}$$

After the irradiation was complete the samples were suspended in the CAE sample access tube to cool for five minutes. The samples were then stored in a lead lined case for seven days to further cool to background. Irradiation times and cooling times were chosen to keep the total dose from the samples and sample containers to researchers below 25 mrem/hr for safety reasons and so that the samples could be removed from the reactor according to the University policy. After the cooling period ended, the PCMs were melted, and three small samples were extracted from each batch and placed in DSC measurement pans. The remaining PCM was returned to the reactor for the next set of irradiations.

Table 2 – MSTR Irradiation Information

Irradiation #	1	2	3	4	5	6
180 kW – Flux: 5.42×10^{12} (n/cm^2-s)						
Irradiation time (min)	6	6	6	6	6	6
Accumulated Radiation Time (min)	6	12	18	24	30	36
Accumulated Fluence ($\times10^{15}$ n/cm^2)	1.95	3.90	5.85	7.80	9.75	11.70
Total Dose (Gy)	470	940	1410	1880	2350	2820
100 kW – Flux: 3.26×10^{12} (n/cm^2-s)						
Irradiation time (min)	10	10	10	10	10	10
Accumulated Radiation Time (min)	10	20	30	40	50	60
Accumulated Fluence ($\times10^{15}$ n/cm^2)	1.95	3.90	5.85	7.80	9.75	11.70
Total Dose (Gy)	470	940	1410	1880	2350	2820

Going back to the Tihange-I reactor the dose rate would be 1.07×10^{-4} Gy/s. This translates to approximately 283 Gy every month. The total dose that the PEW would receive in MSTR after all the irradiations were complete would be approximately 9.9 months inside a nuclear reactor. It should be noted that the information from Tihange-1 is only to estimate the dose expected and that the actual dose in a reactor, such as D.C. Cook, could be significantly different.

3.4.2. MUC. The cyclotron used at The University of Missouri is a GE PETtrace Radiotracer cyclotron. The typical use for this cyclotron is the production of the medical isotope Flourine-18. To do this they accelerate hydrogen atoms into Oxygen-18, which if captured produces Fluorine-18 and a high energy neutron. The facility has several

irradiation locations where they can place a secondary target to be irradiated by the produced neutrons [27]. The samples were irradiated to a 1 MeV equivalent fluence of 10.1×10^{14} n/cm^2. This translates to a dose of approximately 662 Gy which is equivalent to approximately 2.3 months in a nuclear reactor containment. The neutron energy spectrum in the MUC is comprised of fast, unmoderated neutrons, unlike in the MSTR or MURR. Higher energy neutrons are less likely to interact with the material but would cause more damage when they do. Further experiments would be able to show the dependence on neutron energy however that is not the primary goal of this paper. Once the irradiations were done the samples were shipped back to Missouri University of Science and Technology where three DSC samples were prepared.

3.4.3. MURR. MURR is a 10 MW research reactor. The reactor contains a flux trap that, when operating at full power, has a neutron flux of 6×10^{14} n/cm^2-s [28]. This equals a dose rate of 144 Gy/s. Irradiation was performed for 20 seconds yielding a total dose of 2895 Gy. This would be equivalent of approximately 10.2 months inside a nuclear reactor containment.

4. RESULTS AND DISCUSSION

4.1. DSC

Figure 12 (a) and (c) show representative DSC thermographs for the PEW for the unirradiated specimens and specimens irradiated at 50% power and 90% power respectively. Figure 12 (b) and (d) show the integral of the DSC thermographs and shows how the latent heat develops over temperature. Figure 12 (e) and (f) show the representative thermographs and their integrals, respectively, from unirradiated PEW and PEW irradiated

at MUC and MURR. Evaluation of the thermographs show little change in the shape of the curves between the irradiated PCM and unirradiated PCM and that the material has a melting peak that spans from 20°C to 90°C. This melting peak is too wide for a nuclear reactor passive safety system as by the time an accident happens the PCM would have already been partially melted leaving less latent heat for the condensation of steam. The wide melting peak was unexpected as this brand of PEW was advertised to have a narrow melting peak. If PEW were to be used in a nuclear reactor for steam condensation it would need a cooling mechanism or additional PCM to make up for the material being partially melted at the start of the accident. The latent heat develops similarly for all measurements indicating there is no significant change in the material with the current doses.

Figure 13 shows the average latent heat of fusion with a 90% confidence interval evaluated using a Student's t-distribution. This confidence interval takes into consideration the error associated with the DSC and propagates it through the standard deviation using Equation 4:

$$CI = \bar{\varepsilon} + \frac{t}{\sqrt{S}} s \left(1 + \frac{\sum_i^N (\varepsilon_i + \bar{\varepsilon})(x_i - \bar{x})}{\sum_i^N (x_i - \bar{x})^2} \right) \tag{4}$$

where CI is the confidence interval, $\bar{\varepsilon}$ is the average error from the DSC measurement, t is the t-value from the students t distribution, S is the number of data points, s is the standard deviation, ε_i is the DSC error from a particular measurement i, x_i is the latent heat of a particular measurement i, and $\bar{x}$ is the average latent heat.

As can be seen in Figure 13 the 90% confidence interval error bars on most of the latent heat data overlap with the unirradiated data error bars indicating that there was no significant change for those samples. The exceptions to this are between 8-16% different

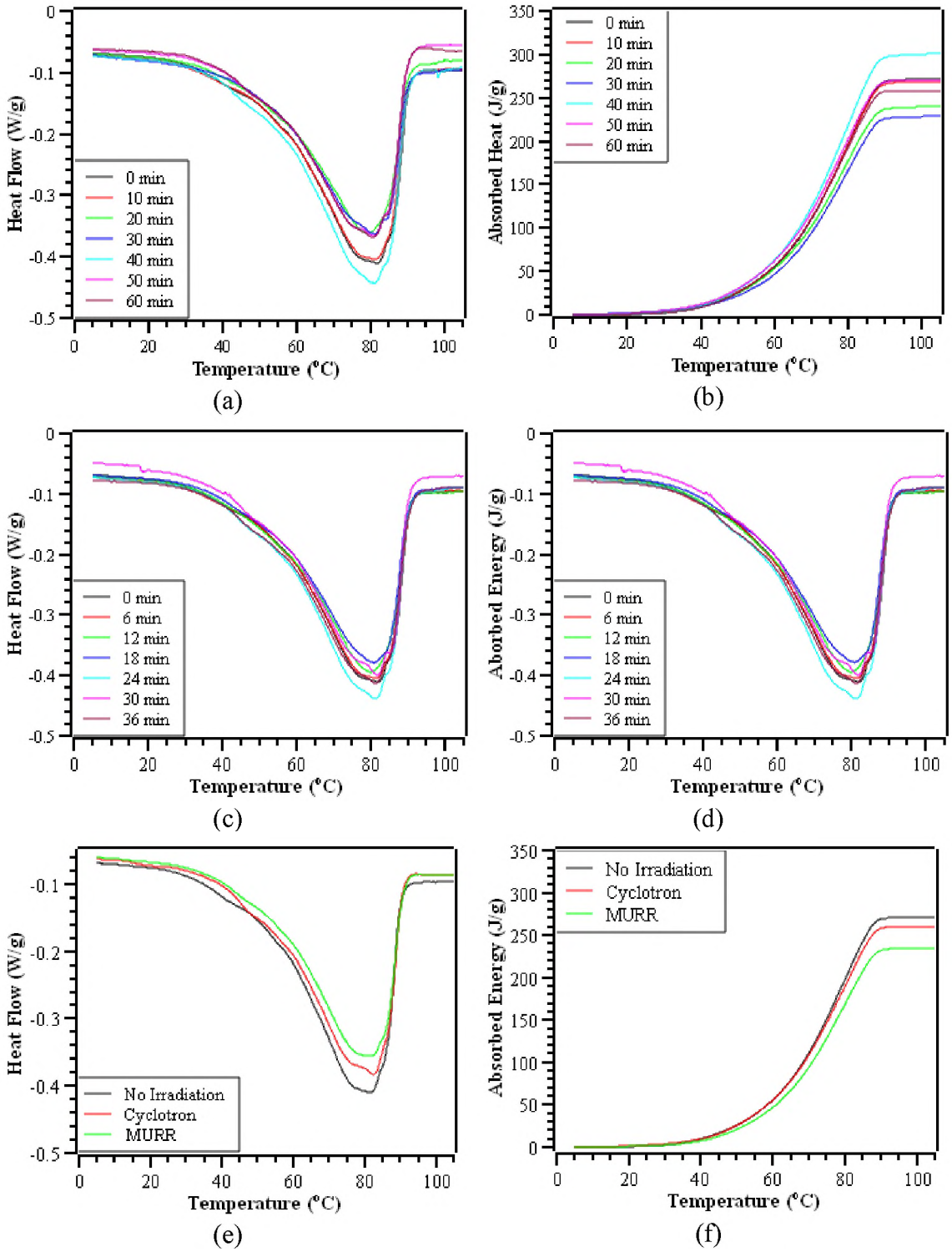

Figure 12 – Representative DSC Thermographs of PEW for Each Irradiation (a) Samples Irradiated at 100 kW (b) Integral of Samples Irradiated 100 kW (c) Samples Irradiated at 180 kW (d) Integral of Samples Irradiated at 180 kW (e) Samples Irradiated at MUC and MURR. (f) Integral of Samples Irradiated at MUC and MURR

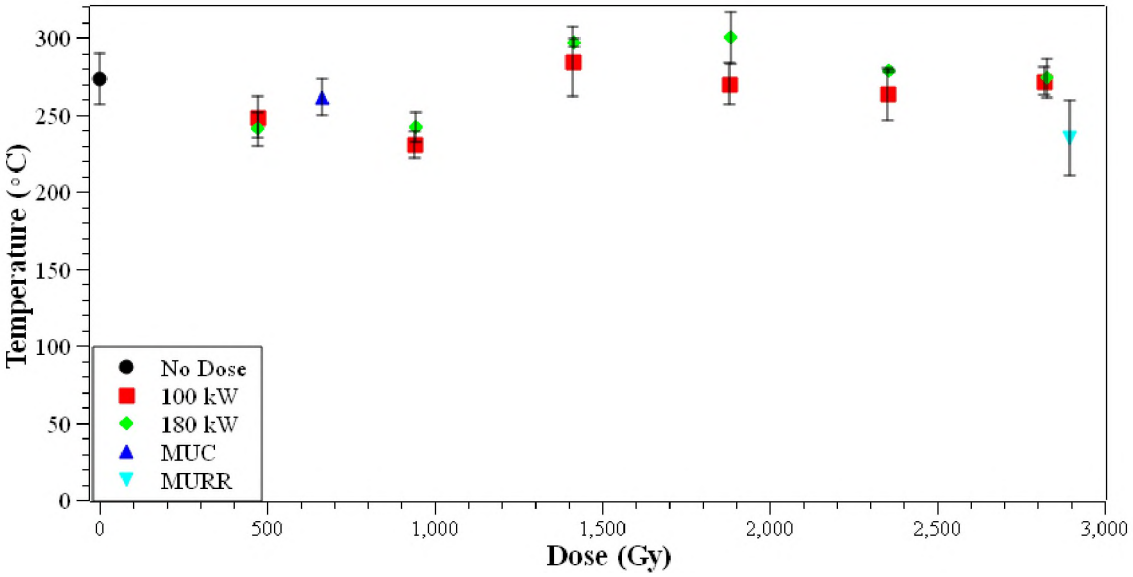

Figure 13 – Average Latent Heat of Fusion of PEW vs. Dose

than the starting value. These exceptions are very close to overlapping with the error bars from the unirradiated PEW and therefore are very likely just artifacts the PEW being inhomogeneous and the fact that some data will always fall outside a 90% confidence interval. This is significantly promising for nuclear applications. The data presented in this paper is somewhat coarse and additional measurements are needed to verify that the small errors seen are only artifacts of random sampling however this lends credibility that up to doses of approximately 3000 Gy there is very little change in the latent heat of PEW.

Figure 14 shows the average melting temperature and the temperature with the maximum melting heat flow with a 90% confidence interval calculated using a Student's t-distribution. As can be seen in the figure the melting temperature, as defined in this paper, is around 50°C. The large error bars in the melting temperature calculation are caused by the small differences in the slope of the leading edge of the melting peak. Due to how shallow the slope of the melt peak for PEW is, it can lead to large errors with small

differences in the slope. Even with the large error bars on some of the measurements it is still significantly lower than the melting temperature that is reported of 88°C. This discrepancy is due to a difference in measurement methodology. The manufacturer used the Standard Test Method for Drop Melting Point of Petroleum Wax, Including Petrolatum (ASTM D127). This method heats a thin film of the material that is solidified on two thermometers and takes the average of the temperatures of when the first drop of the material falls off each of the thermometers. Due to this methodology of determining the melting temperature, it requires the sample to be mostly melted and therefore closer to the maximum heat flux of the material as most of it has melted at that point. The point of maximum heat flow is around 80°C which is much closer to the reported melting temperature. As can be seen in the graph, there is no statistically significant change in the melting temperature or maximum heat flow temperature of the materials with radiation dose. This result is in agreement with the literature because of the relatively low doses that were used in these experiments compared to others.

4.2. RAMAN SPECTROSCOPY

While the DSC measurements provide evidence that the PEW is not undergoing any significant changes with radiation damage Raman spectra were taken to determine if there had been a change that in the materials bonding structure that did not cause a change in the latent heat. Figure 15 (a) shows representative Raman spectra taken for unirradiated PEW, the 36 min irradiation time at 180 kW, MUC and MURR. New peaks were not formed near 854 cm^{-1} or 1655 cm^{-1}. The narrower spectral range shown in Figure 15 (b) reveals several features which differ between specimens. It can be seen that for the

cyclotron measured data there is an additional peak at 150 cm^{-1} and that the peak at 100 cm^{-1} was reduced. This was present in two of the three measurements made for the cyclotron data. It is difficult to say what exactly caused this and should be further studied. One possible explanation is that it could be an additional accordion mode from a longer or shorter molecular chain caused by irradiation damage that is only present in small amounts and found in small pockets in the material.

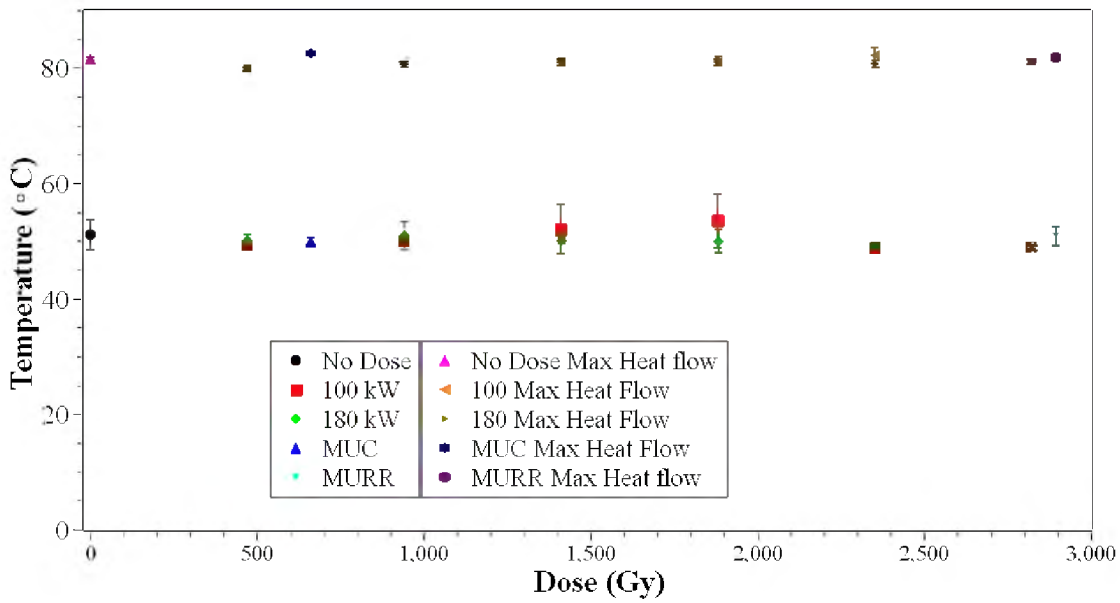

Figure 14 – Average Melting Temperature and Point of Maximum Heat Flow of PEW vs. Dose

Finally, there is no observed decrease in the magnitudes of all the peaks after irradiation. To evaluate this the intensity of the main peaks in polyethylene spectrum were peak fitted and their intensities were compared across irradiation. Figure 16 shows the average intensity of peaks 1065 cm^{-1}, 1132 cm^{-1}, 1460 cm^{-1}, 2884 cm^{-1} with a 90% confidence interval calculated with a student's t-distribution at each irradiation point. It can

be seen in Figure 16 that all of the error bars for the chosen peaks lie within the no dose error bars of that peak. The same is true for all the peaks in the Raman spectrum.

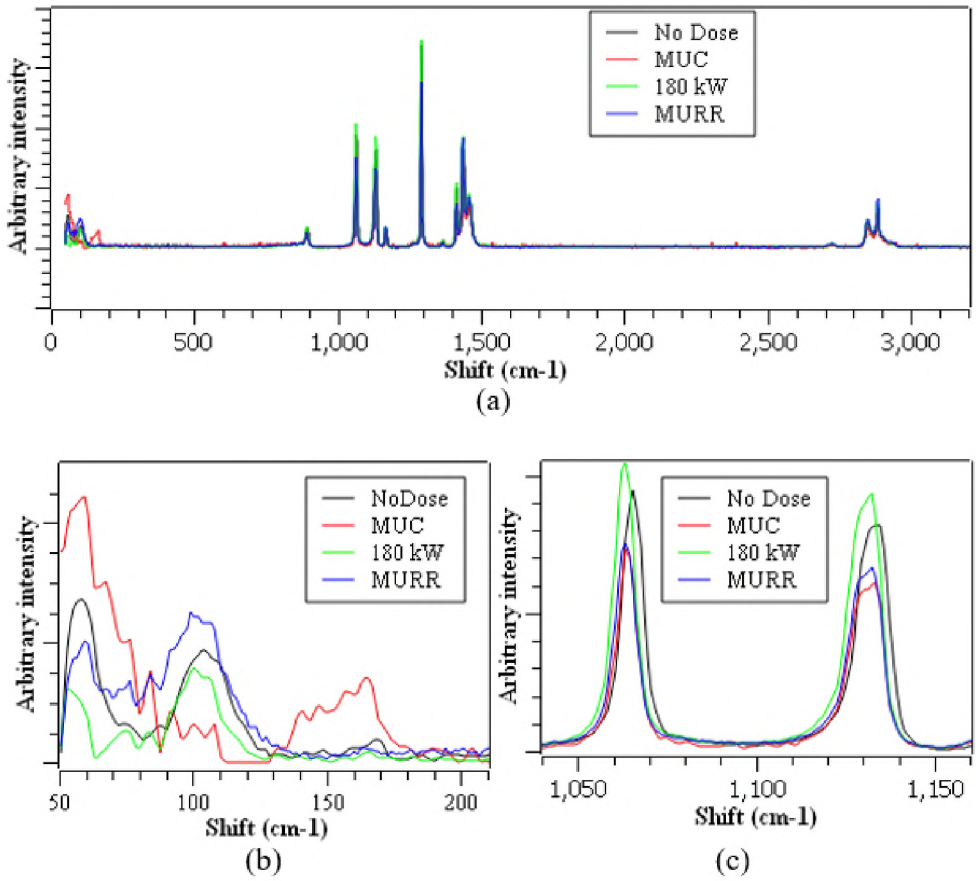

Figure 15 – Representative Raman Spectra of PEW with No Irradiation, Irradiation at MUC, Full 180kW Irradiation, and Irradiation at MURR (a) is the Full Spectrum (b) is Zoomed into the Peaks Between 50 and 220 cm^{-1} (c) is Zoomed into the Peaks Between 1040 and 1160 cm^{-1}

Between the lack of change in the Raman spectra and the minimal change in the latent heat with irradiation it seems that PEW is a good candidate for PCM applications in a nuclear environment. However, this paper was looking specifically at steam condensation. . Due to the wide melting peak of the PEW a significant portion of its latent

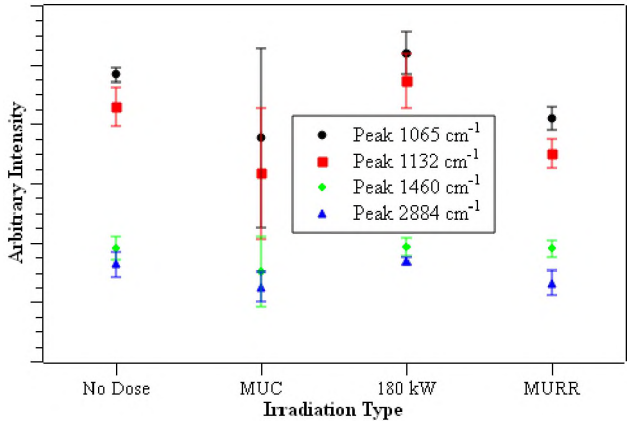

Figure 16 – Average Peak Intensities of Four Distinct PEW Peaks

latent heat would be used at the start of an accident scenario due to the temperature in the containment building. This would mean that active cooling would be required if PEW were to be used as a safety system in a nuclear reactor or that additional PCM would be required to compensate for the missing latent heat. Other materials may be better suited for this application such as Stearic acid which is a fatty acid that has a melting temperature of 69 °C and has a latent heat of 212 J/g. Further testing of both PEW and Stearic acid should be performed to confirm the results from this paper and to determine if the results hold true for other organic materials.

5. CONCLUSIONS

This paper has found that at neutron doses below 2894 Gy there is no observable change to the latent heat of fusion and melting temperature of PEW It was also found that the melting peak of PEW is too wide to be useful for passive steam condensation applications without an additional active cooling system or increasing the amount of PEW

to make up for the difference in latent heat. While this work has shown that PEW is less than ideal for a passive safety system for a nuclear reactor, it has shown that due to the negligible change in the thermal properties and Raman spectra that organic PCMs are still a promising solution. More work should be done to analyze a wider variety of organic PCMs and to further evaluate their performance at higher doses.

ACKNOWLEDGEMENTS

This paper is based upon work supported by the U.S. Nuclear Regulatory Commission, Nuclear Education Program under Award NRC -HQ-13-G-38-0026. The researchers would like to thank the staff at the Missouri University of Science and Technology Research Reactor and the staff at the University of Missouri Research Reactor for the use of their facilities as well as helping perform the experiments. We would also like to thank Dr. John Gahl with the University of Missouri for getting the reactor time at MURR and helping with the shipping and receiving of samples. Thermal characterization was performed using facilities of the Materials Research Center (MRC) located at the Missouri University of Science and Technology and special thanks to Dr. Eric Bohannan for help with the DSC measurements.

REFERENCES

[1] Kosny, J. and Yarbrough, D.W., 2008. Use of PCM-Enhanced Insulations in the Building Envelope (No. 5). Oak Ridge National Laboratory (ORNL); Building Technologies Research and Integration Center.

[2] Onofrei, Elena & Rocha, A. & Catarino, André. (2010). Textiles integrating PCMs-A review. Buletinul Institutului Politehnic din Iasi. Tom LVI (LX). 99-110.

[3] S. Nandakumar, M. Le Gallo, I. Boybat, B. Rajendran, A. Sebastian and E. Eleftheriou, "A phase-change memory model for neuromorphic computing", Journal of Applied Physics, vol. 124, no. 15, p. 152135, 2018. Available: 10.1063/1.5042408.

[4] Demirbas, M.F., 2006. Thermal energy storage and phase change materials: an overview.

[5] Maimon, J.D. et al. "Chalcogenide Memory Arrays: Characterization And Radiation Effects". IEEE Transactions on Nuclear Science 50.6 (2003): 1878-1884. Web.

[6] Union of Concerned Scientists, "Donald C. Cook Unit 2: Bridgeman, MI", 2000

[7] Westinghouse, "Westinghouse Technology Systems Manual Section 5.4 Containment Temperature, Pressure, and Combustible Gas Control Systems."

[8] O. Noori-Kalkhoran, A. Shirani and R. Ahangari, "Simulation of Containment Pressurization in a Large Break-Loss of Coolant Accident Using Single-Cell and Multicell Models and CONTAIN Code", *Nuclear Engineering and Technology*, vol. 48, no. 5, pp. 1140-1153, 2016. Available: 10.1016/j.net.2016.03.008

[9] K. Gillen, R. Clough and L. Jones, "Investigation of cable deterioration in the containment building of the Savannah River Nuclear Reactor", 1982. Available: 10.2172/7094253

[10] M. Brovchenko, B. Dechenaux, K. Burn, P. Console Camprini, I. Duhamel and A. Peron, "Neutron-gamma flux and dose calculations in a Pressurized Water Reactor (PWR)", EPJ Web of Conferences, vol. 153, p. 05008, 2017. Available: 10.1051/epjconf/201715305008

[11] G Fleischer A.S. (2015) Types of PCMs and Their Selection. In: Thermal Energy Storage Using Phase Change Materials. SpringerBriefs in Applied Sciences and Technology. Springer, Cham

[12] D. Zhou, C. Zhao and Y. Tian, "Review on thermal energy storage with phase change materials (PCMs) in building applications", Applied Energy, vol. 92, pp. 593-605, 2012. Available: 10.1016/j.apenergy.2011.08.025.

[13] M. herald and L.F. Cabeza, Heat and cold storage with PCM: An upto date introduction to basics and applications, Verlag Berlin Heidelberg: Springer, 2008

[14] M. Farid, A. Khudhair, S. Razack and S. Al-Hallaj, "A review on phase change energy storage: materials and applications", Energy Conversion and Management, vol. 45, no. 9-10, pp. 1597-1615, 2004. Available: 10.1016/j.enconman.2003.09.015.

[15] A. Solé, H. Neumann, S. Niedermaier, L. Cabeza and E. Palomo, "Thermal Stability Test of Sugar Alcohols as Phase Change Materials for Medium Temperature Energy Storage Application", Energy Procedia, vol. 48, pp. 436-439, 2014. Available: 10.1016/j.egypro.2014.02.051.

[16] R. Singh, S. Sadeghi and B. Shabani, "Thermal Conductivity Enhancement of Phase Change Materials for Low-Temperature Thermal Energy Storage Applications", Energies, vol. 12, no. 1, p. 75, 2018. Available: 10.3390/en12010075.

[17] Z. Qureshi, H. Ali and S. Khushnood, "Recent advances on thermal conductivity enhancement of phase change materials for energy storage system: A review", International Journal of Heat and Mass Transfer, vol. 127, pp. 838-856, 2018. Available: 10.1016/j.ijheatmasstransfer.2018.08.049.

[18] "Chemical Name Search", Webbook.nist.gov. [Online]. Available: https://webbook.nist.gov/chemistry/name-ser/.

[19] Georgia institute of Technology, "Radiation Effects on Organic Materials in Nuclear Plants", Electric Power Research Institute, 1981.

[20] A. Charlesby, "The cross-linking and degradation of paraffin chains by high-energy radiation", Proceedings of the Royal Society of London. Series A. Mathematical and Physical Sciences, vol. 222, no. 1148, pp. 60-74, 1954. Available: 10.1098/rspa.1954.0052.

[21] R. Saeed, J. Schlegel, C. Castano and R. Swafta, "Uncertainty of Thermal Characterization of Phase Change Material by Differential Scanning Calorimetry Analysis", International Journal of Engineering Research & Technology, vol. 5, no. 1, pp. 405-412, 2016.

[22] D. Lin-Vien, N. Colthup, W. Fateley and J. Grasselli, The Handbook of Infrared and Raman Characteristic Frequencies of Organic Molecules. San Diego: Academic Press, 1991.

[23] H. Abou Zeid, Z. Ali, T. Abdel Maksoud and R. Khafagy, "Structure-property behavior of polyethylene exposed to different types of radiation", Journal of Applied Polymer Science, vol. 75, no. 2, pp. 179-200, 2000. Available: 10.1002/(sici)1097-4628(20000110)75:2<179::aid-app1>3.0.co;2-b.

[24] C. Warren and D. Hooper, "Chain Length Determination of Fatty Acids by Raman Spectroscopy", Canadian Journal of Chemistry, vol. 51, no. 23, pp. 3901-3904, 1973. Available: 10.1139/v73-581

[25] Baker Hughes Incorporated, "POLYWAX Polyethylenes: Specialty Polymers and Waxes to meet your needs", 2011.

[26] Los Alamos Scientific Laboratory. Group X-6. MCNP : a General Monte Carlo Code for Neutron and Photon Transport. Los Alamos, N.M. : [Springfield, Va.] :Dept. of Energy, Los Alamos Scientific Laboratory ; [for sale by the National Technical Information Service], 1979.

[27] C. Algiere, "Chronomorphic characterization and radiolytic degradation analysis of polyurethane with monte carlo modeling of the neutron spectra surrounding age pettrace cyclotron", 2018. Available: https://hdl.handle.net/10355/66223.

[28] R. Berliner, "The university of Missouri Research Reactor (MURR)", Neutron News, vol. 2, no. 4, pp. 13-19, 1991. Available: 10.1080/10448639108218740.

II. NEUTRON AND GAMMA RADIATION EFFECTS ON THERMAL STORAGE PROPERTIES OF AN ORGANIC EUTECTIC PCM

ABSTRACT

NASA has recently started analyzing the effects of micro-gravity on a phase change material (PCM) heat exchanger that could be used on a mission to Mars. It is important that this heat exchanger can withstand the high levels of radiation expected with space travel. The effect of neutron and gamma radiation on two PCMs, a eutectic of methyl palmitate and lauric acid (EMPaLA) and EMPaLA with 10% by weight of graphene nanoplatelets (E-NP), are evaluated in this paper. Irradiation was performed in the Missouri University of Science and Technology Research Reactor (MSTR), the University of Missouri Cyclotron (MUC), and the University of Missouri Research Reactor (MURR). Doses that were achieved are on the order of 10^3 Gy which is approximately what is expected on a mission to Mars. This research found that while there was some scatter in the data, overall, there was no significant change in the latent heat of the PCMs. Raman spectra were also obtained from the PCMs and it showed that there was no significant change in the bonding within the material further proving that there was no change in the material. This lends credibility to the radiation resistance of organic PCMs over the dose ranges expected on a mission to Mars. Further work should be done to assure that the results from this paper are also applicable to the high energy protons and ions expected from Galactic Cosmic Rays.

1. INTRODUCTION

Phase change materials (PCMs) can store and release large amounts of thermal energy at a nearly constant temperature by utilizing the latent heat of a phase change. This unique property is used in many applications including enhanced building insulation, temperature regulating textiles, and for energy storage[1-4]. In addition, PCMs are used as a safety system in nuclear reactors in the form of ice condensers and have shown potential for neurons in a neural network [5-6]. PCMs have also been an important addition to many NASA applications including space suits [7]. Recently NASA has been developing a PCM heat exchanger for use on spacecraft for missions to Mars and is currently testing one on the international space station [8]. The heat exchanger absorbs excess heat during high temperature periods and releases the energy at lower temperature periods. This helps to load-shift the periods of higher demand on the spacecraft's radiator system, allowing it to be designed for conditions closer to the average load rather than the maximum. This in turn reduces the size and weight of the radiator for launch. The current test system is designed to accept almost any type of PCM; however, they are only testing Paraffin wax at this time. The current tests are being used to determine how the system works in low gravity

The ideal properties for a PCM for this system would have a latent heat of fusion of greater than 170 J/g and a melting temperature range between 20-25 °C. These values are based off the current tests that NASA is performing with paraffin wax. The latent heat must be greater than 170 J/g because weight is a very large concern for missions in space. If the latent heat is larger then the overall weight of the heat exchanger goes down. The melting temperature range should be between 20-25 °C to keep the spacecraft near room

temperature. As will be discussed in the background the ideal PCM for this application is Organic PCMs. The effect that radiation has on the latent heat of organic materials is not well documented and significant changes with radiation damage could reduce the ability of the PCM to properly store and release the heat in a spacecraft. As is well known there is a significant amount of radiation in space in the form of cosmic rays [9] that could become problematic for a PCM that does not withstand radiation well over the doses experienced during the length of a mission. The goal of this paper is to evaluate the effect that radiation has on the latent heat of a eutectic of Methyl Palmitate and Lauric acid which has ideal properties for room temperature applications.

2. BACKGROUND

2.1. RADIATION ENVIRONMENT IN SPACE

The radiation in space comes from two main sources: the sun and galactic cosmic rays (GCR). The radiation from the sun typically occurs during solar flares where high energy protons are emitted [9]. GCR are much more constant than the suns radiation and come in the form of protons and heavy nuclei. Additionally, Since the primary goal for a PCM heat exchanger is a mission to Mars, there is an increased radiation dose on the surface of Mars compared to earth due to its thinner atmosphere and lack of a magnetic field. This all adds up to large radiation doses to the crew and equipment for a mission to Mars. Current estimates expect that radiation doses could accumulate to the order of 1×10^3 Gy over the course of a mission [10]. It is therefore necessary to make sure that any materials that are on that mission will maintain their ability to perform through doses up to

that limit. Additionally, solar flares and other sources of unpredictable radiation dose are a concern for the materials. These doses are not going to be tested in this paper but will need to be researched in the future if these materials are resilient under the doses tested in this paper.

2.2. PHASE CHANGE MATERIALS

PCMs are materials that have a large latent heat that allows them to absorb a significant amount of energy at a phase transition temperature. There are three main types of PCMs which include organic, inorganic, and eutectic. Organic PCMs consist of paraffins, fatty acids, polymers, and sugar alcohols. Inorganic PCMs consist of salt hydrates, salts, and metals. Eutectic PCMs are any two or more PCMs that are mixed in a particular ratio that they melt and solidify at the same temperature [11-12]. In our current study salt hydrates, paraffins, and fatty acids have the ideal melting temperature [13]. Salt hydrates, while having the highest latent heat, degrade over time due to phase separation [14]. Paraffins and fatty acids do not degrade over time but do suffer from having a low thermal conductivity, on the order of 0.01 W/cm-K [15-16]. For more information on PCMs see previous work [17]. The major difference between paraffins and fatty acids are that fatty acids have a carboxyl group somewhere in their chain. Both paraffins and fatty acids melting temperature and latent heat are affected by their chain length. Fatty acids melting temperature and latent heat are also affected by where their functional group is located and whether they are saturated (all C-C bonds are single bonds) or unsaturated (some C=C double bonds are present).

It was determined that an organic PCM as either a paraffin or fatty acid was the best option for room temperature applications in space craft due to having the appropriate melting temperature, high latent heat, and not having to worry about phase separation. As mentioned the main disadvantage of organic PCMs is a low thermal conductivity which has the potential to limit the amount of heat that it can absorb due to self-shielding however in practical applications this could be alleviated by the design of fins into the material or the addition of nanoparticles [15-16]. In addition, radiation effects on latent heat of organic materials is not well known.

As mentioned before Paraffins melting temperature and latent heat are dependent on their chain lengths which can be seen in Figure 1 [18]. Some examples of fatty acids can be seen in Table 1 [18]. Table 1 shows that even minor modifications in the molecular structure of the material yields significantly different latent heats and melting temperatures. Due to the fact that radiation damage can change the molecular structure of organic molecules its quite possible that significant changes in the latent heat and melting temperature could occur.

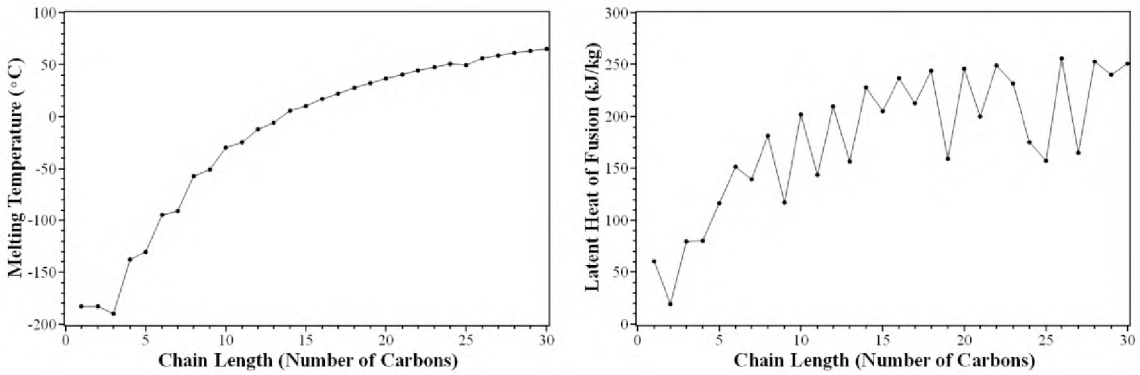

Figure 1 – Melting temperature (Left) and Latent heat (Right) of Paraffins with Different Chain Lengths [18]

Table 1 – Examples of Fatty Acid PCMs and their Melting Properties [18]

Name	Chemical Formula	Melting Temp (°C)	Latent Heat (kJ/kg)
Methyl Palmitate	$C_{17}H_{34}O_2$	32.3	207
Heptadecanoic Acid	$C_{17}H_{34}O_2$	60.2	171
Palmitic Acid	$C_{16}H_{32}O_2$	61.0	210
Lauric Acid	$C_{12}H_{24}O_2$	43.9	181
Stearic acid	$C_{18}H_{36}O_2$	69.3	212
Oleic acid	$C_{18}H_{34}O_2$	13.3	140

Table 2 shows the melting temperature, latent heat, and thermal conductivity of a eutectic of Methyl Palmitate and Lauric Acid (EMPaLA) developed by Saeed et. al [19]. This eutectic was developed for room temperature applications and has a gelling agent at 10% by weight of 2-hydroxypropyl ether cellulose. The gelling agent was introduced to have the phase transition go from solid to gel rather than solid to liquid. This helps to prevent leakage of the PCM in the melt phase. Saeed et. al. also tested EMPaLA with 10% by weight graphene nanoplatelets (E-NP) which the values for can also be seen in Table 2. As can be seen the E-NP has a thermal conductivity that is 100% higher than EMPaLA which makes up for the displaced latent heat. It was also found that the nanoplatelets considerably increased the sensible heat that the material could absorb in areas around that melting temperature [19]. These PCMs should be ideal for room temperature applications on a space craft and will be what is tested for radiation resistance.

Table 2 – Eutectic of Methyl Palmitate and Lauric Acid [19]

Name	Melting Temp (°C)	Latent Heat (kJ/kg)	Thermal Conductivity (W/m-K)
EMPaLA	24.06	177.9	0.17
E-NP	24.29	165.6	0.34

2.3. RADIATION DAMAGE IN ORGANIC MATERIALS

The three main radiation effects in organic materials include scission, crosslinking, and oxidation. A scission occurs when radiation causes a C-C bond to break creating two separate chains each with a free radical. A crosslink occurs when two carbon free radicals from separate chains bond to each other. Oxidation occurs when a carbon free radical bonds with oxygen in the air. Figure 2 shows visualizations of these effects [20].

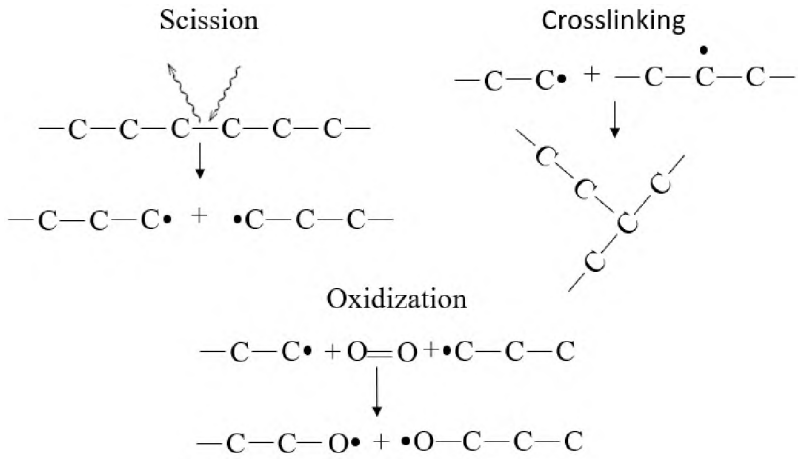

Figure 2 – Visualization of the Main Radiation Damage Mechanisms

Each of these primary mechanisms occur throughout the material however they do have places that they occur most. Scissions occur throughout the material with more occurring where the radiation source is more intense. Oxidation and crosslinking are competing effects as they both require free radicals to occur. Typically, oxidation occurs most on the surface of the material and decreases with depth due to the slow diffusion of oxygen in the materials. Crosslinking occurs more in the center of the material as it does not have to compete with oxygen for the free radicals. If the dose rate is lower oxidation occurs deeper in the material as oxygen has a longer time to diffuse into the material [20].

It has also been found that mechanical stress and temperature can increase or decrease the amount of damage is done in the material and how often a particular type of mechanism occurs.

Scissions cause a decrease in molecular weight of the material which can create gases in the form of small chain hydrocarbons and diatomic hydrogen. In addition, to gas formation it can decrease many mechanical properties such as the Young's modulus, tensile strength, hardness, and elasticity. It can also increase the solubility and elongation of the material. Due to having a decreased molecular weight it is also noted that the melting temperature can decrease [21].

Crosslinking increases the molecular weight of the material and therefore typically has opposite effects as scission meaning the mechanical properties increase or decrease opposite of scissions. Gas formation is still prevalent in the material as it requires losing hydrogen bonds or creating scissions to crosslink. Crosslinking has been shown to cause an increase in melting temperatures and to create a gel like substance that does not melt [20,21].

Oxidation in general yields the same effects that scissions create. This is due to the fact that the free radicals created by the scissions are taken by oxygen instead of by crosslinking. In materials where oxidation is more prevalent than crosslinking the mechanical properties decrease significantly [21].

With this information there is a significant gap in the current literature about the effects of radiation on the latent heat of an organic material. Since latent heat is one of the most important aspects of a PCM it is imperative to know these effects and to be able to predict them if they are to be used in a space craft. As previously mentioned EMPaLA and

E-NP should have ideal properties for this application and will be the PCMs that is tested in this work. For more information on damage mechanisms in organic molecules please see previous work [17].

2.4. MEASUREMENT TECHNIQUES

Differential Scanning Calorimetry (DSC) is used to measure thermal properties of materials [22]. It will be used to obtain information about the latent heat an melting temperature of both the EMPaLA and E-NP using the a similar process as in previous work [17].

Raman spectroscopy uses a laser to excite the molecular bonds in a material and detects the inelastically scattered photons to determine the molecular structure and bonds. The Raman shift for many types of bonds in various molecules are already determined [23]. Figure 3 shows an example spectrum of (a) Methyl Palmitate (b) Lauric Acid (c) Hydroxypropyl Ether Cellulose [24].

As can be seen in Figure 3 the main peaks for each spectrum are labeled with what type of molecular bond and motion it is attributed to [25-28]. The most important peaks for this work are those of the methyl palmitate and lauric acid. This is due to the fact that the main contribution to latent heat is from these molecules. Analysis will focus on these peaks more in depth.

It has been shown that the Raman spectra of Polyethylene irradiated by fast neutrons has several changes such as new peak formation, merging of certain peaks and a decrease in the overall intensities of the peaks [28]. While EMPaLA and E-NP will not

behave the exact same under these conditions similar changes could be expected and will be examined for in the analysis.

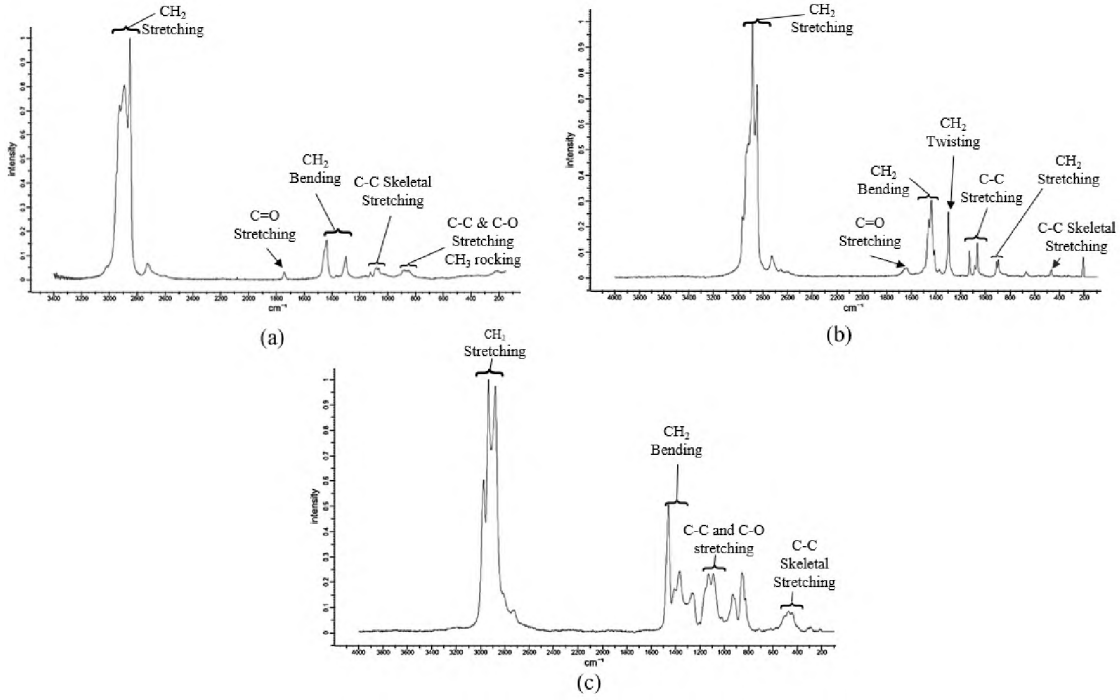

Figure 3 – Example Raman Spectrum EMPaLA Components (a) Methyl Palmitate (b) Lauric Acid and (c) 2-Hydroxypropyl Ether Cellulose [24]

It has also been found that low Raman shift peaks (<500 cm^{-1}) in the Raman spectra of paraffins and fatty acids can be used to determine the approximate chain length of organic compounds due to the accordion motion of long carbon chains [29]. This effect will be looked for in the current work to determine if there was a significant change in the chain lengths of the material.

3. MATERIALS AND METHODS

3.1. EMPaLA AND E-NP

EMPaLA was supplied by Phase Change Energy Solutions. As described in the introduction, EMPaLA is a eutectic of methyl palmitate and lauric acid in a ratio of 60/40, respectively, with a 10% addition by weight of 2-hydroxypropyl which acts as a gelling agent [19]. Methyl palmitate has a melting temperature of 29.6°C and a latent heat of 227 kJ/kg. Lauric acid has a melting temperature of 44.1 °C and a latent heat of 185.5 kJ/kg. When mixed at their eutectic point, they have a melting temperature of 25.6 °C and a latent heat of 205 kJ/kg. When the 2-hydroxypropyl ether cellulose is added to the eutectic mixture, the melting temperature becomes 24°C with a latent heat of 177.9 kJ/kg [19].

Graphene nanoplatelets were supplied by Angstorn. They have a thickness of 10 nm and a width of < 5μm. These particular graphene nanoplatelets were chosen because they have been used with EMPaLA in the past [19]. A 10% by weight addition of nanoplatelets was mixed into EMPaLA.

3.2. DIFFERENTIAL SCANNING CALORIMETER

The DSC instrument used for the melting temperature and latent heat measurements was a TA Instruments DSC 2010 Differential Scanning Calorimeter. The instrument was calibrated using tin, lead, and indium standards. The temperature accuracy, temperature reproducibility, maximum sensitivity and calorimetric precision are ±0.1°C, ±0.05°C, 1μW, and ±0.1% respectively. The samples and DSC were cooled to below 0 °C using liquid nitrogen. A heating rate of 1 °C/min was used up to a temperature of 45 °C.

Aluminum pans with lids from DSC Consumables were used as the sample pans. Thermographic analysis was performed using TA Universal analysis software.

The EMPaLA received had a measured melting temperature of 22.5 °C and a latent heat of 201 kJ/kg. The difference in these properties is likely due to a difference in heating rate between the work done to develop it and this paper. The resulting mixture E-NP resulted in a melting temperature of 21°C and latent heat of 185 J/g.

3.3. RAMAN SPECTROSCOPY

Raman spectra were acquired using a Horiba XploRA Plus confocal Raman microscope with a laser wavelength of 785 nm and a maximum resolution of <1.2 cm^{-1} FWHM. Calibration was performed with a (111) Si standard. For the measurements in this work, the grating was set to 1200 mm^{-1}. Each spectrum was averaged over five 60-second acquisitions. Post processing of the data was performed using the acquisition software, LabSpec6, and spectrum analysis tool Fityk. The noise was reduced using a moving average filter in the LabSpec6 software. Background estimation and removal was performed by Fityk. The background was estimated using a piecewise interpolation function and each of the points were chosen specifically for each spectrum. Spectrum normalization and peak fitting were also performed using the Fityk software. The normalization was such that the areas under the spectra were set to one. Peak fitting was performed using a Pearson VII function.

3.4. RADIATION SOURCES

3.4.1. MSTR. Previous research by this group on the radiation effects of latent heat on polyethylene characterized the flux of the MSTR. It was found that the flux of the reactor in the irradiation location used was 3.26×10^{12} n/cm^2-s at 50% power and 5.42×10^{12} n/cm^2-s at 80% power. From the measured dose and simulated neutron spectra, estimated dose rates were 0.78 Gy/s and 1.3Gy/s at 50% and 80% power respectively. Additional details are provided in the previous work [17].

The experiments were carried out with four batches of EMPaLA and E-NP. Two batches of each sample were irradiated at 100 kW and the remaining two batches were irradiated at 180 kW. Table 3 shows the irradiation times, accumulated irradiation time, accumulated fluence and total dose of the samples irradiated at 180 kW and 100 kW. After each irradiation was complete the samples were left to decay in the reactor for one week. After the cooling period ended, the PCMs were melted, and three small samples were extracted from each batch and placed in DSC measurement pans. The remaining PCM was returned to the reactor for the next set of irradiations.

Given that the total dose in the MSTR reactor is 2820 Gy it shows that the experiments carried out here are of the same order of magnitude as what the PCM would be exposed to during a mission.

3.4.2. MUC. The cyclotron used at The University of Missouri is a GE PETtrace Radiotracer cyclotron. The typical use for this cyclotron is the production of the medical isotope Flourine-18 which is produced by accelerating protons into Oxygen-18. The (p,n) reaction used to produce Fluorine-18 yields a high energy neutron with energy on the order of 10 MeV. The target is surrounded by neutron irradiation locations [30]. Samples of

EMPaLA were irradiated to a 1 MeV equivalent fluence of 10.1×10^{14} n/cm^{2}corresponding to a dose of approximately 662 Gy or about half of the expected dose encountered on a Mars mission.

Table 3 – MSTR Irradiation Information

Irradiation #	**1**	**2**	**3**	**4**	**5**	**6**
180 kW – Flux: 5.42×10^{12} (n/cm^2-s)						
Irradiation time (min)	6	6	6	6	6	6
Accumulated Radiation Time (min)	6	12	18	24	30	36
Accumulated Fluence ($\times10^{15}$ n/cm^2)	1.95	3.90	5.85	7.80	9.75	11.70
Total Dose (Gy)	470	940	1410	1880	2350	2820
100 kW – Flux: 3.26×10^{12} (n/cm^2-s)						
Irradiation time (min)	10	10	10	10	10	10
Accumulated Radiation Time (min)	10	20	30	40	50	60
Accumulated Fluence ($\times10^{15}$ n/cm^2)	1.95	3.90	5.85	7.80	9.75	11.70
Total Dose (Gy)	470	940	1410	1880	2350	2820

3.4.4. MURR. While at full power, MURR operates at 10 MW and has a maximum neutron flux of 6×10^{14} n/cm^2-s in the Flux trap where the samples were irradiated [31]. For EMPaLA and E-NP this equates to a dose rate of approximately 144 Gy/s. Irradiation of EMPaLA was performed for 20 seconds which is a total dose of approximately 2895 Gy. This dose is on the same order of magnitude as a mission to Mars.

4. RESULTS AND DISCUSSION

4.1. DSC

Figure 4 (a) and (c) show representative DSC thermographs for the EMPaLA samples irradiated at 50% power and 90% power, respectively. Figure 4 (b) and (d) show the integral of the DSC corresponding thermographs and shows how the latent heat develops over temperature. Figure 4 (e) and (f) show representative thermographs and their integrals, respectively, for the samples irradiated at MUC and MURR. Figure 5 (a) and (c) show representative DSC thermographs for the E-NP samples irradiated at 50% power and 90% power respectively. Figure 5 (b) and (d) show the integral of the corresponding DSC thermographs and shows how the latent heat develops over temperature. For the irradiations at MSTR, a total of six DSC samples were evaluated for each irradiation (three from each irradiation batch). Two and three DSC samples were evaluated from the MURR and MUC data respectively. Evaluation of the thermographs show that there is very little change in the shape of the curves between the irradiated PCM and unirradiated PCM and that the material has a melting peak that spans from around 20°C to 29°C. The latent heat develops the same throughout every measurement except for the irradiations at MURR where the maximum latent heat is significantly lower than the rest of the measurements.

Figure 6 (a) and (b) shows the average latent heat of fusion with a 90% confidence interval evaluated using a Student's t-distribution of the EMPaLA and E-NP respectively. This confidence interval takes into consideration the error associated with the DSC and propagates it through the standard deviation using Equation 1:

$$CI = \bar{\varepsilon} + \frac{t}{\sqrt{S}} s \left(1 + \frac{\sum_i^N (\varepsilon_i + \bar{\varepsilon})(x_i - \bar{x})}{\sum_i^N (x_i - \bar{x})^2} \right) \quad (1)$$

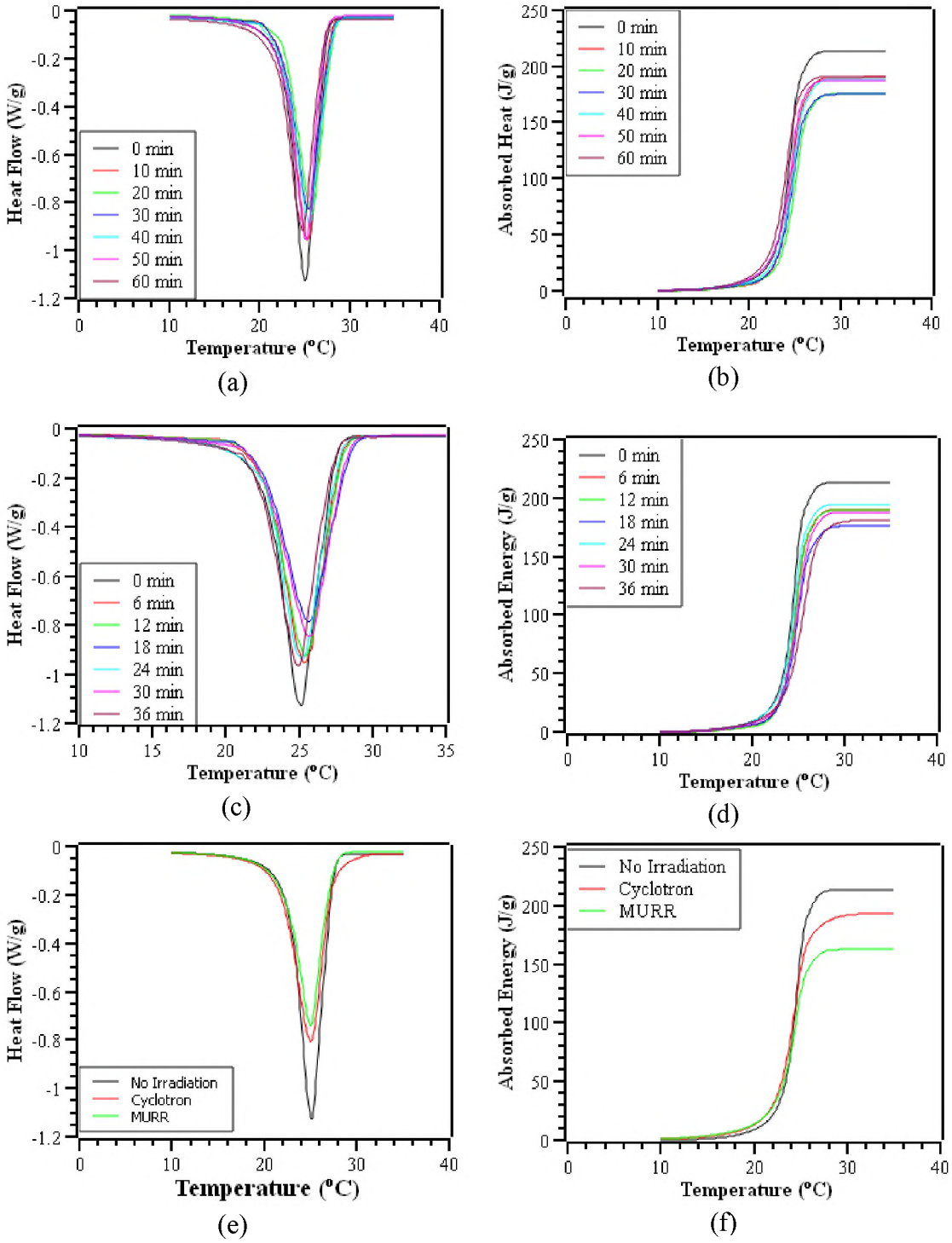

Figure 4 – Representative DSC Thermographs for EMPaLA for each Irradiation and their Integrals (a) Samples Irradiated at 100 kW (b) Integral of Samples Irradiated 100 kW (c) Samples Irradiated at 180 kW (d) Integral of Samples Irradiated at 180 kW (e) Samples Irradiated at MUC and MURR. (f) Integral of Samples Irradiated at MUC and MURR

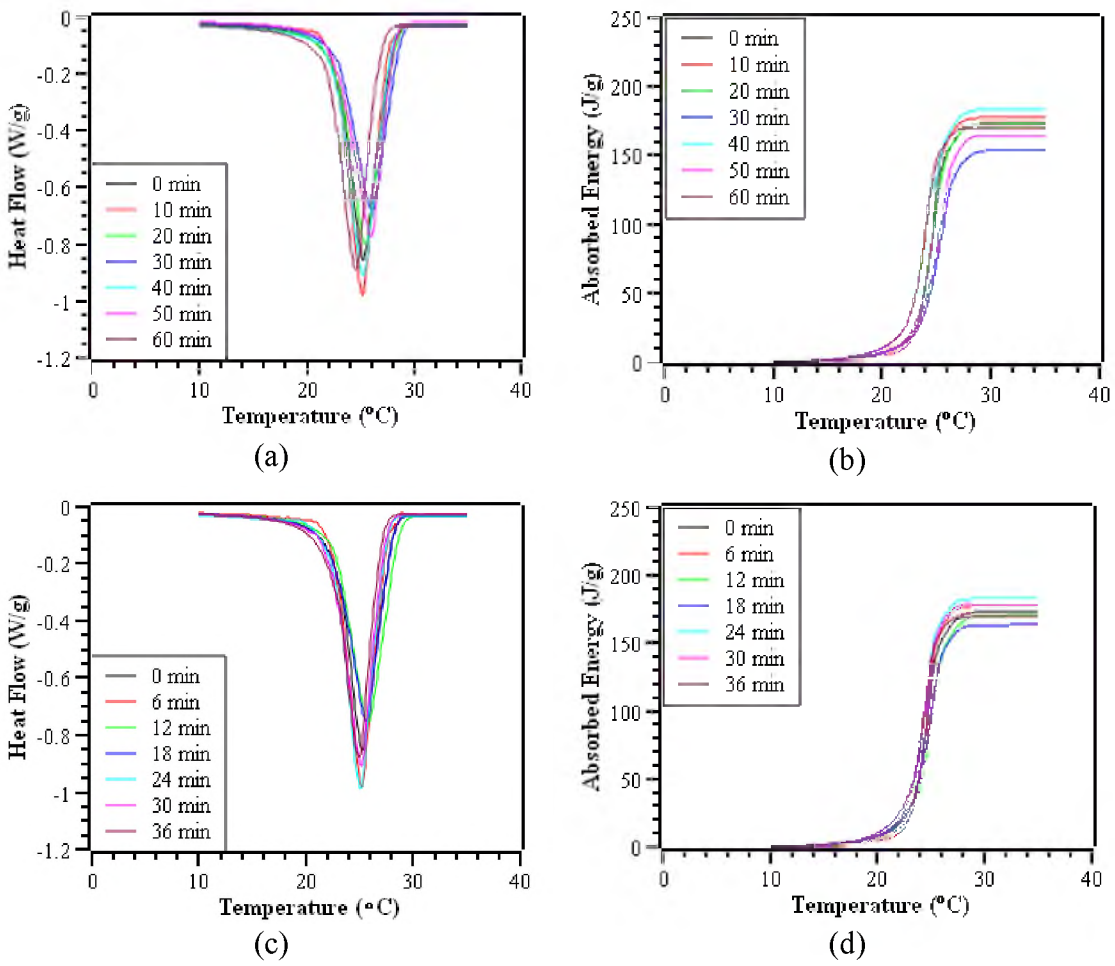

Figure 5 – Representative DSC Thermographs for E-NP for each Irradiation and their Integrals (a) Samples Irradiated at 100 kW (b) Integral of Samples Irradiated 100 kW (c) Samples Irradiated at 180 kW (d) Integral of Samples Irradiated at 180 kW

where CI is the confidence interval, $\bar{\varepsilon}$ is the average error from the DSC measurement, t is the t-value from the students t distribution, S is the number of data points, s is the standard deviation, ε_i is the DSC error from a particular measurement i, x_i is the latent heat of a particular measurement i, and $\bar{x}$ is the average latent heat.

As can be seen in Figure 6 the 90% confidence interval error bars on some of the latent heat data overlap with the unirradiated data error bars indicating that there was no significant change for those samples. The exceptions to this for EMPaLA have differences

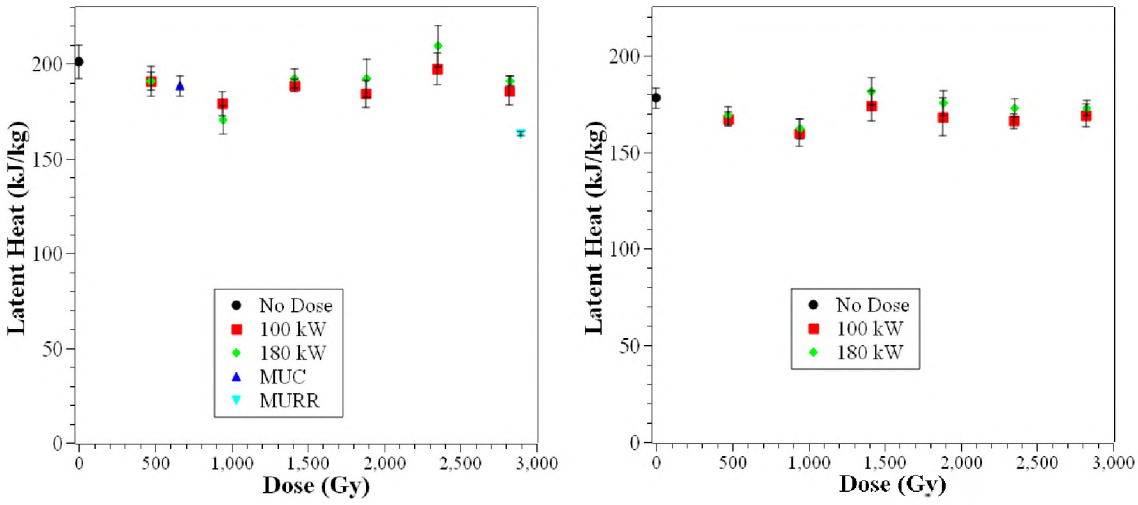

Figure 6 – Average Latent Heat of Fusion of (a) EMPaLA and (b) E-NP vs. Dose

between 6.1 and 18.8% and for E-NP its between 6.1 and 10.1% when compared to the 0-dose measurements.These measurements have error bars that are very close to the 0-dose measurement and are likely not a significant change in the material. The changes could be from heterogeneities in the sample or other factors. It is important this helps to lend some credibility to the radiation resistance of EMPaLA and E-NP for a Mars mission. Further analysis of these materials in higher radiation fields may be necessary for unpredictable radiation events on a mission.

Figure 7 (a) and (b) shows the average melting temperature of EMPaLA and E-NP respectively with a 90% confidence interval calculated using a Student's t-distribution. It can be seen that several of the measurements for both EMPaLA and E-NP are outside the 0-dose melting temperature error bars. The maximum error in these values are 3.8% or 0.38 °C. This change is negligible and is in agreement with the literature because of the relatively low doses that were used in these experiments compared to others. It should be noted that the data at MURR and MUC for EMPaLA significantly wider error bars than

the rest of the data. This is due to only having two DSC measurements for MURR and three DSC measurements at MUC because only a small amount of EMPaLA could be irradiated at each of the facilities.

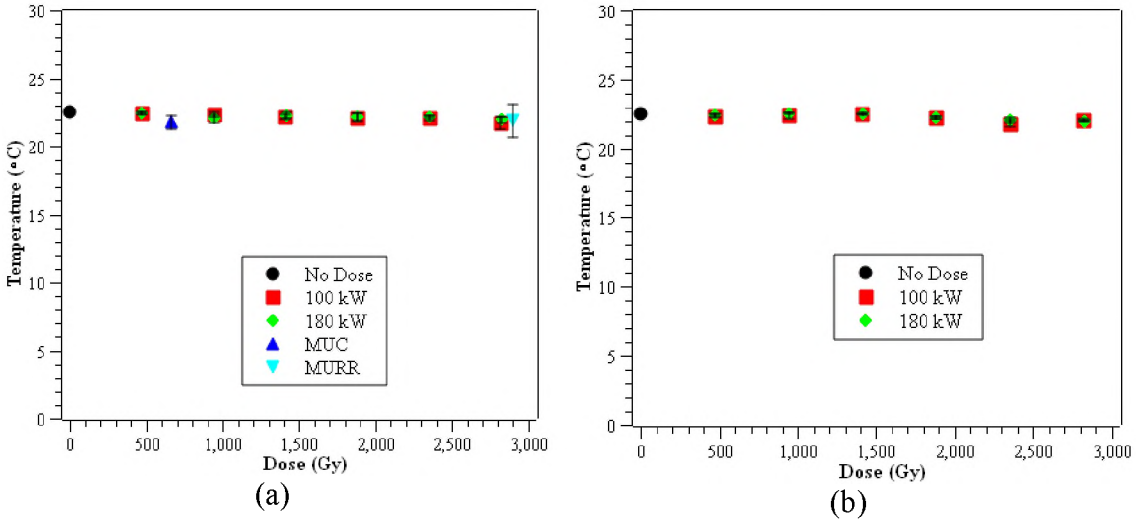

Figure 7 – Average Melting Temperature of (a) EMPaLA and (b) E-NP vs. Dose

4.2. RAMAN SPECTROSCOPY

Raman Spectroscopy was performed in an attempt to confirm the conclusion that there was no significant change EMPaLA after irradiation by analyzing the molecular bond structure. Figure 8 (a) shows representative Raman spectra taken for EMPaLA at no dose, the 6th irradiation at 180kw, MUC and MURR. As previously discussed the main changes that are being looked for is the creation of new peaks, shifting of peaks below 500 cm^{-1}, and lowered intensities across all peaks. Figure 8 (a) shows that there are no new peaks in any of the spectra. Figure 8 (b) zooms into the Raman shift spectra below 600 cm^{-1}. It can be seen that there are peaks in this area that are of the low Raman shift expected from the accordion modes but there is no shift in the peaks. Figure 9 (c) zooms in on the peaks

between 800 and 1800 cm^{-1}.It can be seen that there again are no additional peaks between these points and that there is no shift in the peak locations.

Finally, radiation damage in the material is supposed to decrease the magnitude of all the peaks. To evaluate this the intensity of the main peaks in in the EMPaLA spectrum were peak fitted and their intensities were compared across irradiation. Figure 10 shows the average intensity of peaks with a 90% confidence interval calculated with a student's t-distribution at each irradiation point. The peaks chosen for this graph were 127 cm^{-1}, 1197 cm^{-1}, 1296 cm^{-1}, and 1459 cm^{-1}. It can be seen in Figure 9 that all of the error bars for the chosen peaks lie within the no dose error bars of that peak. The same is true for all the peaks in the Raman specta.

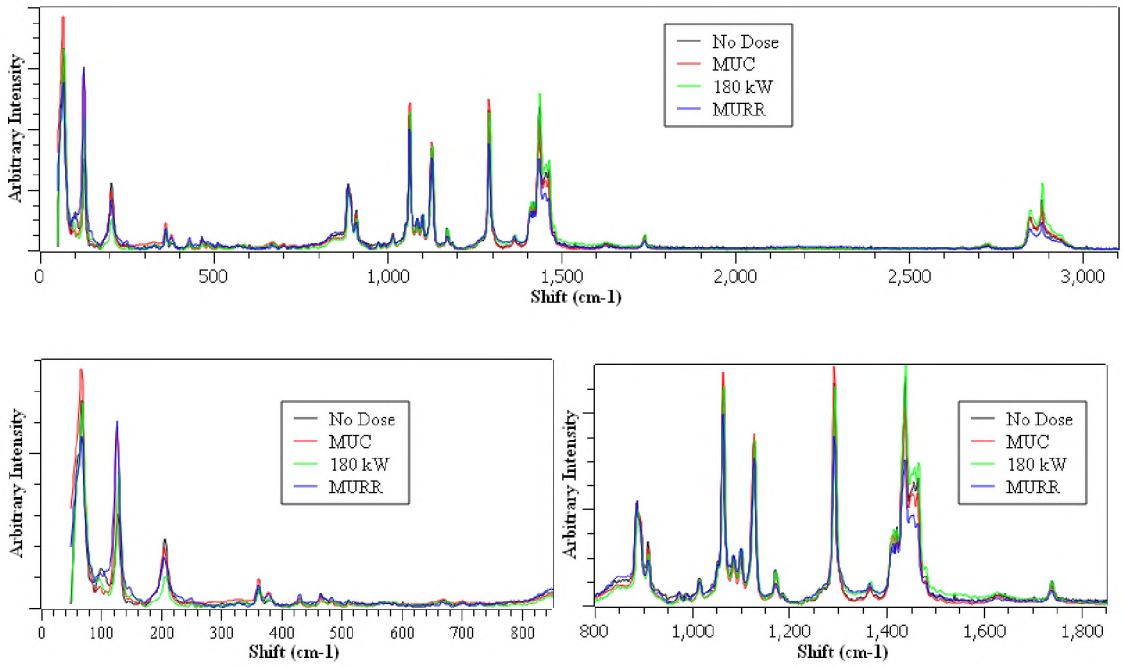

Figure 8 – Representative Raman Spectra of EMPaLA with No Irradiation, Irradiation at MUC, full 180kW Irradiation, and Irradiation at MURR (a) is the Full Spectrum (b) is Zoomed into the Peaks at the Start of the Spectra Between 50 and 220 cm^{-1} (c) is Zoomed into the Peaks Between 1040 and 1160 cm^{-1}

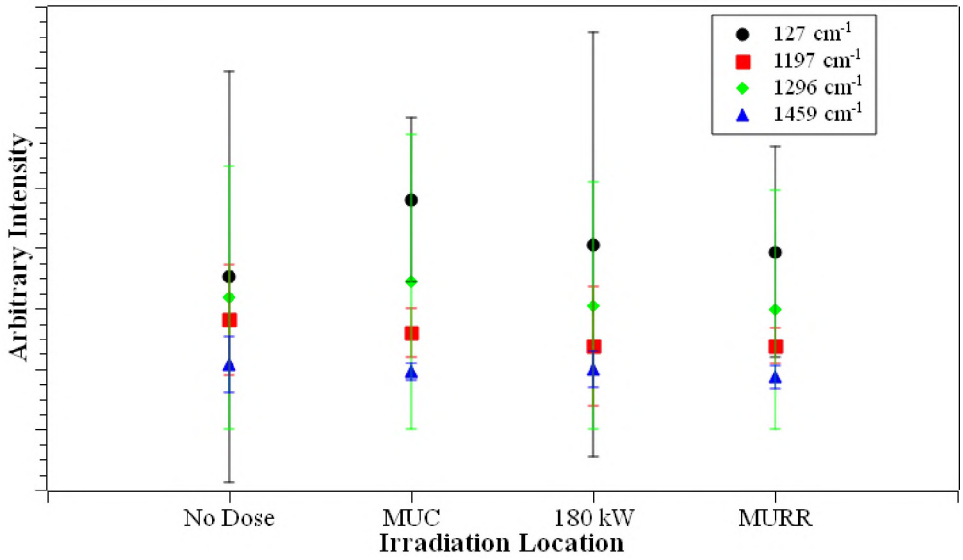

Figure 9 – Average Peak Intensities of Four Distinct EMPaLA Peaks

The lack of change in the Raman spectra indicates that there is minimal change in the bond structure of the EMPaLA. Between the Raman spectra being unchanged and the lack of change in the latent heat lends some credibility of EMPaLA or E-NP to be used for a mission to Mars. Future work would be to make sure the results are true for radiation damage caused by the energetic protons and heavy ions associated with GCR. In addition, these materials should be tested at higher dose to help predict what changes may occur during a solar flare or other cosmic radiation event.

5. CONCLUSIONS

The latent heat and melting temperature of EMPaLA and E-NP were found to be stable (within 20%) when exposed to neutrons from a nuclear reactor up to a dose of ~3 kGy. These doses are comparable to the estimated doses expected on a Mars mission.

Failure to observe a significant change in the properties with radiation dose lends credibility to these materials being used in a mission to Mars. Further work should be done to make sure that the radiation damage from high energy protons and heavy ions do not change these results. It may be necessary to test these materials under higher doses in the event of a solar flare or other unexpected radiation exposure.

ACKNOWLEDGEMENTS

This paper is based upon work supported by the U.S. Nuclear Regulatory Commission, Nuclear Education Program under Award NRC-HQ-13-G-38-0026. The researchers would like to thank the staff at the Missouri University of Science and Technology Research Reactor and the staff at the University of Missouri Research Reactor for the use of their facilities as well as helping perform the experiments. We would also like to thank Dr. John Gahl with the University of Missouri for getting the reactor time at MURR and helping with the shipping and receiving of samples. Thermal characterization was performed using facilities of the Materials Research Center (MRC) located at the Missouri University of Science and Technology and special thanks to Dr. Eric Bohannan for help with the DSC measurements.

REFERENCES

[1] Kosny, J. and Yarbrough, D.W., 2008. Use of PCM-Enhanced Insulations in the Building Envelope (No. 5). Oak Ridge National Laboratory (ORNL); Building Technologies Research and Integration Center.

[2] Onofrei, Elena & Rocha, A. & Catarino, André. (2010). Textiles integrating PCMs-A review. Buletinul Institutului Politehnic din Iasi. Tom LVI (LX). 99-110.

[3] S. Nandakumar, M. Le Gallo, I. Boybat, B. Rajendran, A. Sebastian and E. Eleftheriou, "A phase-change memory model for neuromorphic computing", Journal of Applied Physics, vol. 124, no. 15, p. 152135, 2018. Available: 10.1063/1.5042408.

[4] Maimon, J.D. et al. "Chalcogenide Memory Arrays: Characterization And Radiation Effects". IEEE Transactions on Nuclear Science 50.6 (2003): 1878-1884. Web.

[5] Demirbas, M.F., 2006. Thermal energy storage and phase change materials: an overview.

[6] Union of Concerned Scientists, "Donald C. Cook Unit 2: Bridgeman, MI", 2000

[7] L. Trevino and E. Orndoff, "Advanced Space Suit Insulation Feasibility Study", SAE Technical Paper Series, 2000. Available: 10.4271/2000-01-2479

[8] "NASA to Begin Testing Next Generation of Spacecraft Heat Exchangers", NASA, 2016. [Online]. Available: https://www.nasa.gov/feature/nasa-to-0-begin-testing-next-generation-of-spacecraft-heat-exchangers.

[9] L. Simonsen and C. Zeitlin, "Mars Radiation Environment- what have we learned?", Briefing to NAC HEO/SMD Joint Committee Meeting, 2017.

[10] R. Maurer, M. Fraeman, M. Martin and D. Roth, "Harsh Environments: Space Radiation Environment, Effects, and Mitigation", Johns Hopkins APL Technical Digest, vol. 28, no. 1, pp. 17-29, 2008.

[11] G Fleischer A.S. (2015) Types of PCMs and Their Selection. In: Thermal Energy Storage Using Phase Change Materials. SpringerBriefs in Applied Sciences and Technology. Springer, Cham

[12] D. Zhou, C. Zhao and Y. Tian, "Review on thermal energy storage with phase change materials (PCMs) in building applications", Applied Energy, vol. 92, pp. 593-605, 2012. Available: 10.1016/j.apenergy.2011.08.025.

[13] M. herald and L.F. Cabeza, Heat and cold storage with PCM: An up to date introduction to basics and applications, Verlag Berlin Heidelberg: Springer, 2008

[14] M. Farid, A. Khudhair, S. Razack and S. Al-Hallaj, "A review on phase change energy storage: materials and applications", Energy Conversion and Management, vol. 45, no. 9-10, pp. 1597-1615, 2004. Available: 10.1016/j.enconman.2003.09.015.

[15] R. Singh, S. Sadeghi and B. Shabani, "Thermal Conductivity Enhancement of Phase Change Materials for Low-Temperature Thermal Energy Storage Applications", Energies, vol. 12, no. 1, p. 75, 2018. Available: 10.3390/en12010075.

[16] Z. Qureshi, H. Ali and S. Khushnood, "Recent advances on thermal conductivity enhancement of phase change materials for energy storage system: A review", International Journal of Heat and Mass Transfer, vol. 127, pp. 838-856, 2018. Available: 10.1016/j.ijheatmasstransfer.2018.08.049.

[17] R. Steere, et al. (2021) " Radiation Effects on Thermal Storage Properties of Polyethylene Wax". Under Review

[18] "Chemical Name Search", Webbook.nist.gov. [Online]. Available: https://webbook.nist.gov/chemistry/name-ser/.

[19] R. Saeed, J. Schlegel, C. Castano and R. Sawafta, "Preparation and enhanced thermal performance of novel (solid to gel) form-stable eutectic PCM modified by nano-graphene platelets", Journal of Energy Storage, vol. 15, pp. 91-102, 2018. Available: 10.1016/j.est.2017.11.003.

[20] Georgia institute of Technology, "Radiation Effects on Organic Materials in Nuclear Plants", Electric Power Research Institute, 1981.

[21] A. Charlesby, "The cross-linking and degradation of paraffin chains by high-energy radiation", Proceedings of the Royal Society of London. Series A. Mathematical and Physical Sciences, vol. 222, no. 1148, pp. 60-74, 1954. Available: 10.1098/rspa.1954.0052.

[22] R. Saeed, J. Schlegel, C. Castano and R. Swafta, "Uncertainty of Thermal Characterization of Phase Change Material by Differential Scanning Calorimetry Analysis", International Journal of Engineering Research & Technology, vol. 5, no. 1, pp. 405-412, 2016.

[23] D. Lin-Vien, N. Colthup, W. Fateley and J. Grasselli, The Handbook of Infrared and Raman Characteristic Frequencies of Organic Molecules. San Diego: Academic Press, 1991.

[24] "SpectraBase", Spectrabase.com, 2021. [Online]. Available: https://spectrabase.com/.

[25] A. Miranda et al., "Line shape analysis of the Raman spectra from pure and mixed biofuels esters compounds", Fuel, vol. 115, pp. 118-125, 2014. Available: 10.1016/j.fuel.2013.06.038.

[26] J. De Gelder, K. De Gussem, P. Vandenabeele and L. Moens, "Reference database of Raman spectra of biological molecules", Journal of Raman Spectroscopy, vol. 38, no. 9, pp. 1133-1147, 2007. Available: 10.1002/jrs.1734

[27] F. Adar, "Characterizing Modified Celluloses Using Raman Spectroscopy", Wright's Media, 2016.

[28] H. Abou Zeid, Z. Ali, T. Abdel Maksoud and R. Khafagy, "Structure-property behavior of polyethylene exposed to different types of radiation", Journal of Applied Polymer Science, vol. 75, no. 2, pp. 179-200, 2000. Available: 10.1002/(sici)1097-4628(20000110)75:2<179::aid-app1>3.0.co;2-b.

[29] C. Warren and D. Hooper, "Chain Length Determination of Fatty Acids by Raman Spectroscopy", Canadian Journal of Chemistry, vol. 51, no. 23, pp. 3901-3904, 1973. Available: 10.1139/v73-581

[30] C. Algiere, "Chronomorphic characterization and radiolytic degradation analysis of polyurethane with monte carlo modeling of the neutron spectra surrounding age pettrace cyclotron", 2018. Available: https://hdl.handle.net/10355/66223.

[31] R. Berliner, "The university of Missouri Research Reactor (MURR)", Neutron News, vol. 2, no. 4, pp. 13-19, 1991. Available: 10.1080/10448639108218740.

III. STATISTICAL DAMAGE MODEL FOR ORGANIC MOLECULES

ABSTRACT

Phase change materials (PCMs) are unique in that they can be used to store large amounts of thermal energy at nearly constant temperature due to phase change. Two applications for PCMs is an environmental control system on a space craft and a passive safety system in a nuclear reactor. The ideal PCMs for these applications are organics. Unfortunately, these applications have radiation environments which is known to degrade organic materials overtime Recent work has gone into determining how well certain PCMs maintain their properties under radiation environments. The current work attempts to model the changes in organic molecules to extrapolate the change in the latent heat of the PCM. The current model uses a damage per atom (DPA) model and statistics to predict the scissions that occur in an organic molecule. This model is compared to a similar model made by Charlesby and it was found that the maximum absolute error was less than 0.15 under the tested conditions. The current model improves upon the Charlesby model by removing the need to calculate the probability of a C-C break for every radiation environment it is used for. Further analysis showed that not implementing chain recombination and crosslinking does not allow the current model to accurately predict the change in the latent heat provided in previous work. Future work should go into determining the probability of free radicals, cross linking, and chain recombination.

1. INTRODUCTION

Phase change materials (PCMs) are unique in that their high latent heat lets them absorb large amounts of thermal energy at nearly a constant temperature while changing phase. PCMs have uses in many applications including building insulation, textiles, and energy storage [1-6]. Some of the more interesting applications that PCMs are used for is in environmental control mechanisms in space craft and as passive safety systems in nuclear reactors [7-9]. In a space craft, PCMs would allow the radiator, used to reject heat into space, to be designed with the average heat load rather than the maximum heat load which reduces the size of the radiator. In a nuclear reactor, PCMs would be used to condense steam in the event of a loss of coolant accident reducing the temperature and pressure inside the containment structure. Both space and nuclear applications have the unique feature of being in a radiation environment. It is important for any PCM used in these applications to maintain their melting properties through the irradiation.

To properly make a PCM selection for radiation environments it is important to be able to predict the change in the major properties of the PCM, mainly melting temperature and latent heat. As will be discussed further in the background the best type of PCM for these applications are organic PCMs however the effect of radiation on their latent heat is largely unknown and has only recently been investigated [10-11]. This paper develops a simple model to predict the change expected in the original molecules of an organic PCM which should correlate to the change in the latent heat of the PCM.

2. BACKGROUND

2.1. PHASE CHANGE MATERIALS

PCMs are materials with a large latent heat that allows them to absorb a large amount of thermal energy at their phase transition temperature. Most PCMs that are currently in use have a solid-liquid phase transition. While other phase transitions can be used they typically either have too low of a latent heat or too large a volume change for practical purposes. Within the solid-liquid type PCMs there are three main categories: organic, inorganic, and eutectic. Organic PCMs are typically paraffins, fatty acids, sugar alcohols and polymers. Inorganic PCMs are typically salt hydrates, salts, and metals. Eutectic PCMs are a combination of any two PCMs in a particular ratio, called the eutectic point, that melt and freeze as one material [12-13]. It was found that the ideal PCM categories for space and nuclear applications were organic and eutectic PCMs [10-11]. The main reasons organic and eutectic PCMs are ideal is that they have an appropriate melting temperature for both applications and their melting properties remain constant over many melt/freeze cycles. It should be noted that sugar alcohols, while an organic PCM, are not considered ideal due to their potential to burn after melting which can be a safety hazard [14]. The major downside to organic PCMs is their low thermal conductivity (approximately 0.01 W/cm-K) which results in a self-shielding effect where the PCM will melt on the outside but can't transfer the heat into the bulk of the material fast enough for it to be effective over a short period of time. This is easily engineered around with the addition of fins or nanoparticles [15-16].

In organic PCMs the melting temperature and latent heat is highly dependent on the chain length of the molecules as well as any functional groups that are attached to the chains. Figure 1 shows the change in the melting temperature and latent heat of paraffins with carbon chain length [17]. It can be seen that larger chain lengths have higher melting temperatures and higher latent heats. An interesting observation is that even chain lengths tend to have slightly higher melting temperatures and significantly higher latent heat compared to their odd counterparts. It is this change in the chain length that will be the basis for the model developed. A change in the chain length would result in a loss of latent heat under the appropriate temperature range for a given application. By estimating the change in the original molecules, it should be possible to estimate the change in the latent heat of the material at the original melting temperature.

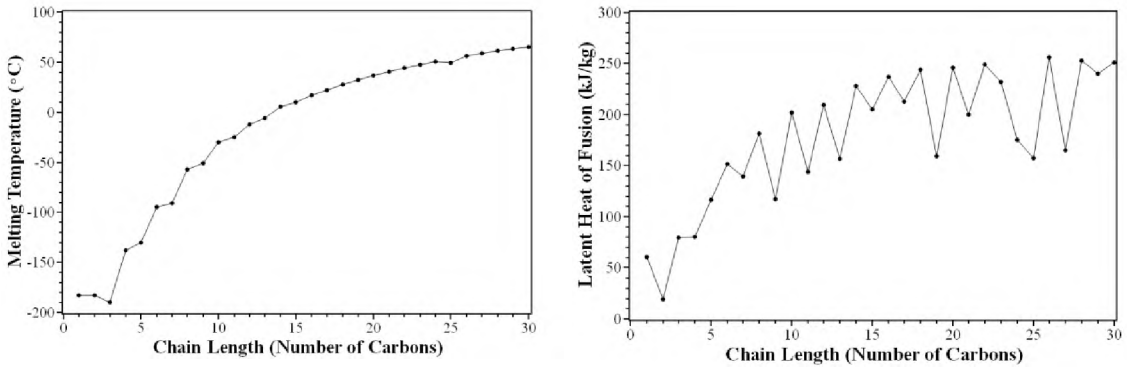

Figure 1 – Melting Temperature (Left) and Latent Heat (Right) of Paraffins with Different Chain Lengths [17]

2.2. RADIATION ENVIRONMENTS

The radiation environments in space and a nuclear reactor containment are very different from one another. The radiation environment in space consists mostly of galactic

cosmic rays (GCR) and solar radiation. The GCR consists mostly of high energy protons as well as high energy heavy nuclei and the solar radiation is primarily protons and electrons [18]. The total dose on a mission to Mars from a radiation space environment would be on the order of 10^3 Gy. In a nuclear reactor containment, the primary source of radiation is gammas and neutrons [19]. The dose rate in a reactor containment is approximately 9 Gy/day. Current lifetimes for nuclear reactors are approximately 60 years which correlates to almost 200 kGy of total radiation dose. Considering that the applications for PCMs in radiation environments have very different types of radiation it is important to make the model general enough that any type of radiation damage could be evaluated.

2.3. DAMAGE MECHANISMS IN ORGANIC MOLECULES

There are three main damage mechanisms in organic molecules due to radiation damage: Scission, crosslinking, and oxidation. Figure 2 shows illustrations of these damage mechanisms. During chain scission the radiation breaks a bond between two carbon atoms that are on the main chain of the molecule. Chain scissions reduce the molecular weight of the material and reduces the Youngs modulus, tensile strength, hardness, elasticity, and melting temperature while increasing solubility and elongation of the irradiated material [20-21]. As was seen in Figure 1 the correlation of chain length to latent heat shows that in general the latent heat reduces with scission. Crosslinking and oxidation both require free radicals to exist for them to occur. These free radicals can come from scission or the loss of a hydrogen atom in the molecules. Crosslinking typically makes chains longer or branched which increases the molecular weight and has the opposite effects on the

mechanical and thermal properties of the material as compared to scission [20-21]. Both scission and crosslinking produce gasses in the form of hydrogen and short chain hydrocarbons. Oxidation occurs when free oxygen in the air bonds to a free radical of the original material. Oxidation competes with crosslinking for free radicals and has similar effects to scission as it prevents the material from crosslinking by taking up the free radicals in the material [20-21].

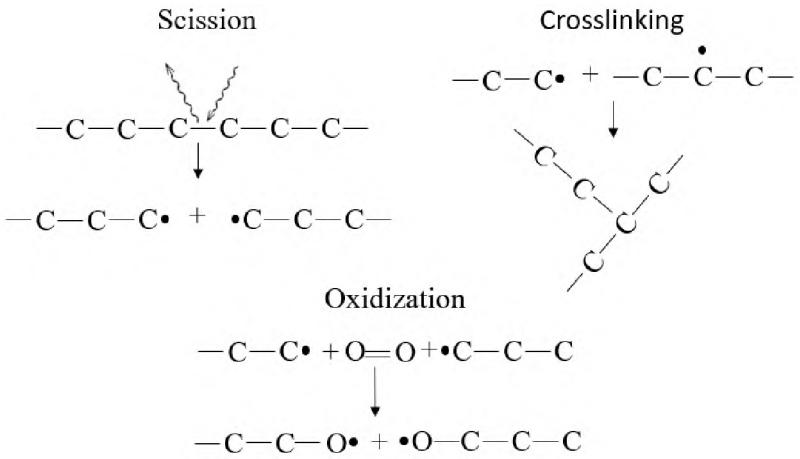

Figure 2 – Visualization of the Three Main Damage Mechanisms in Organic Materials

2.4. PREDICTIVE MODELING

Typically, when considering the radiation damage in an organic material, molecular dynamics or Monte Carlo simulations are used to model the change in the structure. These types of models are very computationally intensive and as such take a long time to run or require expensive computer parts to run more efficiently. A simple analytical model was presented by Charlesby [22] to determine the distribution of molecular chain lengths of polymers after irradiation in the Harwell B.E.P.O. pile. This model only accounts for chain scissions and neglects crosslinking and oxidation. Equation 1 is Charlesby's model for an

infinite chain length and Equation 2 shows the model for molecules of finite length. The model assumes that all bonds are equally likely to be affected and neglects side chains as well as recombination of the broken molecule.

$$P_{l_k}(R) = Z(1 - e^{-pR})^2 * e^{-(k-1)pR} \quad (1)$$

$$P_{l_k}(R) = Z(1 - e^{-pR})^2 * e^{-(k-1)pR} + P_{l_k}(0) * e^{-(k+1)pR} + (1 - e^{-pR_0}) * e^{-kpR} * (2k - (k-1) * e^{pR} - (k+1)e^{-pR}) \quad (2)$$

In Equations 1 and 2 $P_{l_k}(R)$ is the number of molecules with chain length k after R radiation, Z is the initial number of Carbon atoms in the main chain, p is the probability of a C-C break at the Harwell B.E.P.O reactor per unit of radiation exposure, R is the unit of radiation exposure per 10^{17} neutrons/cm^2, and R_0 is a virtual radiation to establish a distribution of chain lengths from an infinite chain when a distribution is needed. If the distribution is already known a virtual radiation dose can be assumed to be zero and thus the last term in Equation 2 equals zero.

This model estimates how much damage has been done to an organic material significantly more quickly than Monte Carlo or Molecular Dynamic simulations. Unfortunately, it requires data for p and R that is difficult to estimate directly without doing experiments first. In this paper one unit of radiation was defined as 10^{17} neutrons/cm^2 and the value for p was estimated to be ~0.004 by how much methane, ethane, propane, and butane escaped from the irradiated samples [22]. The value of p is very strongly dependent on the unit of radiation used and the type of radiation that is being used. This highly limits the predictive nature of this model as p would have to be experimentally determined for every radiation field that needs to be analyzed.

3. MODEL DEVELOPMENT

This model was made to evaluate the reduction of the original chain lengths of the organic molecules in a material after irradiation. Of the three main damage mechanisms this model accounts only for scission. Oxidation was not considered because its effect is very similar to scissions and therefore can be lumped into this term. Crosslinking will be discussed in more depth however it will not be implemented in the model. Ideally this model will be able to predict the amount of deviation from the original chain lengths after irradiation to make it possible to determine the deviation in the latent heat under the appropriate melting temperature. The model in this paper will utilize a displacements per atom (DPA) calculation to statistically determine the number of scissions that occur per chain. While the DPA calculation in this paper will be specific for neutrons it can be used for other types of particles as long as a cross section can be found or derived.

3.1. MODEL DERIVATION

3.1.1. Scission. To determine the damage done within the organic molecule a DPA calculation is needed. Equation 3 is used to find DPA per second within a material. In Equation 3, $\dot{H}$ is the DPA per second, Φ is the neutron flux as a function of energy, σ_d is the displacement cross section as a function of energy, and E is the neutron energy. For a given application the energy dependent flux would need to be known or estimated.

$$\dot{H} = \int \Phi(E)\sigma_d(E)dE \tag{3}$$

The displacement cross section can be calculated from Equation 4 where σ_s is the energy dependent scattering cross section of the target atom, m_n is the neutron mass, m_T

is the mass of the target atom, E is the energy of the neutron, and E_m is the energy needed to break a single C-C bond. It should be noted that the masses are needed to determine the maximum fraction of energy that a neutron can impart onto the target atom.

$$\sigma_d = \sigma_s \frac{4m_n m_T}{(m_n + m_T)^2} \frac{E}{E_m} \tag{4}$$

For scission the only bonds that are significant are the C-C bonds. Therefore, only a DPA calculation involving carbon will be used. The displacement energy is determined by the C-C bond which has an energy of 6.23 eV [23]. This is the value that will be used for E_m. ENDF data will be used to obtain the energy dependent cross section of carbon and can be seen in Figure 3 [24]. It can be seen that a smooth function for this cross section is not feasible and therefore the integral in Equation 3 will have to be solved numerically.

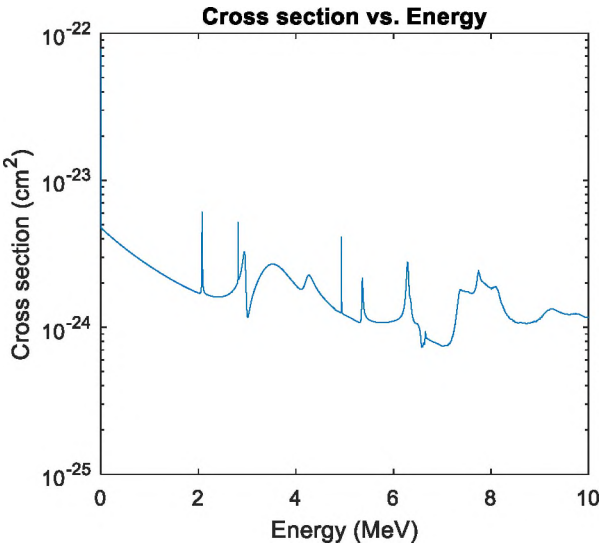

Figure 3 – Carbon Scattering Cross Section vs. Energy

The neutron flux that will interact with material being evaluated will vary depending on the situation. The scission portion of this code will be compared to

Charlesby's model for verification. Due to Charlesby's model only being valid with the known terms for the Harwell B.E.P.O pile it is necessary for this code to assume a flux distribution. It will be assumed that the spectrum in the Harwell B.E.P.O pile is a Watt's Fission spectrum. Equation 5 gives a normalized Watts Fission Spectrum and Figure 4 shows what the distribution looks like. The results of this program will also be compared to the change in the thermal properties of a PCM irradiated in the Missouri University of Science and Technology Research Reactor (MSTR). Figure 5 shows the flux profile of the MSTR at 180 kW and 100 kW as used in the previous paper [10-11]. For this paper only the 180 kW spectrum will be considered.

$$P(E) = 0.48455 * \sinh\left(\sqrt{2E}\right) e^{-E} \tag{5}$$

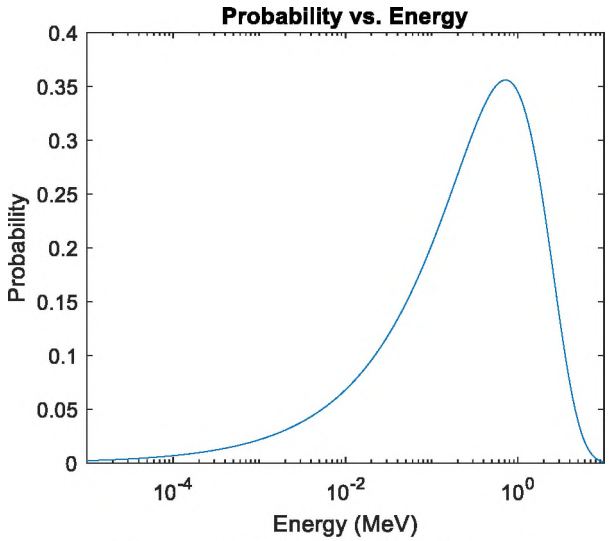

Figure 4 – Watts Fission Spectrum

After the DPA/s calculation has been made it can be multiplied by the irradiation time to obtain the total DPA of the material for carbon. To determine the probability of scissions per chain the carbon DPA will be multiplied by the number of carbons in a

molecule to give the Damage per Chain (DPC). Because the neutrons have an equal probability of interacting with each carbon atom in the chain, a Poisson distribution can be used to determine the probability of a given molecule having a certain number of breaks which can be seen in Equation 6.

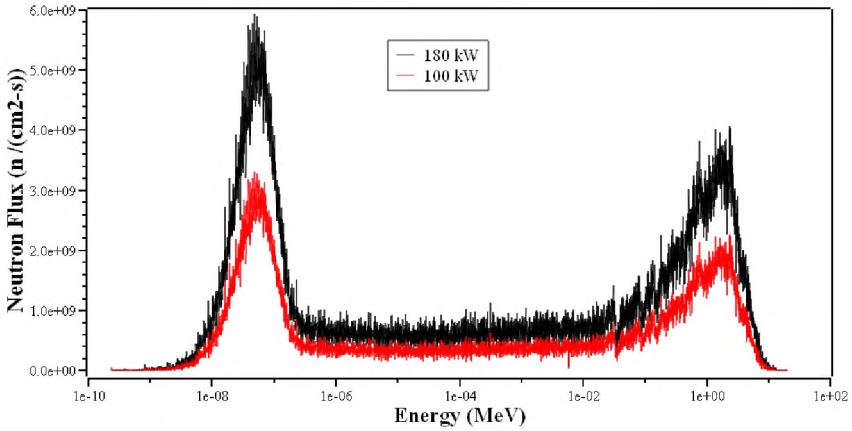

Figure 5 – Flux Profile of the MSTR Obtained from MCNP at 180 kW and 100 kW

Using the same logic for the Poisson distribution, it can be assumed that the chain distribution after irradiation will follow an exponential distribution except for at the starting chain length. Equation 7 shows a modified exponential distribution that was used to determine the distribution of chain lengths after irradiation. The modification to the distribution was that the starting chain length would be the sum of all the predicted chain lengths higher than the starting. To do this an integral from the starting chain length to infinity of the chain distribution equation was used

$$P_{sc}(k) = \frac{(G)^k * e^{-G}}{k!} \tag{6}$$

$$P_{cl}(l) = \begin{cases} H * e^{-H*l}, & l < l_{st} \\ \int_{l_{st}}^{\infty} H * e^{-H*l}\, dl, & l = l_{st} \end{cases} \tag{7}$$

In Equations 6 and 7, P_{sc} is the probability of a given number of scissions per chain, k is the number of breaks in a chain, G is the damage per chain, P_{cl} is the Chain length distribution, H is the damage per atom, l_{st} is the starting chain length in the PCM, and l is the length of a carbon chain. Equations 6 and 7 are normalized to give probability distributions of breaks per chain and chain length distribution. By comparing the change in the starting chain lengths after irradiation to post irradiation it should be possible to determine how much of a decrease in latent heat can be expected under the original melting temperature.

3.1.2. Cross Linking. As mentioned previously this paper will not add crosslinking into the model developed, however one theoretical method for implementing it will be discussed. To account for crosslinking the loss of hydrogen atoms would be the main source of free radicals on a chain. These free radicals then have a particular chance to form a crosslink which is dependent on the number of free radicals present in the system [25]. In order to calculate the number of free radicals produced from hydrogen loss a similar method to the scission calculation could be used. Using Equations 3 and 4 would yield the DPA/s for hydrogen with the major differences being σ_s, m_T, and E_a where σ_s would be the energy dependent scattering cross section of hydrogen, m_T would be the mass of hydrogen, and E_a would be the energy of a C-H bond. After the DPA is calculated it is multiplied by the number of hydrogen atoms in the molecule which would yield the DPC. It should be noted that the DPC can be determined for undamaged chains as well as chains that have undergone scission by multiplying by the correct number of hydrogen atoms per chain. This is then turned into a Poisson distribution similarly to Equation 6 which yields

a probability distribution for the number of Hydrogen atoms lost per chain and provides the production of free radicals which can be seen in Equation 8.

$$P_{FP}(z) = \frac{(G)^z * e^{-G}}{z!} \tag{8}$$

In Equation 8, P_{FP} is the percent of chains with z free radicals produced from hydrogen loss, z is the number of hydrogen bonds broken, G is the damage per chain for hydrogen. As was stated previously each free radical has a particular probability to form a cross link and this probability is dependent on the free radical concentration in the material. By adding cross linking into the model, it complicates determining the distribution of chain lengths in the material after irradiation due to the possible combinations of chain segments. It becomes much simpler to look at what percent of molecules were unaffected by the irradiation to extrapolate the change in the materials latent heat. Equation 9 is one possible method that could be used to determine the probability that a molecule does not form a cross link.

$$P_t = \sum_{z=0} P_{FP}(z) * nc^z \tag{9}$$

In Equation 9, P_t is the total probability of chains not forming a crosslink, FP is the free radical production on a given chain, nc is the probability of a given free radical on the chain not forming a crosslink, and z is the number of cross links on a chain. Once P is calculated multiplying that by the number of unaffected chains after scission yields the total percent change in the original chain length. The main reason that this cannot be implemented into the current model is the lack of information on nc which would need to be experimentally discovered. As was mentioned nc is dependent on the free radical concentration and therefore any experimental investigation intended to evaluate it would

need to do a thorough investigation including: many dose rates for various free radical concentrations, free radical measurements in the material, and determination of the total cross links that occur throughout the material. The radiation environments in the applications being considered in this paper, namely the nuclear reactor containment and deep space exploration vehicles, have very low dose rates but are expected to see a large dose overall. Due to this it is expected that crosslinking would have a minimal effect on the actual applications being discussed.

3.1.3. Latent Heat Estimation. The end goal of this model is to be able to predict the latent heat of the material after irradiation. It will be assumed that for a given material the latent heat at the original melting temperature would change identically with the change in the mass of the original molecules, as the shorter molecules would 'melt' at lower temperatures. It is important to note that the code currently determines chain length distribution of the material which does not directly correspond to mass. Equation 10 uses the chain distribution to determine the mass distribution of molecules with a given chain length. In Equation 10, P_m is the mass of chains with k carbons, P_{cl} is the chain distribution of molecules with k carbons, m is the molar mass of a molecule with k carbons, $P_{m_{v0}}$ is the mass of molecules with v carbons prior to irradiation.

$$P_m = P_{cl} * m_k * \sum_v \frac{P_{m_{v0}}}{m_v} \tag{10}$$

It is important to note that Equation 10 has a few limitations. Equation 10 is only fully valid for materials that start off fully as either pure paraffin or a mixture of paraffins and can be used to predict the mass of all subsequent paraffins that would be generated due to scission. For non-paraffins, Equation 10 can only be used to determine the mass of the

unchanged molecules. This is due to non-paraffins having functional groups that change the properties, and mass, of the material. Figure 6 shows a fatty acid that undergoes scission. It can be seen in figure 6 that the scission yields one fatty acid and one paraffin that have the same chain length but have significantly different masses due to the carboxyl group on the fatty acid. In the current model there is no method for determining which chains have the functional group and which ones do not therefore making it impossible to accurately determine the mass of chains that underwent scission. The final limitation to Equation 10 is that it assumes that there is no mass loss in the material due to gas generation.

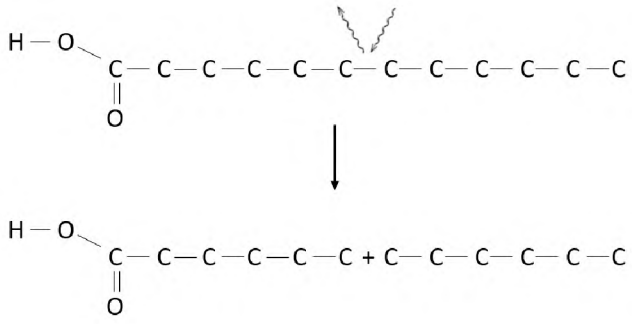

Figure 6 – Example of Radiation Damage Leading to Different Masses for the Same Chain Length

To determine the latent heat of the material after irradiation Equation 11 is used. In Equation 11, LH is latent heat, P_{m_Δ} is the mass of chain lengths that underwent the most mass change from unirradiated to irradiated, the subscript i represents after irradiation, the subscript 0 represents before irradiation. For a pure substance P_{m_Δ} is the starting chain length of a material. For a mixture, such as a eutectic, P_{m_Δ} will have to be determined for

each of the starting chain lengths and the chain length that has the most change will have to be determined by your eutectic point.

$$LH_i = LH_0 \frac{P_{m_{\Delta i}}}{P_{m_{\Delta 0}}} \tag{11}$$

3.2. CODE IMPLEMENTATION

This model was implemented using MATLAB. Figure 7 shows a flow chart for the methodology for estimating the change in the chain lengths with radiation. As can be seen in top part of Figure 7 the first step was initializing all the basic parameters such as energy range, total flux in the reactor, mass of carbon, etc. Then the percent of each molecule of the original substance is calculated. In this paper two different materials will be used, icosane and a eutectic of methyl palmitate and lauric acid (EMPaLA) in a ratio of 60/40 by mass [11]. Icosane is a paraffin that is 20 carbons long and will be used to compare this model to Charlesby's model. EMPaLA is made of two fatty acids that have chain lengths of 16 and 12 for methyl palmitate and lauric acid, respectively. The change in latent heat of EMPaLA with radiation damage has been tested to some extent and will be compared to the change in the initial chain lengths predicted with this code. After the molecular percentages are found a function, made in MATLAB, determines the damage distribution and chain length distribution for each molecule that is present in the material. For materials with multiple starting chain lengths such as EMPaLA, the damage distributions and chain length distributions of each are superimposed using the molecular percentages. Finally, a cumulative probability density function is created.

The red box in Figure 7 shows a flow chart for the function used to calculate the damage and chain length distributions. First, it generates the Neutron flux energy

distribution as a symbolic function in MATLAB or reads in flux data for the necessary application. In this instance the Watts fission spectrum will be used for the icosane when comparing it to Charlesby's model and data will be read in from the MSTR data for EMPaLA. The ENDF data for the energy dependent scattering cross section is then read in from a text document and the values for energy are converted from eV to MeV and the cross sections are converted from barns to cm2. The cross-section data is then converted into a piecewise function by linearly interpolating between each point. Depending on whether the radiation data was a function or data determines how the next portion of the code runs. If the data is a function, the integral of the flux function times the linearly interpolated cross section times energy is performed numerically for each part of the cross section function. If the data is numerical then it too is linearly interpolated and integrals with each of the interpolated functions are made with bounds based on the piecewise limits for each function. Once the integrals are calculated the DPA/s is multiplied by irradiation time to obtain DPA in the material which is then converted into DPC. Equation 6 is then directly solved from this assuming that there will be no more dislocations than carbon atoms in the molecule. Equation 7 is then formed into a symbolic equation and solved up to the starting chain length. The equation is then numerically integrated from the starting chain length to infinity to determine the value for the starting chain length after irradiation.

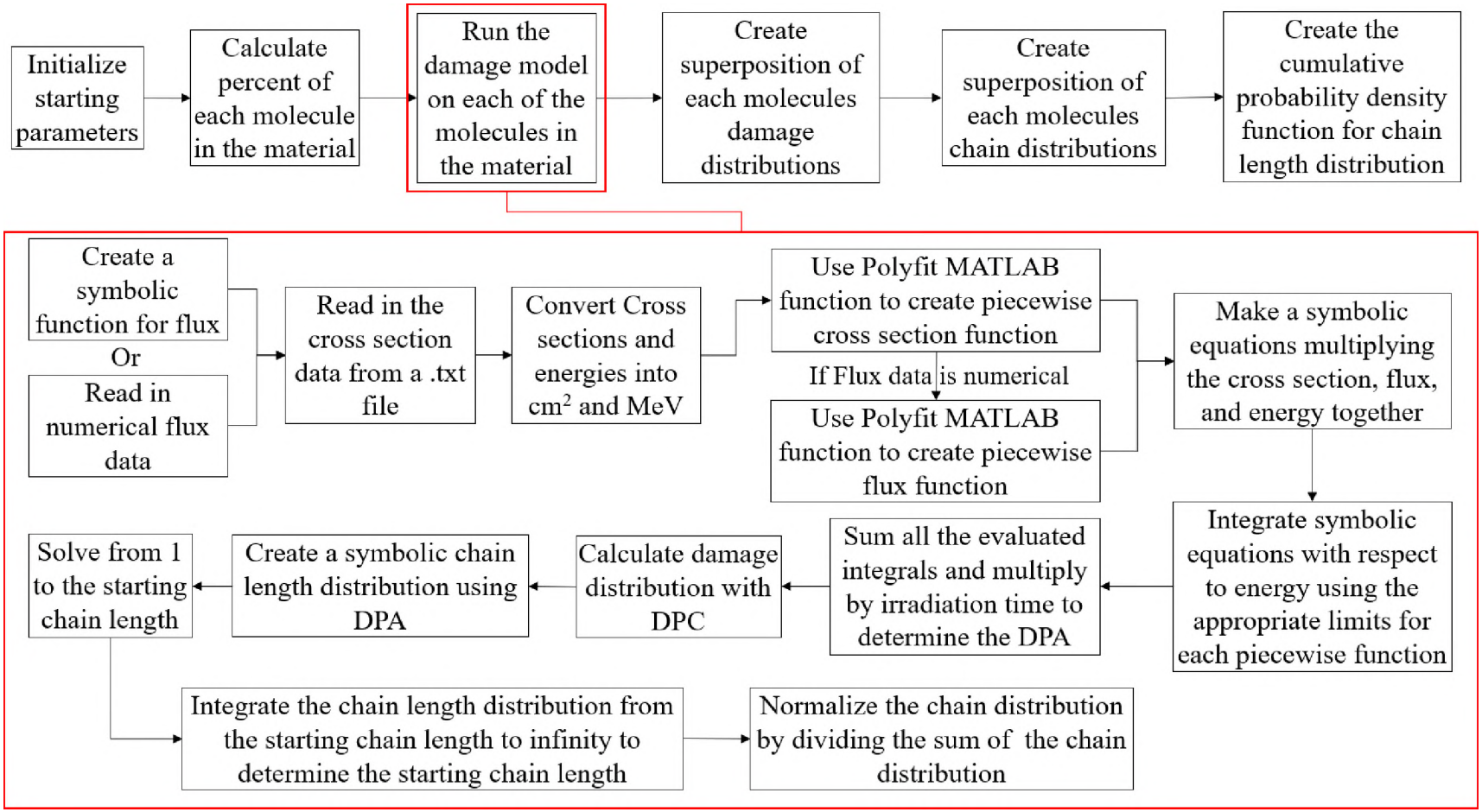

Figure 7 – Damage Modeling Flow Chart

4. RESULTS

4.1. MODEL COMPARISON

The model that has been developed is very similar to Charlesby's model. The main difference between the two models is that the current model is more general in that it is not necessary to determine the probability of a C-C break for each radiation source that the model is applied to. To compare these two models a couple of assumptions need to be made about each. First, Due to the limitations of Charlesby's model both models will assume fluences of 10^{17}, $2x10^{17}$, $3x10^{17}$, $4x10^{17}$, $5x10^{17}$, and $6x10^{17}$. This allows for R in Charlesby's model to be 1, 2, 3, 4, 5, and 6 for each fluence. The value for p will use the same value that is listed in the paper, 0.004. The current model will assume that it takes 1 minute for the samples to receive a fluence of 10^{17} which allows irradiation times of 1, 2, 3, 4, 5, and 6 minutes. The model developed here will also assume a Watt's fission spectrum since an energy distribution is not given in the paper by Charlesby. Both models will assume a starting distribution of 100% Icosane (C20H42). In Charlesby's model there is a virtual irradiation of R0 that is used to create a chain length distribution when one isn't known. This value will be set to 0 since its assumed to be 100% Icosane. Figure 8 (a) and (b) shows results of Charlesby's model, (c) and (d) shows the results of the current model, and (e) and (f) show the absolute error between them.

As can be seen in Figure 8 the shapes of the chain length distributions and cumulative chain distributions are similar for both models. The errors in Figure 8 (E) and (F) were calculated with a general error function as seen in Equation 12.

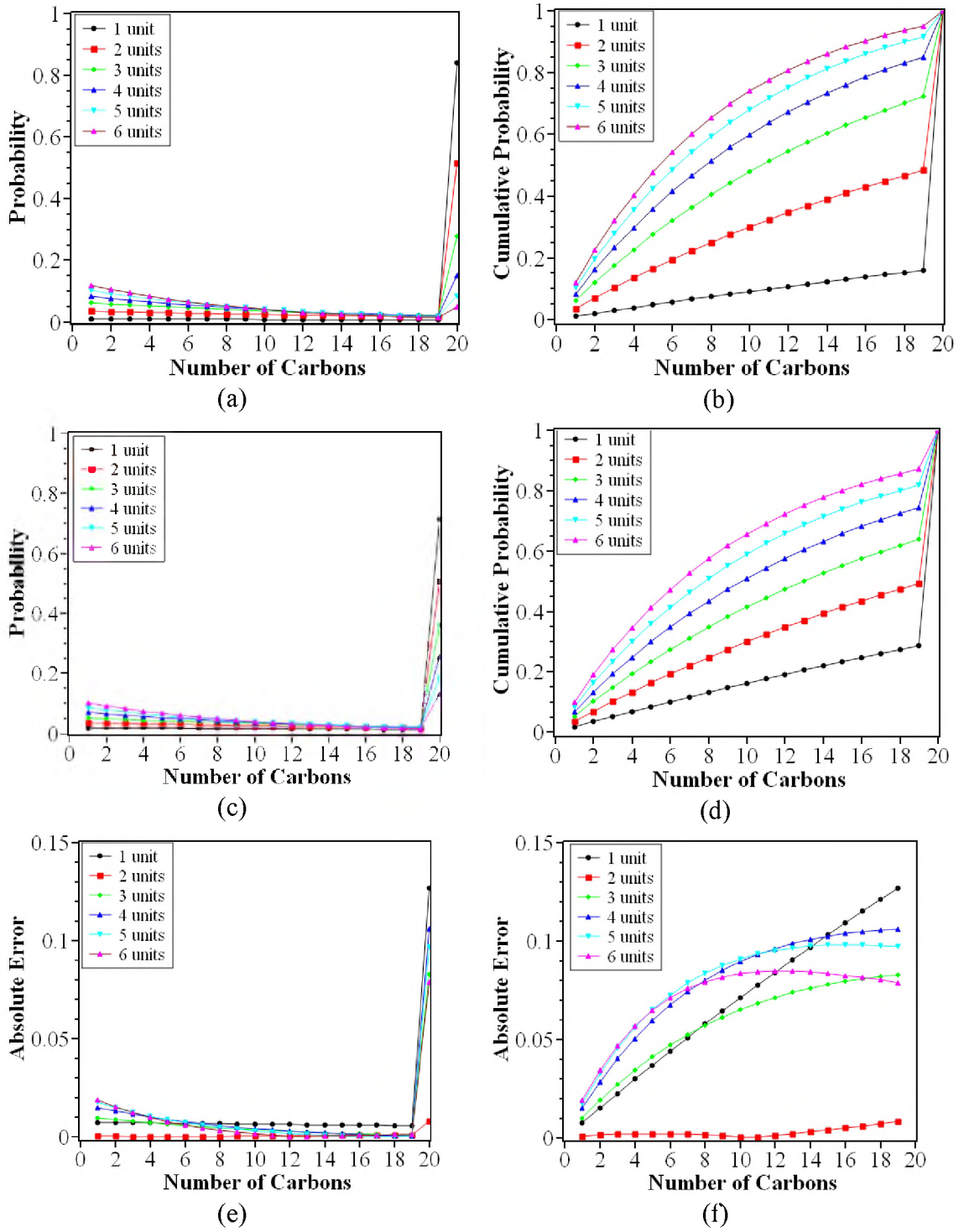

Figure 8 – Comparison of Charlesby's model and the Current Model Using a 20 Carbon Chain Length (a) Charlesby's Chain Distribution (b) Charlesby's Cumulative Chain Distribution (c) Current Model's Chain Length Distribution (d) Current Models Cumulative Chain Distribution (e) Chain Length Distribution Error (f) Cumulative Chain Distribution Error.

In Equation 12, CM is the value of the current model and Ch is the value for Charlesby's model. In Figure8 (F) the error at a chain length of 20 will always be equal to 0 due to the lack of chains higher than the starting chain length and the values were omitted from the graph. It can be seen in Figure 8 (e) that the chain length distribution error at chain length 20 are rather large compared to all of the other chain lengths. This is likely due to the method of calculating the starting chain length with an integral however the error is still less than 0.15 and is an acceptable difference. Another cause of the errors in these values could be caused due to lack of a proper neutron spectrum included in the paper for the Charlesby's model and the assumption that it followed a watt's fission spectrum. Overall, the current model shows good agreement with Charlesby's model and is more general in that it can be used with any radiation field as long as the energy spectrum of the field is known or can be estimated.

$$\varepsilon = |CM - Ch| \tag{12}$$

4.2. COMPARISON OF MODEL WITH LATENT HEAT DATA

Previous work has been done to determine the effect that radiation damage has on PCMs. One paper investigated the effect on a 60/40 Eutectic of Methyl Palmitate and Lauric Acid (EMPaLA). The samples were irradiated in the University of Missouri Science and Technology Research Reactor (MSTR) at 180 kW for 6, 12, 18, 24, 30 and 36 minutes. Figure 5 shows the energy dependent flux of the MSTR. Figure 9 (a), (b), and (c) show, respectively, the predicted chain distribution, damage per chain and cumulative chain probability density of EMPaLA after the irradiations. Since EMPaLA is a eutectic of 60% methyl palmitate and 40% lauric acid by weight, and because the methyl palmitate

molecules are heavier than the lauric acid molecules, the initial chain length distribution has a probability of 52% and 48% at chain length 16 and 12, respectively. It is important to note that even though methyl palmitate has a total of 17 carbon atoms only 16 are on the carbon backbone which is what this model focuses on. Figure 9 shows that very little scission damage occurred in the irradiations. By utilizing Equation 10 it was found that the mass percent of undamaged Methyl Palmitate and Lauric Acid was 59.9 and 40% respectively. The 40% on the Lauric Acid is the same as the initial amount due to rounding in MATLAB and to how little damage was estimated. This shows that the quantity of Methyl Palmitate will govern the amount of eutectic present in the irradiated sample. Using Equation 11 it was found that the latent heat of EMPaLA after 36 minutes of irradiation would be 99.99% of its starting value.

Figure 10 shows the change in the latent heat of EMPaLA with irradiation dose in the MSTR at 180 kW and 100 kW [11]. Each data point is an additional 6 minutes of irradiation . It can be seen that at the second point with 12 minutes of irradiation there is the largest change for both 100 and 180 kW from the no dose measurement. While this measurement does fall outside the 90% confidence interval the error bars were so close together that it was assumed in the previous research that this was just due to random error. That means that during the irradiations there was no observable difference in the latent heat data. This helps to corroborate the values given by the proposed model. Future work would be to evaluate the changes at higher dose rates to see if a change in the latent heat does occur and to determine if the change is proportional to the change in predicted chain lengths.

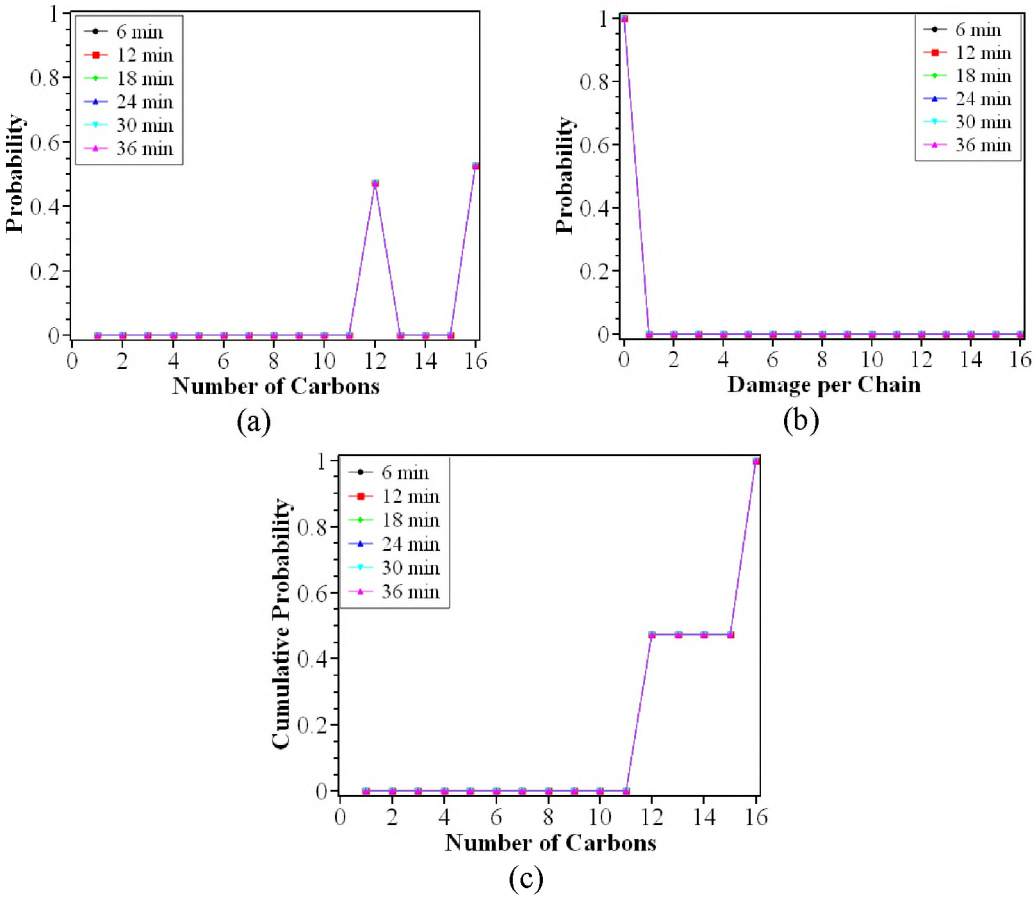

Figure 9 – Model Predictions for EMPaLA in MSTR (a) Chain Length Distribution (b) Scissions per Chain (c) Cumulative Chain Distribution in MSTR

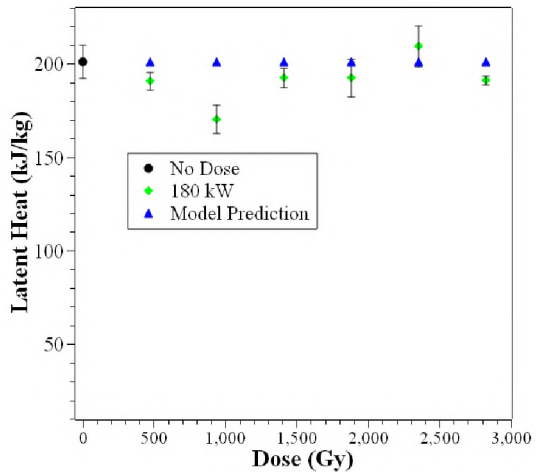

Figure 10 – Latent Heat of EMPaLA Irradiated at 180 kW in the MSTR Experimentally Determined and Estimated with Current Model

4.3. CROSS LINKING IMPLEMENTATION

To further improve the predictive capabilities of this code it is extremely important to add cross linking to the code. As was previously mentioned it is necessary to determine the probability that a free radical will create a cross link in the material and that increased free radical concentration leads to increased cross linking. A series of experiments should be conducted that test the free radical concentration and crosslinking in materials that have been irradiated. To determine the effect that free radical concentration has on crosslinking varied dose rates should be used to increase free radical production however total dose should remain constant. It is proposed that dose rates of 102, 103, 104, 105, and 106 Gy/min be used at minimum with total dose reaching an order of magnitude of 104 Gy. One method to measure the free radical concentration in the materials is electron spin resonance (ESR) which uses a magnetic field and microwaves to excite free electrons which then emit a photon that can be detected. To measure the crosslinking in the sample it may be possible to use High Performance Liquid Chromatography (HPLC). HPLC can determine the components in a material by dissolving the sample in a liquid solvent and passing it through a solid adsorbent material which changes the flow rates for different compounds in a sample. Ideally the samples would be irradiated while ESR measurements were being performed however that may not be realistically achievable. Therefore, to calculate the total concentration of free radicals several ESR measurements should be taken after irradiation to see how the free radical concentration changes with time after irradiation has finished in an effort to back calculate the maximum free radical concentration in the material. If there is a significant change in the free radical concentration with time after irradiation several HPLC measurements should be taken to determine how cross linking

was affected over time after irradiation was concluded. As little time as reasonably achievable should be between the end of the irradiation and the first ESR and HPLC measurements. After all the data has been collected a curve fit should be made between free radical concentration and cross linked molecules to yield the probability of a free radical forming a cross link. Additionally, the free radical concentration could be used to determine the accuracy of the free radical production equation proposed in this paper.

5. CONCLUSIONS

A simple model has been created to determine the scission damage caused by radiation on organic chains. It has been compared to a similar model made by Charlesby and found to be in good agreement with absolute errors lower than 0.15. The model in this paper is significantly more general than the Charlesby model as it is useful in many applications with the only necessary knowledge being the molecular chain(s) to be irradiated, the energy spectrum of the radiation field, and the nuclear cross sections of the material. Charlesby's model required a probability of a C-C break for a given dose of radiation which would have to be experimentally determined for each radiation field it is used for which severely limits its usefulness. It was found that the current model is unable to predict the change in the latent heat of a material irradiated likely due to assumptions made that the chains do not recombine and because cross linking was ignored. Future work should go into adding chain recombination and cross linking into the code however it is necessary to find the probability of free radicals creating cross links and what the probability of chain recombination is.

ACKNOWLEDGEMENTS

This paper is based upon work supported by the U.S. Nuclear Regulatory Commission, Nuclear Education Program under Award NRC-HQ-13-G-38-0026.

REFERENCES

[1] Kosny, J. and Yarbrough, D.W., 2008. Use of PCM-Enhanced Insulations in the Building Envelope (No. 5). Oak Ridge National Laboratory (ORNL); Building Technologies Research and Integration Center.

[2] Onofrei, Elena & Rocha, A. & Catarino, André. (2010). Textiles integrating PCMs-A review. Buletinul Institutului Politehnic din Iasi. Tom LVI (LX). 99-110.

[3] S. Nandakumar, M. Le Gallo, I. Boybat, B. Rajendran, A. Sebastian and E. Eleftheriou, "A phase-change memory model for neuromorphic computing", Journal of Applied Physics, vol. 124, no. 15, p. 152135, 2018. Available: 10.1063/1.5042408.

[4] Maimon, J.D. et al. "Chalcogenide Memory Arrays: Characterization And Radiation Effects". IEEE Transactions on Nuclear Science 50.6 (2003): 1878-1884. Web.

[5] Demirbas, M.F., 2006. Thermal energy storage and phase change materials: an overview.

[6] Union of Concerned Scientists, "Donald C. Cook Unit 2: Bridgeman, MI", 2000

[7] L. Trevino and E. Orndoff, "Advanced Space Suit Insulation Feasibility Study", SAE Technical Paper Series, 2000. Available: 10.4271/2000-01-2479

[8] "NASA to Begin Testing Next Generation of Spacecraft Heat Exchangers", NASA, 2016. [Online]. Available: https://www.nasa.gov/feature/nasa-to-begin-testing-next-generation-of-spacecraft-heat-exchangers.

[9] Sargent & Lundy (2015). D.C. Cook PWR Nuclear Generating Station Ice Condenser Ice Machine System Replacement Project Profile. Chicago, IL.

[10] R. Steere, et al. (2021) " Radiation Effects on Thermal Storage Properties of Polyethylene Wax". Under Review

[11] R. Steere, et al. (2021) " Radiation Effects on Thermal Storage Properties of an Organic Eutectic PCM". Under Review

[12] G Fleischer A.S. (2015) Types of PCMs and Their Selection. In: Thermal Energy Storage Using Phase Change Materials. SpringerBriefs in Applied Sciences and Technology. Springer, Cham

[13] D. Zhou, C. Zhao and Y. Tian, "Review on thermal energy storage with phase change materials (PCMs) in building applications", Applied Energy, vol. 92, pp. 593-605, 2012. Available: 10.1016/j.apenergy.2011.08.025.

[14] A. Solé, H. Neumann, S. Niedermaier, L. Cabeza and E. Palomo, "Thermal Stability Test of Sugar Alcohols as Phase Change Materials for Medium Temperature Energy Storage Application", Energy Procedia, vol. 48, pp. 436-439, 2014. Available: 10.1016/j.egypro.2014.02.051.

[15] R. Singh, S. Sadeghi and B. Shabani, "Thermal Conductivity Enhancement of Phase Change Materials for Low-Temperature Thermal Energy Storage Applications", Energies, vol. 12, no. 1, p. 75, 2018. Available: 10.3390/en12010075.

[16] Z. Qureshi, H. Ali and S. Khushnood, "Recent advances on thermal conductivity enhancement of phase change materials for energy storage system: A review", International Journal of Heat and Mass Transfer, vol. 127, pp. 838-856, 2018. Available: 10.1016/j.ijheatmasstransfer.2018.08.049.

[17] “Chemical Name Search", Webbook.nist.gov. [Online]. Available: https://webbook.nist.gov/chemistry/name-ser/.

[18] L. Simonsen and C. Zeitlin, "Mars Radiation Environment- what have we learned?", Briefing to NAC HEO/SMD Joint Committee Meeting, 2017.

[19] M. Brovchenko, B. Dechenaux, K. Burn, P. Console Camprini, I. Duhamel and A. Peron, "Neutron-gamma flux and dose calculations in a Pressurized Water Reactor (PWR)", EPJ Web of Conferences, vol. 153, p. 05008, 2017. Available: 10.1051/epjconf/201715305008

[20] Georgia institute of Technology, "Radiation Effects on Organic Materials in Nuclear Plants", Electric Power Research Institute, 1981.

[21] A. Charlesby, "The cross-linking and degradation of paraffin chains by high-energy radiation", *Proceedings of the Royal Society of London. Series A. Mathematical and Physical Sciences*, vol. 222, no. 1148, pp. 60-74, 1954. Available: 10.1098/rspa.1954.0052.

[22] A. Charlesby, "Cross-linking of polythene by pile radiation", Atomic Energy Research Establishment, vol. 215, no. 1121, pp. 187-214, 1952.

[23] Darwent, B. (1970). Bond Dissociation Energies In Simple Molecules. U.S. DEPARTMENT OF COMMERCE NATIONAL BUREAU OF STANDARD.

[24] Www-nds.iaea.org. (2017). ENDF: Evaluated Nuclear Data File. [online] Available at: https://www-nds.iaea.org/exfor/endf.htm

[25] A. Mosieh, A. Hahn and C. Smith, "Physics-Based Probabilistic Model of the Effects of Ionizing Radiation on Polymeric Insulators of Electric Cables used in Nuclear Power Plants", NEUP U.S. Department of Energy, 2019.

SECTION

3. CONCLUSIONS AND RECOMMENDED FUTURE WORK

3.1. CONCLUSIONS

Phase change materials (PCMs) present a unique opportunity for environmental control in space craft and passive safety in nuclear reactors. The work presented in this dissertation shows that organic PCMs are somewhat resilient to radiation damage upto a total dose of nearly 3000 Gy. The maximum change in latent heat was approximately 20% at just below 1500 Gy and then the latent heat returned to normal. The doses that were used in these experiments were equivalent to approximately 10 months in a nuclear reactor containment and on the same order of magnitude as expected for a trip to Mars. It was found that PEW is not ideal passive safety applications, due to its wide melting peak. PEW could still be useful for other radiation environment applications, or it could be engineered around to add additional PEW to a passive safety system to account for the portion of the latent heat that is already used during normal reactor operations. Additionally, other materials may have better melting peaks. EMPaLA and E-NP were found to be good candidates for the space craft applications however.With a maximum change of 20% in the latent heat, it may be necessary to add additional shielding or PCM mass to make sure the system is consistently effective.

It was found that with the radiation damage between the 6^{th} irradiation at MSTR and the irradiation at MURR there was only a 70 Gy difference, however the latent heat dropped approximately 20% more. This was seen in both the EMPaLA and PEW samples.

This difference indicates that dose rate has a large effect on the change in the latent heat likely due to increased crosslinking. However in the applications of interest the dose rates should be lower than those tested which implies that there should be less crosslinking and the damage should primarily be due to scission and oxidation. This indicates that the overall damage should be lower for the real-world applications.

Finally, a simple model was created to determine the scission damage caused by radiation on organic chains. It has been compared to a similar model by Charlesby with absolute errors lower than 0.15. It improves on a previous model by Charlesby by eliminating the need for determining the probability of a C-C break for a given dose of radiation for each radiation source. The model in this dissertation uses a DPA calculation rather than the probability of a C-C break by using the radiation flux and scattering cross sections of carbon. This makes the model significantly more general than the Charlesby model and makes it easier to use in different applications. Additionally, the scission model was used to try to extrapolate the change in the latent heat of PCMs that were irradiated in the MSTR. It was found that the current model shows little change in the latent heat with the doses used in these papers. This is consistent with the data from MUC and MSTR however is less true with the data from MURR. This difference is likely due to the much higher radiation dose rate at MURR where the assumption that crosslinking and recombination is negligible may not be valid.

3.2. FUTURE WORK

It would be advantageous to test other materials' radiation resistance, especially ones applicable for the nuclear reactor passive safety applications such as Stearic Acid that

has a much narrower melting peak. In addition, it could be beneficial to test these materials and others at higher total doses and at additional dose rates to determine how much of an effect dose rate has on the change in latent heat.

The main reason cross linking was excluded from the model that was developed was a lack of information on the probability for a free radical produced by radiation damage to develop a crosslink. It would be very beneficial to add this to the model to improve the prediction of the latent heat from the radiation damage. Potential experiments to determine this parameter were proposed in the paper.

APPENDIX A.

MATLAB CODE USED FOR CHAIN DISTRIBUTION MODELING

This is the MATLAB code used to evaluate the damage in the MSTR after 6, 12, 18, 24, 30, and 36 minutes. It uses a function called damagemodeldataV2 that is included under it. The main purpose of this part is to initialize the necessary information for the function, to find the percent of each molecule in the mixture, and to superimpose the data for each molecule for each distribution.

```
%Ryan Steere
%EMPaLA damage model
clear
clc

%Energy range MeV
E=0:0.0001:10;
%carbon mass in amu
Carmass=12.0107;
%hydrogen mass in amu
Hydmass=1.0078;
%Neutron mass in amu
Neutmass=1.008664;
%energy needed to break a C –C bond
BreakEng=6.23864517488E –6; %MeV
%energy needed to break a C –H bond
DisEn=4.99E –6; %MeV
%name of the flux data
fluxdata='MSTRfluxprofilemcnp.xlsx';
%name of the carbon cross section file
carcrsection='CxsData.txt';
%methylpalmitate chainlength
ChainlengthMP=16;
ChainlengthLA=12;
%irradiation time in sec
Irradiationtime=[1,2,3,4,5,6]*6*60;
%percent of MP in the Eutectic
MPperw=60/100;
%percent of LA in the Eutectic
LAperw=1 –MPperw;

C=Carmass;
H=Hydmass;
O=15.999;
```

```
MPmolmass=C*17+H*34+O*2;
LAmolmass=C*12+H*24+O*2;
MPper=MPperw/MPmolmass/(MPperw/MPmolmass+LAperw/LAmolmass);
LAper=LAperw/LAmolmass/(MPperw/MPmolmass+LAperw/LAmolmass);

tic
%calculates for Methyl Palmitate
for i=1:length(Irradiationtime)
   [damagedisthold, chainlenghold,
CPDFhold]=damagemodeldataV2(Carmass,Neutmass,BreakEng,carcrsection,ChainlengthMP,Irradiationtime(i),fluxdata);
   MPdamagedist(i,:)=damagedisthold;
   MPchainleng(i,:)=chainlenghold;
   MPCPDF(i,:)=CPDFhold;

end
toc

tic
%calculates for Lauric Acid
for i=1:length(Irradiationtime)
   [damagedisthold, chainlenghold,
CPDFhold]=damagemodeldataV2(Carmass,Neutmass,BreakEng,carcrsection,ChainlengthLA,Irradiationtime(i),fluxdata);
   LAdamagedist(i,:)=damagedisthold;
   LAchainleng(i,:)=chainlenghold;
   LACPDF(i,:)=CPDFhold;
end
toc

% calculates the values for the Eutectic

damagedist=MPdamagedist*MPper;
chainleng=MPchainleng*MPper;

damagedist(:,1:size(LAdamagedist,2))=damagedist(:,1:size(LAdamagedist,2))+LAdamagedist*LAper;
chainleng(:,1:size(LAchainleng,2))=chainleng(:,1:size(LAchainleng,2))+LAchainleng*LAper;


% Creates a cummulative probabilty density function
CPDF(:,1)=chainleng(:,1);
for i=2:ChainlengthMP
CPDF(:,i)=chainleng(:,i)+CPDF(:,i-1);
end
```

```
%normalizes that CPDF function
for i=1:length(CPDF)
   CPDF(:,i)=CPDF(:,i)./CPDF(:,end);
end

k=0:1:ChainlengthMP;

p.MarkerIndices=1:1:damagedist(1,:);
figure(1)
p=plot(k,damagedist(1,:),' –or');
hold on
p=plot(k,damagedist(2,:),' –sy');
p=plot(k,damagedist(3,:),' –*g');
p=plot(k,damagedist(4,:),' –xb');
p=plot(k,damagedist(5,:),' –dm');
p=plot(k,damagedist(6,:),' –hk');
hold off
title('Probability Density of a Given Number of Chain Scissions')
ylabel('Probability Density')
ylim([0 1])
xlabel('Carbons Displaced per Molecule')
legend('6min Irradiation', '12min Irradiation', '18min Irradiation', '24min Irradiation',
'30min Irradiation', '36min Irradiation')
set(gca,'FontName','Times New Roman')

markerspace=1;

l=1:1:ChainlengthMP;
figure(2)
p=plot(l,chainleng(1,:),' –or');
p.MarkerIndices=1:markerspace:length(chainleng(1,:));
hold on
p=plot(l,chainleng(2,:),' –sy');
p.MarkerIndices=1:markerspace:length(chainleng(1,:));
p=plot(l,chainleng(3,:),' –*g');
p.MarkerIndices=1:markerspace:length(chainleng(1,:));
p=plot(l,chainleng(4,:),' –xb');
p.MarkerIndices=1:markerspace:length(chainleng(1,:));
p=plot(l,chainleng(5,:),' –dm');
p.MarkerIndices=1:markerspace:length(chainleng(1,:));
p=plot(l,chainleng(6,:),' –hk');
p.MarkerIndices=1:markerspace:length(chainleng(1,:));
hold off
title('Probability Density of Chain Length Distribution after Irradiation')
ylabel('Probability Density')
ylim([0 1])
```

```
xlabel('Carbon Atoms')
legend('6min Irradiation', '12min Irradiation', '18min Irradiation', '24min Irradiation',
'30min Irradiation', '36min Irradiation')
set(gca,'FontName','Times New Roman')

figure(3)
p=plot(l,CPDF(1,:),' –or');
p.MarkerIndices=1:markerspace:length(CPDF(1,:));
hold on
p=plot(l,CPDF(2,:),' –sy');
p.MarkerIndices=1:markerspace:length(CPDF(1,:));
p=plot(l,CPDF(3,:),' –*g');
p.MarkerIndices=1:markerspace:length(CPDF(1,:));
p=plot(l,CPDF(4,:),' –xb');
p.MarkerIndices=1:markerspace:length(CPDF(1,:));
p=plot(l,CPDF(5,:),' –dm');
p.MarkerIndices=1:markerspace:length(CPDF(1,:));
p=plot(l,CPDF(6,:),' –hk');
p.MarkerIndices=1:markerspace:length(CPDF(1,:));
hold off
title('Cumulative Probability of Chain Length Distribution')
ylabel('Cumulative Probability Density')
ylim([0 1])
xlabel('Carbon Atoms')
legend( '6min Irradiation', '12min Irradiation', '18min Irradiation', '24min Irradiation',
'30min Irradiation', '36min Irradiation')
set(gca,'FontName','Times New Roman')
```

This is the function that does the bulk of the work. It calculates the damage distribution and chain length distributions for each molecule by utilizing a DPA model. For this particular version it calculates these values based off data of a flux spectrum a separate function would be used if the flux can be estimated by a function.

```
function [damagedist, chainleng, CPDF]=damagemodeldataV2(targetmass,...
   projmass,BreakEng,Cross,Chainlength,Time,fluxprofile)

% this code statistically determines the damage that will be caused in an
% organic molecule utilizing the concept of DPA. It assumes both a Watt
% fission spectrum and that the events will happen indepently as well as
% that the damage will follow a poisson distribution and that the chain
% distribution will follow a modified exponential distribution

% inputs are
```

```
% E = Energy range and step size in MeV
% fluxtotal= the total flux of the system n/cm^2 –s
% targetmass= mass of the target element in amu
% projmass= mass of the projectile hitting target amu
% BreakEng= Energy needed to break the bond
% Cross = the file name for the approriate cross section
% chainlength= number of atoms in chain
% Time = irradiation time in seconds

% outputs are
% damagedist = The probability distribution of the damage per chain
% chainleng= The probability distribution of chain lengths after an
%           irradiation
% CPDF= the probability distribution of the cumulative chain lengths

% This is a probability function for the watt fission spectrum which is
% integrated from 0 to the max energy to normalize and then setup the
% total flux distribution
flux=xlsread(fluxprofile);
fluxenergy=flux(:,1);
fluxvalue=flux(:,2);
fluxvalue=filter(ones(20,1)./20,1,fluxvalue);

% fluxvalue=filter(ones(1,10)/10,1,fluxvalue);
% fluxvalue=fluxvalue./sum(fluxvalue)*norm;

%gamma value for a target/proj interaction
gamma=4*targetmass*projmass/(targetmass+projmass)^2;

%reads in cross section data
Cxs=dlmread(Cross);

%turns cross section energy into MeV
CE=Cxs(:,1).*10^ –6;

%This turns cross section data into cm^2
Cxs=Cxs(:,2).*10^ –24;

% calculates the integral with respect to Flux * E* Cross section
% numerically by interpolating the cross section linearly between points
j=1;
while CE(j)<fluxenergy(1)
   j=j+1;
end
Coeff= polyfit([CE(j-1) CE(j)], [Cxs(j-1) Cxs(j)], 1);
m = Coeff(1);
```

```
b = Coeff(2);
Coeff2= polyfit([fluxenergy(1) fluxenergy(2)], [fluxvalue(1) fluxvalue(2)], 1);
m2=Coeff2(1);
b2=Coeff2(2);
DPAEQ=@(E)(m2*E+b2).*(m*E+b).*E;
Fluxener(1)=integral(DPAEQ,0,fluxenergy(1));
for i=2:max(size(fluxvalue))

    Coeff2= polyfit([fluxenergy(i-1) fluxenergy(i)], [fluxvalue(i-1) fluxvalue(i)], 1);
    m2=Coeff2(1);
    b2=Coeff2(2);


    check=0;
    j=0;
    while check<fluxenergy(i-1)
       j=j+1;
       check=CE(j);
    end
    k=j-1;
    while check<fluxenergy(i)
       j=j+1;
       check=CE(j);
    end
    Coeff = polyfit([CE(k) CE(j)], [Cxs(k) Cxs(j)], 1);
    m = Coeff(1);
    b = Coeff(2);

    DPAEQ=@(E)(m2*E+b2).*(m*E+b).*E;
    Fluxener(i)=integral(DPAEQ,fluxenergy(i-1),fluxenergy(i));

end

% Calculates the DPA/s of the radiation in the material
DPAperS=sum(Fluxener)*gamma/(BreakEng);

% Calculates DPA for each irradiation time
DPA=DPAperS*Time;

% Calculates the damage per chain for each irradiation time
DPC=DPA*Chainlength;

% creates the damage per chain distribution of the irradiation
% k is the number of damage incidents per chain
k=0:1:Chainlength;
damagedist=exp( –DPC)*(DPC).^k./factorial(k);
```

```
% number of carbons in a chain length
l=1:1:Chainlength;

% % this makes the normalization constant for the chain length distribution
% % by integrating from 1 to inf the chain length dist
% chainlengcheck=@(l) DPA*exp( –DPA.*l);
% normcconstant=1/integral(chainlengcheck,1,inf);
%
%this calculates the full distribution
chainlengeq=@(l) (DPA.*exp( –DPA.*l));%.*normcconstant;
chainleng(1,:)=chainlengeq(l);

% any chain lengths greater than the max are summed into the max chain
% length
chainleng(1,Chainlength)=integral(chainlengeq,Chainlength,inf);

chainleng=chainleng/sum(chainleng);

% Creates a cummulative probabilty density function for chain length
CPDF(1,1)=chainleng(1);
for i=2:Chainlength
CPDF(1,i)=chainleng(1,i)+CPDF(1,i-1);
end

end
```

APPENDIX B.

RAW DATA DSC AND RAMAN DATA

The following tables show the DSC sample masses for each irradiation and what power they were irradiated at as well as where they were irradiated.

No Irradiation

Sample masses (mg)	EMPaLA	E-NP	PEW
sample 1	21.8	23.2	11.1
sample 2	17.5	13.5	13.3
sample 3	13.9	11.2	13.3
sample 4	11.5	17.8	7.7
sample 5	14.3	24.6	10.9
sample 6	23.1	12.4	12.9

MSTR Irradiation 1

Sample masses (mg)	EMPaLA		E-NP		PEW	
Reactor Power	100kW	180kW	100kW	180kW	100kW	180kW
sample 1	23.999	21.5	24.628	28.6	8	13.2
sample 2	30.5	15.4	26.796	19.8	10.1	14.2
sample 3	19.3	10.8	33.1	19.7	4.8	11.4
sample 4	23.1	26.5	12.7	28.7	16.1	9.77
sample 5	18.7	21.9	27	23.5	12.88	16.3
sample 6	26.2	19.86	19.4	21.6	9.6	9.2

MSTR Irradiation 2

Sample masses (mg)	EMPaLA		E-NP		PEW	
Reactor Power	100kW	180kW	100kW	180kW	100kW	180kW
sample 1	16.8	22.9	26.3	23.2	16.2	13.2
sample 2	28.283	16.3	22.4	33.9	10.8	5.4
sample 3	20.351	18.5	27	23.6	11.1	10.9
sample 4	31.8	18.5	18	20.7	9.35	14.7
sample 5	17.4	16.1	20	26.1	8.961	10.4
sample 6	18	25.5	15.7	15.8	9.419	16

MSTR Irradiation 3

Sample masses (mg)	EMPaLA		E-NP		PEW	
Reactor Power	100kW	180kW	100kW	180kW	100kW	180kW
sample 1	18.7	10.4	23.134	25.2	8.1	9.6
sample 2	16.2	19.2	21.288	13	9.3	11.8
sample 3	25.4	7.9	23.676	13	7.098	6.9
sample 4	12.8	12.3	18.5	21.745	7.291	5.8
sample 5	15.3	15	16.7	17.402	11	7.9
sample 6	15.3	18.07	18.8	8.35	12.1	7.3

MSTR Irradiation 4

Sample masses (mg)	EMPaLA		E-NP		PEW	
Reactor Power	100kW	180kW	100kW	180kW	100kW	180kW
sample 1	15	15.3	17.5	20.7	8.5	12.283
sample 2	13.7	10.3	24.5	17.3	15.6	9.749
sample 3	17.5	8.1	16.227	12.7	12.2	6.3
sample 4	19.2	20.3	18.244	13.6	11.5	7.2
sample 5	15.1	7.1	13.384	12.7	16.5	9.4
sample 6	13.3	23.7	14.9	24.7	8.4	6.1

MSTR Irradiation 5

Sample masses (mg)	EMPaLA		E-NP		PEW	
Reactor Power	100kW	180kW	100kW	180kW	100kW	180kW
sample 1	24	8.1	16.7	18.685	10	7.3
sample 2	28.8	7.2	8.9	16.2	6.244	5.7
sample 3	16.3	14.85	20.3	16.1	10.948	6.3
sample 4	8.5	10.6	16.09	17.618	15.7	5.205
sample 5	10.931	10.9	20.79	15	4	4.3
sample 6	7.921	13.8	12.5	17.563	5.9	8.9

MSTR Irradiation 6

Sample masses (mg)	EMPaLA		E-NP		PEW	
Reactor Power	100kW	180kW	100kW	180kW	100kW	180kW
sample 1	20.4	14.747	15.6	19.6	9.9	16.9
sample 2	15.9	21.435	14.1	27.36	15.5	11.6
sample 3	12.1	13.87	18.4	31.5	14.1	12.6
sample 4	11.8	19.6	15.3	15.026	10.9	5.345
sample 5	19	17	18.4	16.12	11.3	10.95
sample 6	18.4	13.1	15.9	15.315	8.5	7.3

MUC

Sample masses (mg)	EMPaLA	PEW
sample 1	28.3	15.3
sample 2	27.2	10.8
sample 3	20.5	11.2

MURR

Sample masses (mg)	EMPaLA	PEW
sample 1	17.1	10.0
sample 2	18.4	17.4
sample 3	–	19.3

Raw DSC data for all measurements including melting temperature in °C (MT) and latent heat in J/g (LH). For PEW, the point of maximum heat flow (max) in °C was also added. Values with a – had either a poor curve or the algorithm for calculating melting temperature was unsuccessful due to noise in the peaks.

No Irradiation

	EMPaLA		E-NP		PEW		
	MT	LH	MT	LH	MT	LH	max
Sample1	22.56	191.9	22.7	172.7	54.35	276.5	81.03
Sample2	22.53	190	22.52	169.9	49.83	268.5	81.41
Sample3	–	205.7	22.38	185.1	49.81	244.2	81.86
Sample4	–	211.4	–	177.3	31.32	306.2	81.21
Sample5	22.63	213.4	22.55	177.5	–	270.6	81.53
Sample6	22.45	193.6	22.5	185.1	50.44	271.4	81.97

Irradiation 1-100kW

	EMPaLA		E-NP		PEW		
	MT	LH	MT	LH	MT	LH	max
Sample1	22.33	190.9	22.44	171.2	50.74	239.8	79.28
Sample2	22.29	188.5	22.34	167.1	49.38	228.9	79.72
Sample3	22.58	175.7	22.36	162.1	48.74	277.6	79.35
Sample4	22.43	204.5	22.04	163.1	49.05	250.2	80.57
Sample5	22.36	196.1	22.53	172.6	48.85	241.9	79.87
Sample6	22.45	190.3	22.46	165.6	48.92	251	79.74

Irradiation 1-180kW

	EMPaLA		E-NP		PEW		
	MT	LH	MT	LH	MT	LH	max
Sample1	22.47	192	22.47	172.2	49.37	240.9	80.55
Sample2	22.29	195.5	22.45	176.4	52.3	253.7	80.08
Sample3	22.53	194.4	22.32	169.9	49.42	242	80.04
Sample4	22.5	192.6	22.45	170.3	49.72	219	79.17
Sample5	22.51	180.4	22.44	162.9	49.16	246.6	80.32
Sample6	22.35	189.8	22.53	161.6	49.58	280.1	79.82

Irradiation 2-100kW

	EMPaLA		E-NP		PEW		
	MT	LH	MT	LH	MT	LH	max
Sample1	22.6	178.5	22.56	153.6	49.59	228.4	80.62
Sample2	22.26	180.3	22.5	66.87	50.24	228.6	80.63
Sample3	22.47	175.2	22.5	159.3	50.07	226.8	80.46
Sample4	22.33	177.5	22.43	154.4	50.64	250.4	81.22
Sample5	22.33	192.5	22.47	174.4	49.36	228.5	81.18
Sample6	22	170.6	21.99	158.1	50.7	220.3	81.11

Irradiation 2-180kW

	EMPaLA		E-NP		PEW		
	MT	LH	MT	LH	MT	LH	max
Sample1	22.14	183.3	22.63	166.1	–	230	80.83
Sample2	21.88	172.4	22.59	160.1	54.74	260	80.19
Sample3	22.57	102.7	22.53	163.5	50.05	225	80.72
Sample4	22.41	164.8	22.49	152.3	50.3	235.6	79.86
Sample5	21.56	155.5	22.43	170.5	49.57	246.9	80.91
Sample6	22.31	176.1	22.63	159.8	49.24	236.1	81.37

Irradiation 3-100kW

	EMPaLA		E-NP		PEW		
	MT	LH	MT	LH	MT	LH	max
Sample1	22.44	188.6	22.52	170.8	50.23	277.8	80.58
Sample2	21.85	189.5	22.47	183	50.08	292.2	81.26
Sample3	22.31	181.4	22.51	176.3	49.56	300.8	81.24
Sample4	22.09	191.5	22.49	164.9	50.46	323.2	81.36
Sample5	22.17	192	22.52	185.9	–	261.6	79.69
Sample6	22.18	188.9	22.53	163.7	59.97	249.8	81.31

Irradiation 3-180kW

	EMPaLA		E-NP		PEW		
	MT	LH	MT	LH	MT	LH	max
Sample1	22.18	186.2	22.57	170.1	51.33	292	82.02
Sample2	22.36	187.8	22.6	182.9	49.76	295.3	81.55
Sample3	–	–	22.57	194.2	49.87	301.2	80.96
Sample4	21.91	194.4	22.39	175.3	50.28	296.7	81.31
Sample5	22.47	199.4	22.5	182.8	49.8	296.7	81.38
Sample6	22.44	194.4	22.54	183.5	49.52	296.6	80.82

Irradiation 4-100kW

	EMPaLA		E-NP		PEW		
	MT	LH	MT	LH	MT	LH	max
Sample1	22.17	195.6	22.26	184.3	51.86	274.8	81.42
Sample2	21.42	180.7	22.39	161.1	50.13	286.3	81.35
Sample3	22.17	171.5	22.45	164.5	52.97	258.5	82.33
Sample4	22.38	189.4	22.23	152.7	76.83	256.7	80.37
Sample5	22.21	180.5	22.19	179.2	80.71	253	82.44
Sample6	22.3	187.2	22.1	167.1	59.13	290.2	85.21

Irradiation 4-180kW

	EMPaLA		E-NP		PEW		
	MT	LH	MT	LH	MT	LH	max
Sample1	22.23	200.1	–	169.1	54.65	276.2	81.32
Sample2	22.15	175.2	22.35	178.9	48.86	279.1	81.92
Sample3	22.34	204.7	22.28	163.9	48.31	291.2	81.73
Sample4	22.23	187.9	22.18	176	50.66	312.1	79.43
Sample5	21.45	203.1	22.16	184.5	48.63	311	81.56
Sample6	22.39	183.6	22.18	179	48.41	328.1	81.47

Irradiation 5-100kW

	EMPaLA		E-NP		PEW		
	MT	LH	MT	LH	MT	LH	max
Sample1	21.93	190.9	22.14	173.8	–	261.4	81.19
Sample2	21.81	188.4	21.33	162.6	48.57	269.5	80.49
Sample3	22.17	194	21.7	163.3	49.36	242.8	81.29
Sample4	22.25	214.8	21.82	169.7	48.51	248.7	81.8
Sample5	21.77	202.9	21.87	163.8	48.89	300.1	81.02
Sample6	22.22	193.5	22.13	162.9	48.81	257.2	80.59

Irradiation 5-180kW

	EMPaLA		E-NP		PEW		
	MT	LH	MT	LH	MT	LH	max
Sample1	22.11	227.3	22.08	170.5	48.96	268	80.73
Sample2	22.07	205	22.02	172.4	50.11	289.8	79.39
Sample3	22.17	191.4	22.26	169.9	48.79	278.6	81.27
Sample4	22.12	215.4	21.64	166.2	49.27	295.7	80.44
Sample5	22.13	217.3	22.19	176.4	49.37	279.3	80.69
Sample6	22.33	199.5	22.19	181.6	49.05	257.9	81.27

Irradiation 6-100kW

	EMPaLA		E-NP		PEW		
	MT	LH	MT	LH	MT	LH	max
Sample1	20.6	172	22.1	179.7	49.72	265.9	79.48
Sample2	21.7	180.6	22.21	175.9	49.11	277.2	81.62
Sample3	21.91	190.9	22.09	164.9	49.11	261.1	81.34
Sample4	22.13	197.6	21.95	163.2	48.89	264.3	81.16
Sample5	22.02	183	22.12	163.8	48.54	270.4	81.25
Sample6	21.74	190.6	21.94	167.2	48.56	290.6	80.87

Irradiation 6-180kW

	EMPaLA		E-NP		PEW		
	MT	LH	MT	LH	MT	LH	max
Sample1	21.98	187	21.97	169.1	48.58	265.6	80.81
Sample2	21.4	187.8	21.96	180.2	48.09	292.9	81.2
Sample3	22	193.7	21.99	168.1	48.96	274.8	81.7
Sample4	22.03	192.4	22.09	170.6	48.61	289.2	80.93
Sample5	22.05	192.6	22.03	176	48.63	265	80.93
Sample6	22.21	192.8	22.06	172.8	49.63	254.8	81.3

MUC

	EMPaLA		PEW		
	MT	LH	MT	LH	max
Sample1	21.56	184.4	49.83	259.5	82.47
Sample2	22.11	187.4	49.68	252.8	82.39
Sample3	21.64	193.3	50.35	271.3	82.73

MURR

	EMPaLA		PEW		
	MT	LH	MT	LH	max
Sample1	21.66	163.6	52	214.8	81.82
Sample2	22.05	162.6	50.49	234	81.53
Sample3	–	–	50.1	255.8	82.02

The following graphs are the raw thermographs from the DSC. Only the range with the important data is in each graph for EMPaLA and E-NP that is from 5 to 35 °C and for PEW that is from 5 to 105 °C

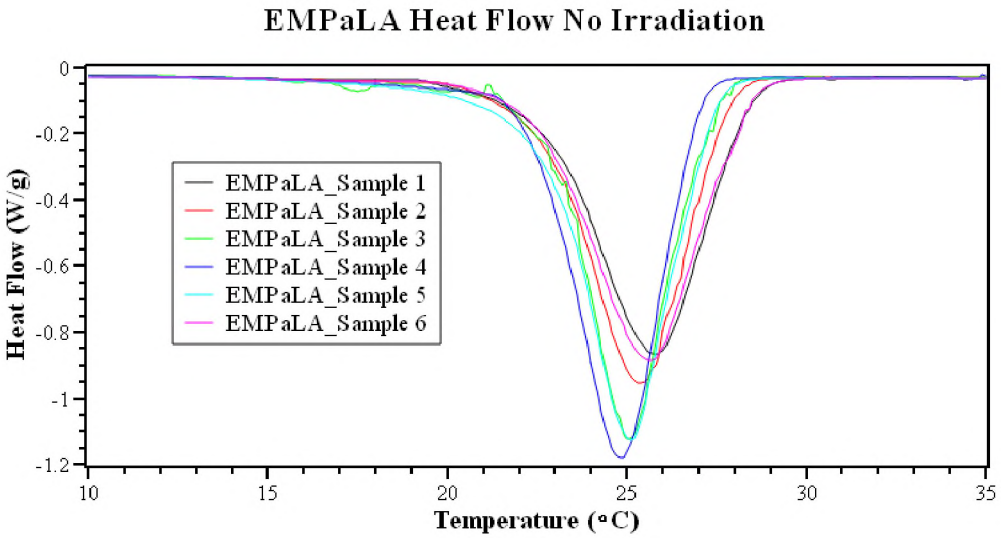

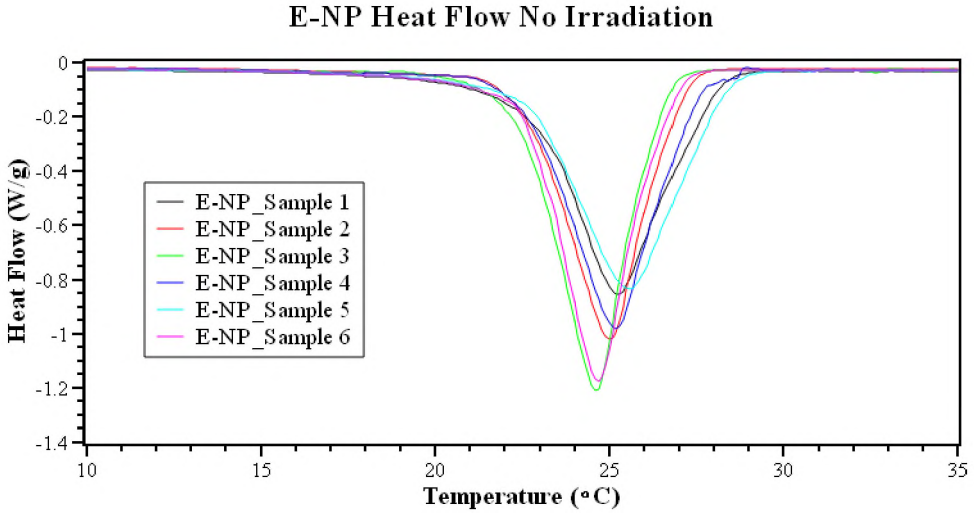

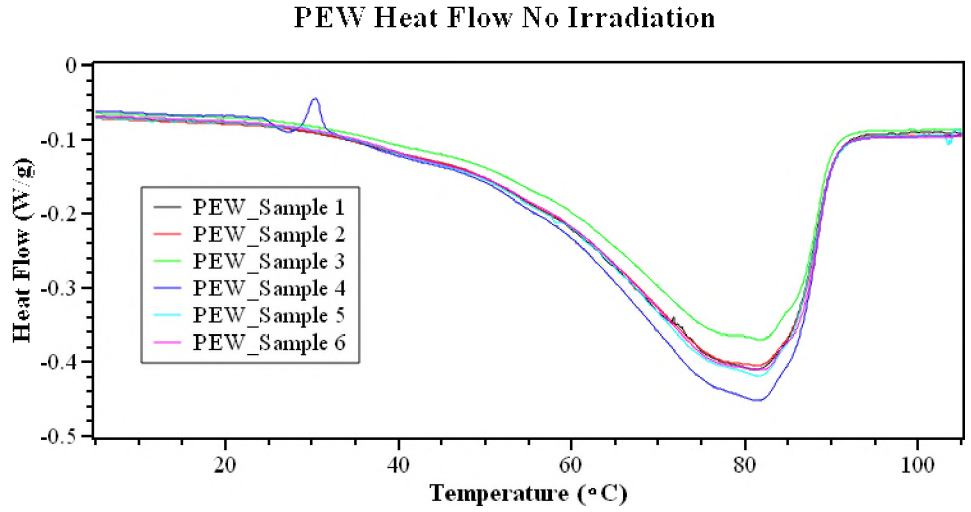
PEW Heat Flow No Irradiation
Heat Flow (W/g)
Temperature (°C)
PEW_Sample 1
PEW_Sample 2
PEW_Sample 3
PEW_Sample 4
PEW_Sample 5
PEW_Sample 6
0
-0.1
-0.2
-0.3
-0.4
-0.5
20
40
60
80
100

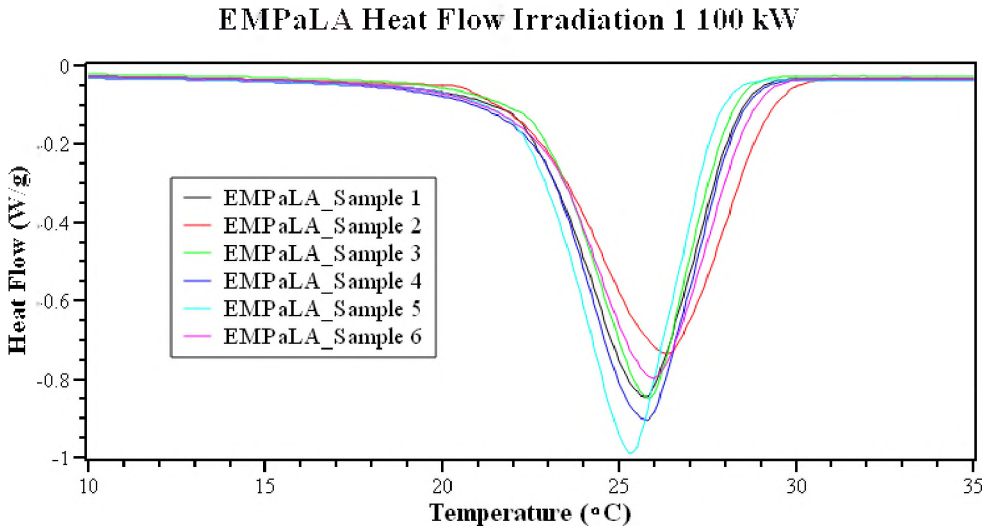
EMPaLA Heat Flow Irradiation 1 100 kW
Heat Flow (W/g)
Temperature (°C)
EMPaLA_Sample 1
EMPaLA_Sample 2
EMPaLA_Sample 3
EMPaLA_Sample 4
EMPaLA_Sample 5
EMPaLA_Sample 6
0
-0.2
-0.4
-0.6
-0.8
-1
10
15
20
25
30
35

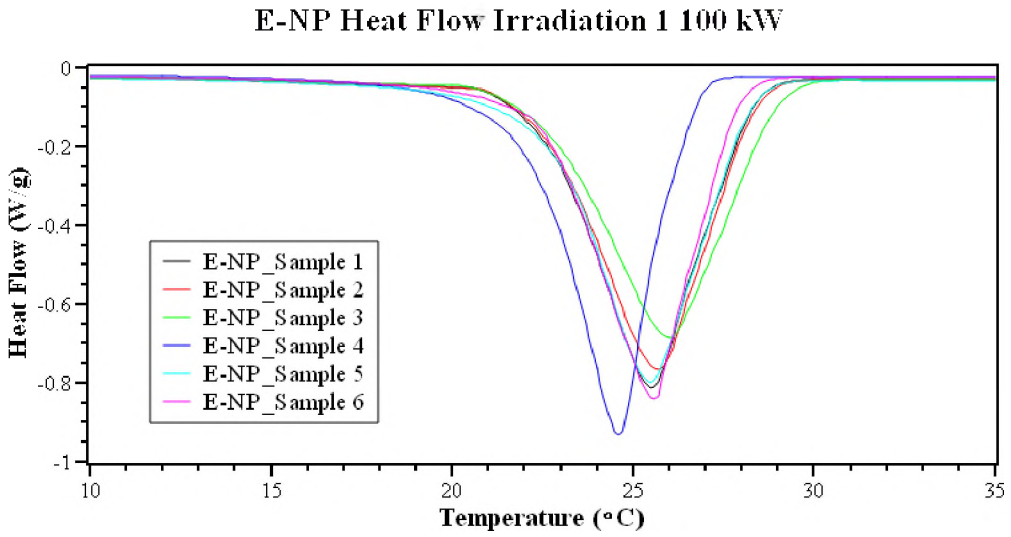
E-NP Heat Flow Irradiation 1 100 kW
Heat Flow (W/g)
Temperature (°C)
E-NP_Sample 1
E-NP_Sample 2
E-NP_Sample 3
E-NP_Sample 4
E-NP_Sample 5
E-NP_Sample 6

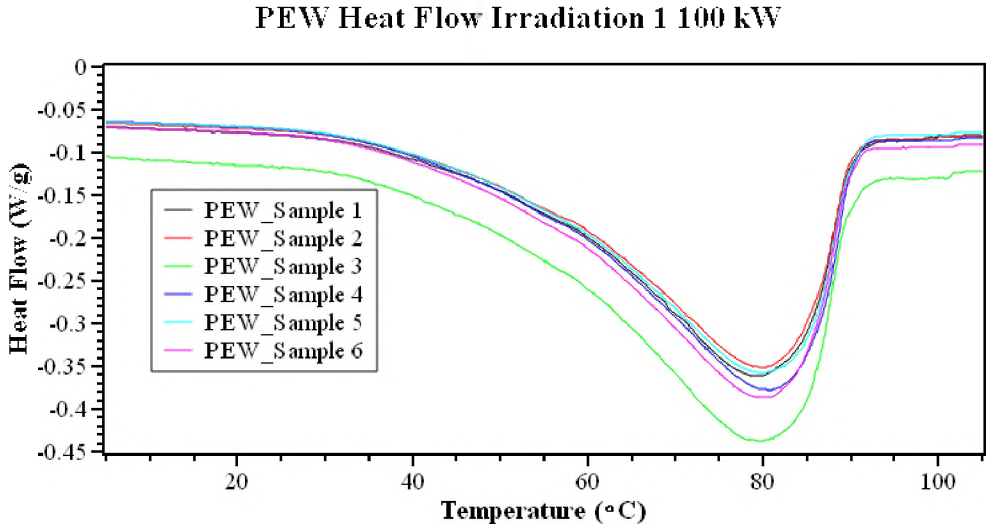
PEW Heat Flow Irradiation 1 100 kW
Heat Flow (W/g)
Temperature (°C)
PEW_Sample 1
PEW_Sample 2
PEW_Sample 3
PEW_Sample 4
PEW_Sample 5
PEW_Sample 6

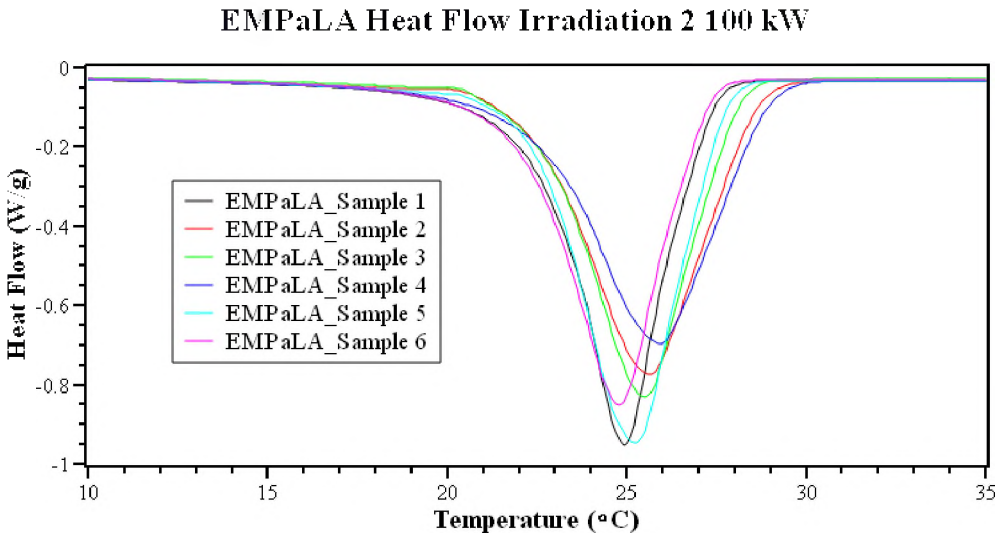
EMPaLA Heat Flow Irradiation 2 100 kW
Heat Flow (W/g)
Temperature (°C)
EMPaLA_Sample 1
EMPaLA_Sample 2
EMPaLA_Sample 3
EMPaLA_Sample 4
EMPaLA_Sample 5
EMPaLA_Sample 6

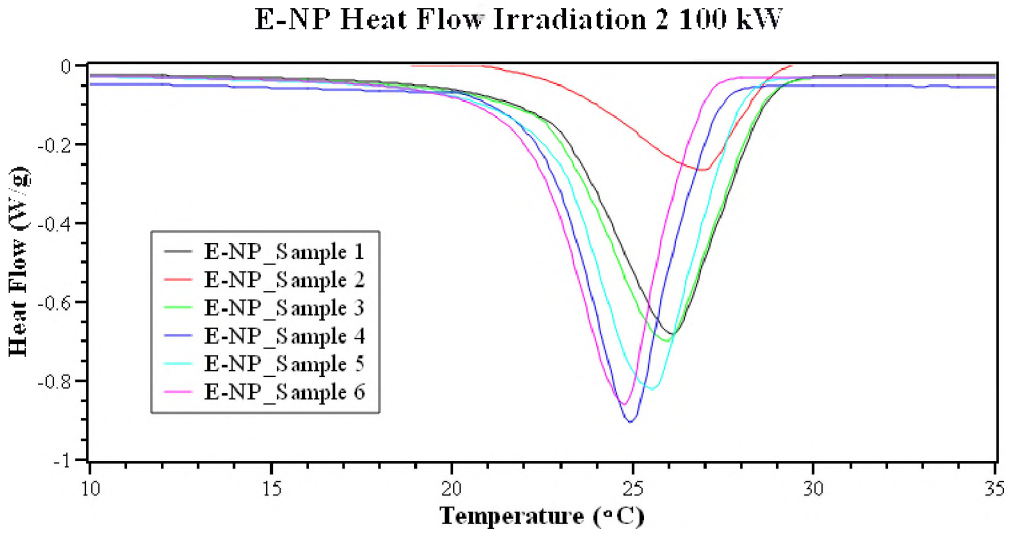
E-NP Heat Flow Irradiation 2 100 kW
Heat Flow (W/g)
Temperature (°C)
E-NP_Sample 1
E-NP_Sample 2
E-NP_Sample 3
E-NP_Sample 4
E-NP_Sample 5
E-NP_Sample 6

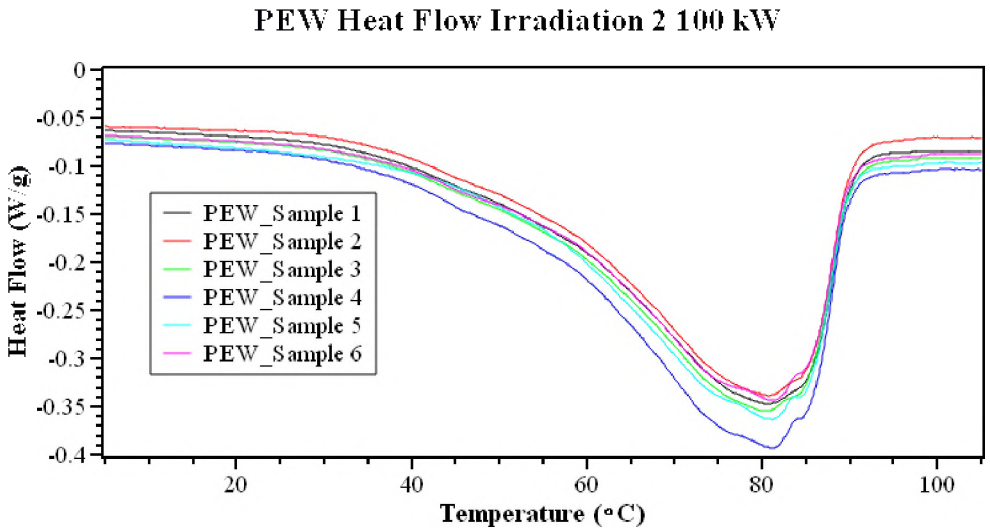
PEW Heat Flow Irradiation 2 100 kW
Heat Flow (W/g)
Temperature (°C)
PEW_Sample 1
PEW_Sample 2
PEW_Sample 3
PEW_Sample 4
PEW_Sample 5
PEW_Sample 6
0
-0.05
-0.1
-0.15
-0.2
-0.25
-0.3
-0.35
-0.4
20
40
60
80
100

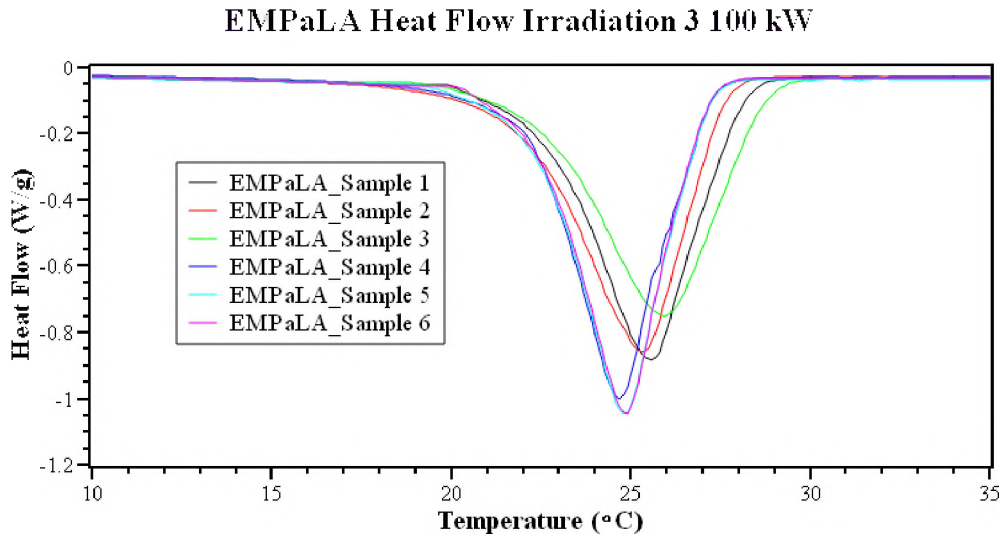
EMPaLA Heat Flow Irradiation 3 100 kW
Heat Flow (W/g)
Temperature (°C)
EMPaLA_Sample 1
EMPaLA_Sample 2
EMPaLA_Sample 3
EMPaLA_Sample 4
EMPaLA_Sample 5
EMPaLA_Sample 6
0
-0.2
-0.4
-0.6
-0.8
-1
-1.2
10
15
20
25
30
35

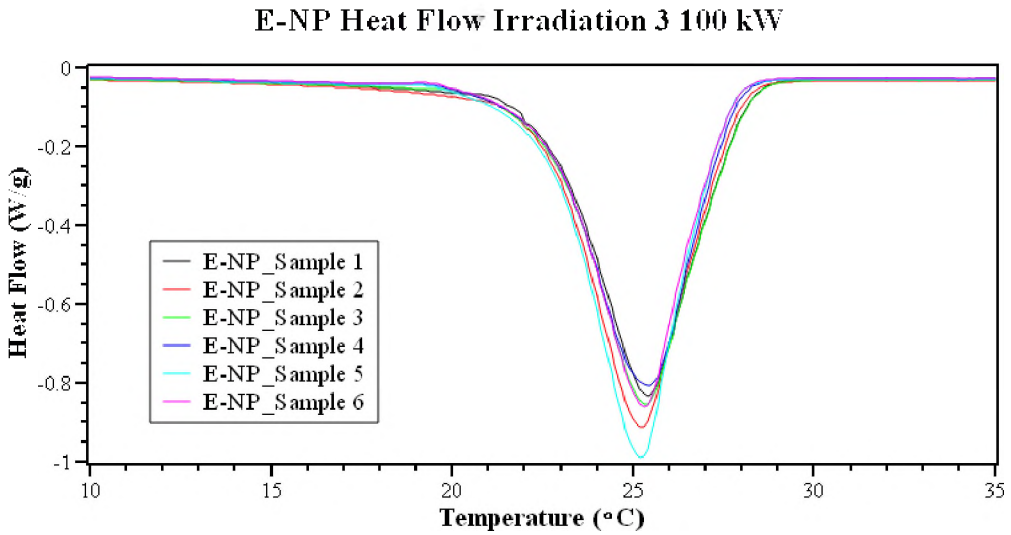
E-NP Heat Flow Irradiation 3 100 kW
Heat Flow (W/g)
Temperature (°C)
E-NP_Sample 1
E-NP_Sample 2
E-NP_Sample 3
E-NP_Sample 4
E-NP_Sample 5
E-NP_Sample 6

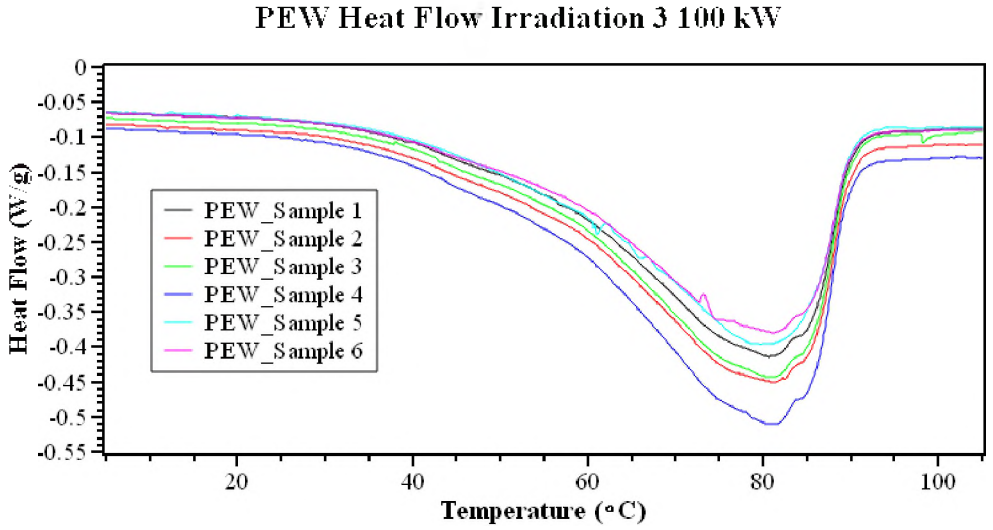
PEW Heat Flow Irradiation 3 100 kW
Heat Flow (W/g)
Temperature (°C)
PEW_Sample 1
PEW_Sample 2
PEW_Sample 3
PEW_Sample 4
PEW_Sample 5
PEW_Sample 6

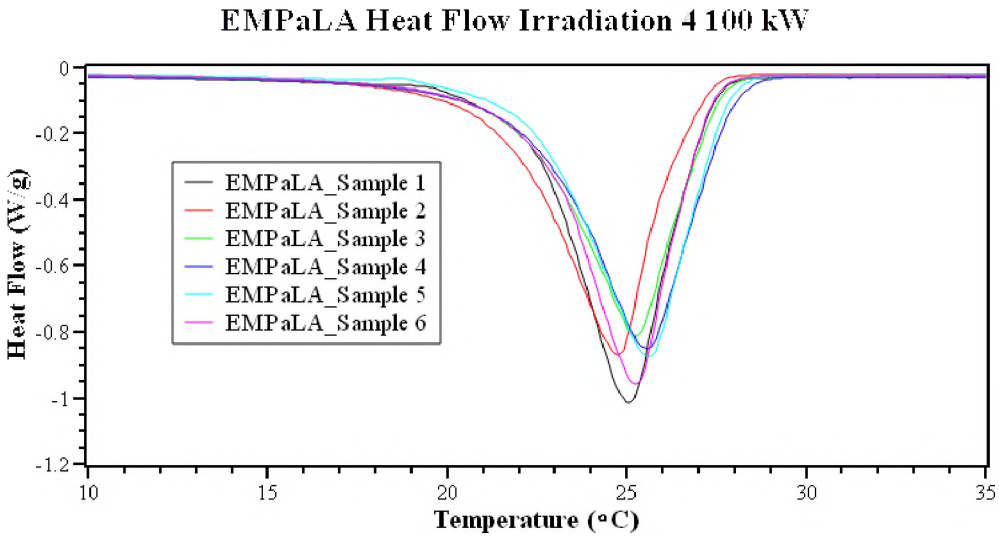
EMPaLA Heat Flow Irradiation 4 100 kW
Heat Flow (W/g)
Temperature (°C)
EMPaLA_Sample 1
EMPaLA_Sample 2
EMPaLA_Sample 3
EMPaLA_Sample 4
EMPaLA_Sample 5
EMPaLA_Sample 6

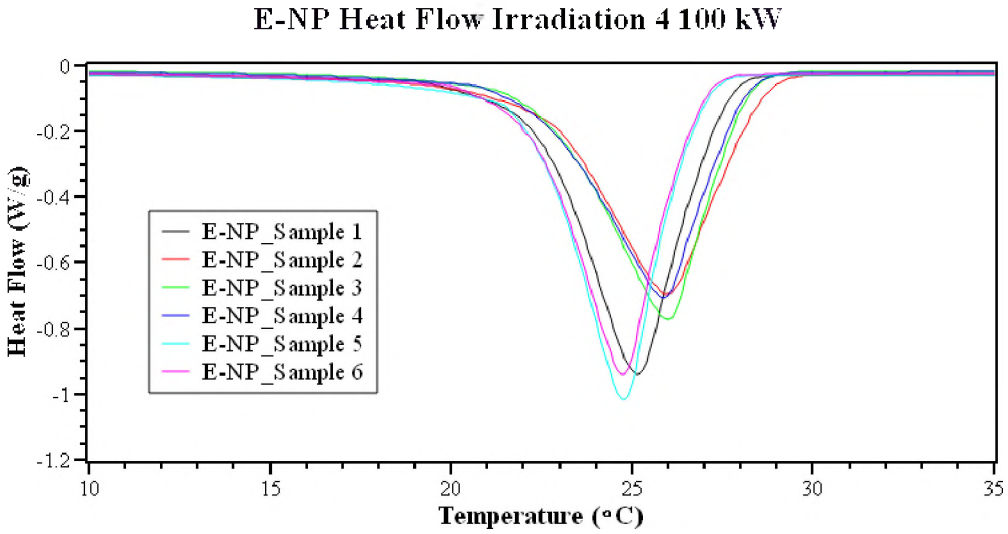
E-NP Heat Flow Irradiation 4 100 kW
Heat Flow (W/g)
Temperature (°C)
E-NP_Sample 1
E-NP_Sample 2
E-NP_Sample 3
E-NP_Sample 4
E-NP_Sample 5
E-NP_Sample 6

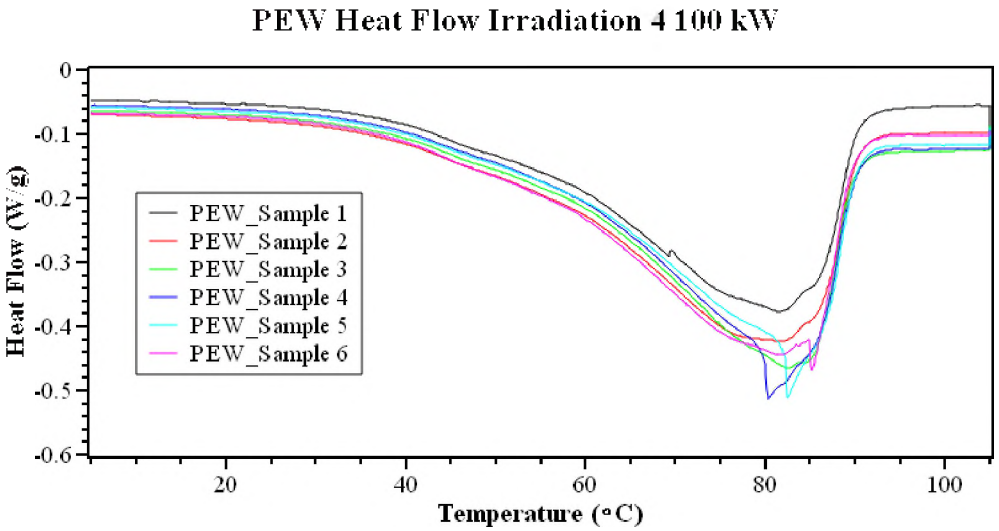
PEW Heat Flow Irradiation 4 100 kW
Heat Flow (W/g)
Temperature (°C)
PEW_Sample 1
PEW_Sample 2
PEW_Sample 3
PEW_Sample 4
PEW_Sample 5
PEW_Sample 6
0
-0.1
-0.2
-0.3
-0.4
-0.5
-0.6
20
40
60
80
100

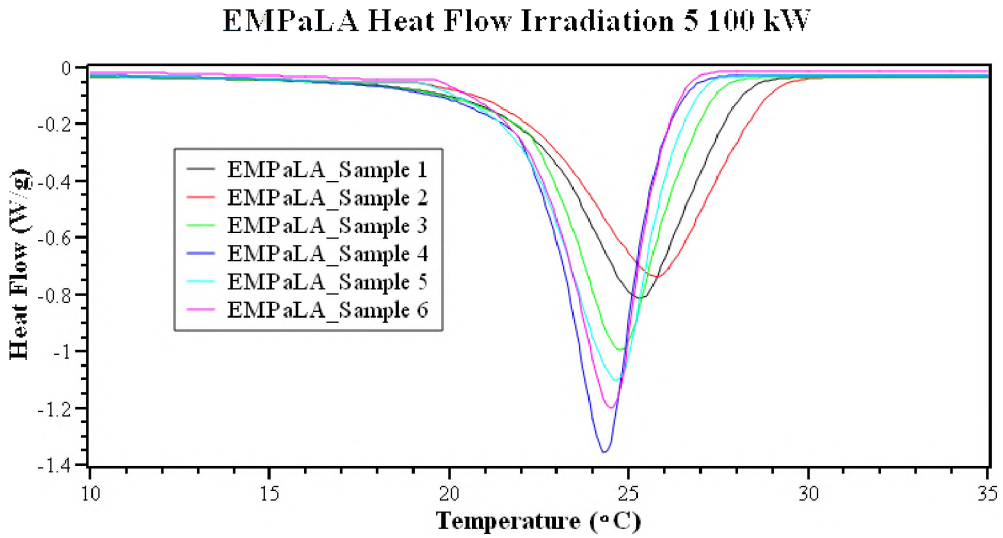
EMPaLA Heat Flow Irradiation 5 100 kW
Heat Flow (W/g)
Temperature (°C)
EMPaLA_Sample 1
EMPaLA_Sample 2
EMPaLA_Sample 3
EMPaLA_Sample 4
EMPaLA_Sample 5
EMPaLA_Sample 6
0
-0.2
-0.4
-0.6
-0.8
-1
-1.2
-1.4
10
15
20
25
30
35

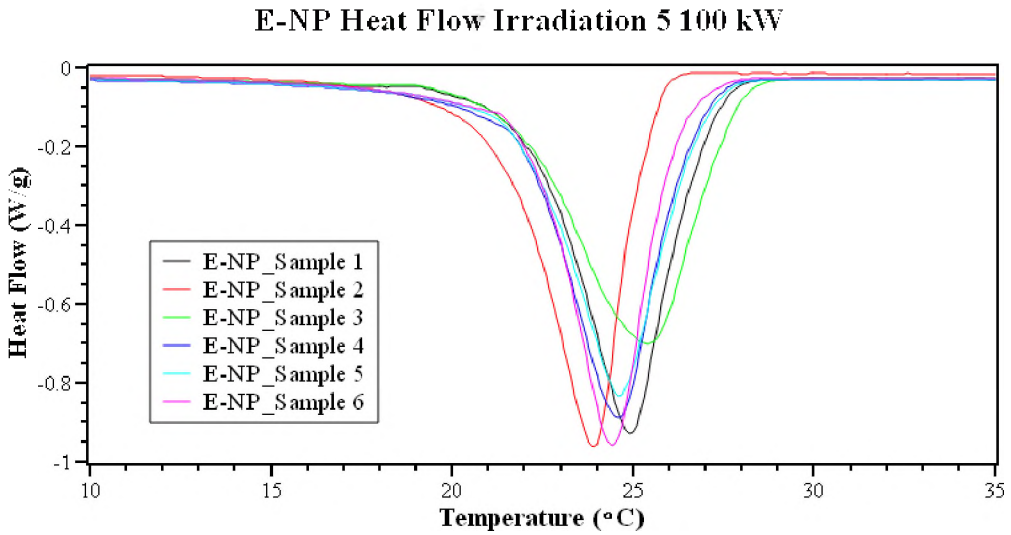
E-NP Heat Flow Irradiation 5 100 kW
Heat Flow (W/g)
Temperature (°C)
E-NP_Sample 1
E-NP_Sample 2
E-NP_Sample 3
E-NP_Sample 4
E-NP_Sample 5
E-NP_Sample 6

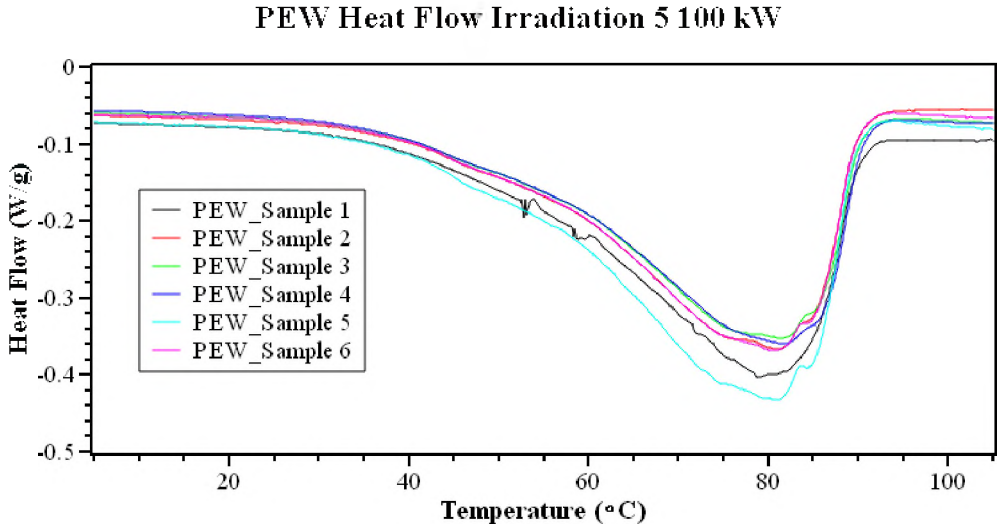
PEW Heat Flow Irradiation 5 100 kW
Heat Flow (W/g)
Temperature (°C)
PEW_Sample 1
PEW_Sample 2
PEW_Sample 3
PEW_Sample 4
PEW_Sample 5
PEW_Sample 6

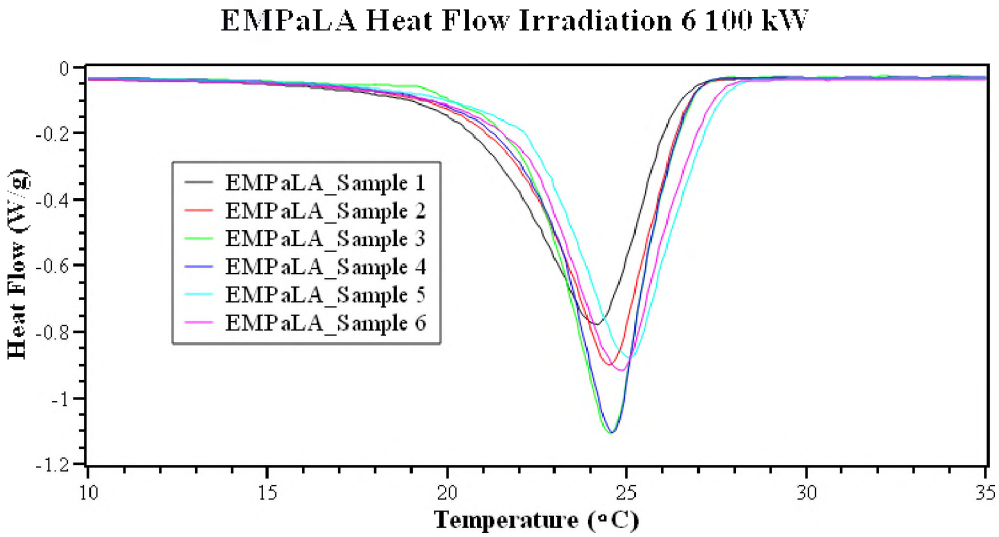
EMPaLA Heat Flow Irradiation 6 100 kW
Heat Flow (W/g)
Temperature (°C)
EMPaLA_Sample 1
EMPaLA_Sample 2
EMPaLA_Sample 3
EMPaLA_Sample 4
EMPaLA_Sample 5
EMPaLA_Sample 6

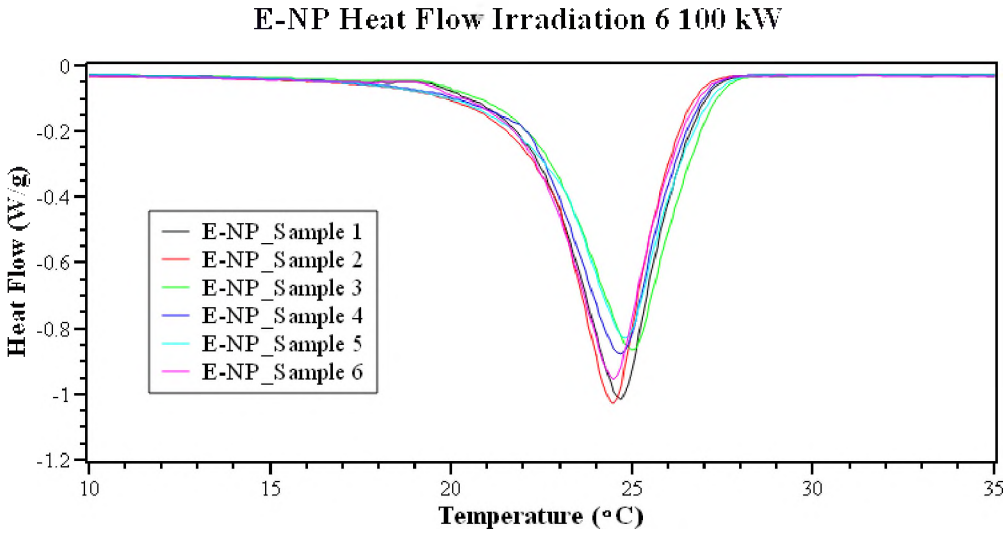
E-NP Heat Flow Irradiation 6 100 kW
Heat Flow (W/g)
Temperature (°C)
E-NP_Sample 1
E-NP_Sample 2
E-NP_Sample 3
E-NP_Sample 4
E-NP_Sample 5
E-NP_Sample 6

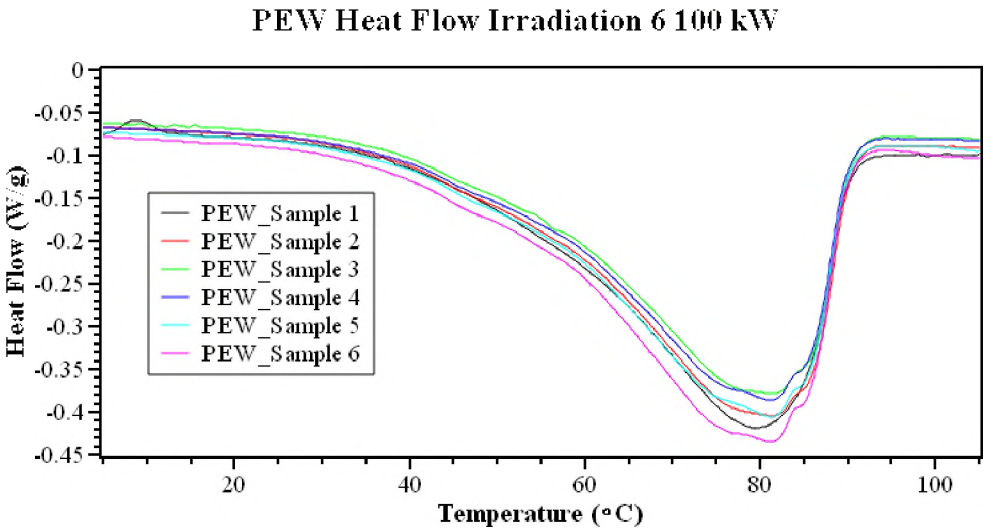
PEW Heat Flow Irradiation 6 100 kW
Heat Flow (W/g)
Temperature (°C)
PEW_Sample 1
PEW_Sample 2
PEW_Sample 3
PEW_Sample 4
PEW_Sample 5
PEW_Sample 6

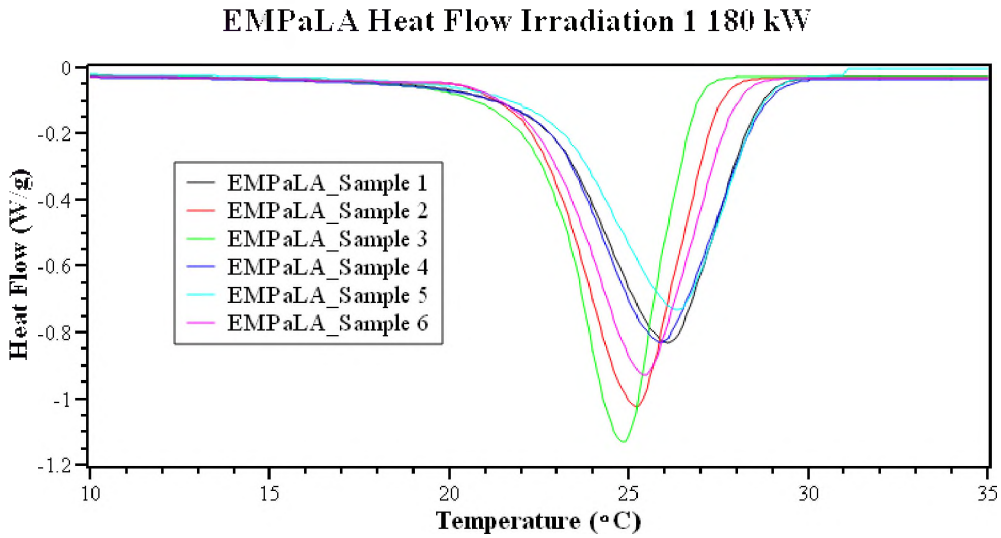
EMPaLA Heat Flow Irradiation 1 180 kW
Heat Flow (W/g)
Temperature (°C)
EMPaLA_Sample 1
EMPaLA_Sample 2
EMPaLA_Sample 3
EMPaLA_Sample 4
EMPaLA_Sample 5
EMPaLA_Sample 6

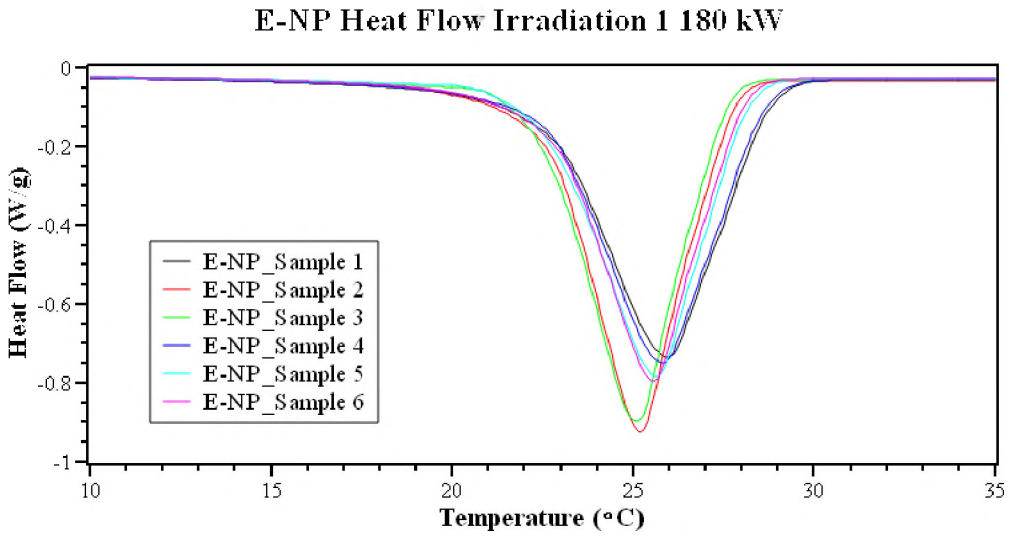
E-NP Heat Flow Irradiation 1 180 kW
Heat Flow (W/g)
Temperature (°C)
E-NP_Sample 1
E-NP_Sample 2
E-NP_Sample 3
E-NP_Sample 4
E-NP_Sample 5
E-NP_Sample 6

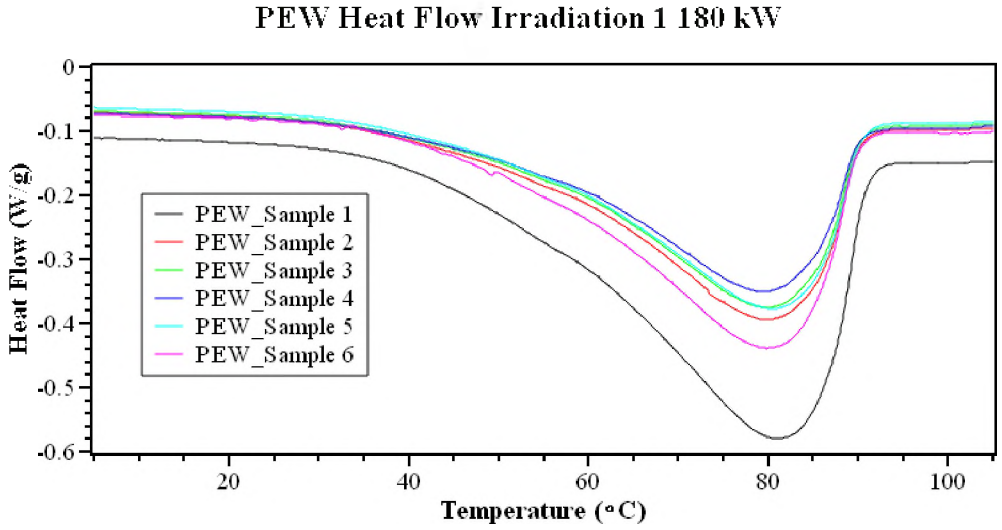
PEW Heat Flow Irradiation 1 180 kW
Heat Flow (W/g)
Temperature (°C)
PEW_Sample 1
PEW_Sample 2
PEW_Sample 3
PEW_Sample 4
PEW_Sample 5
PEW_Sample 6

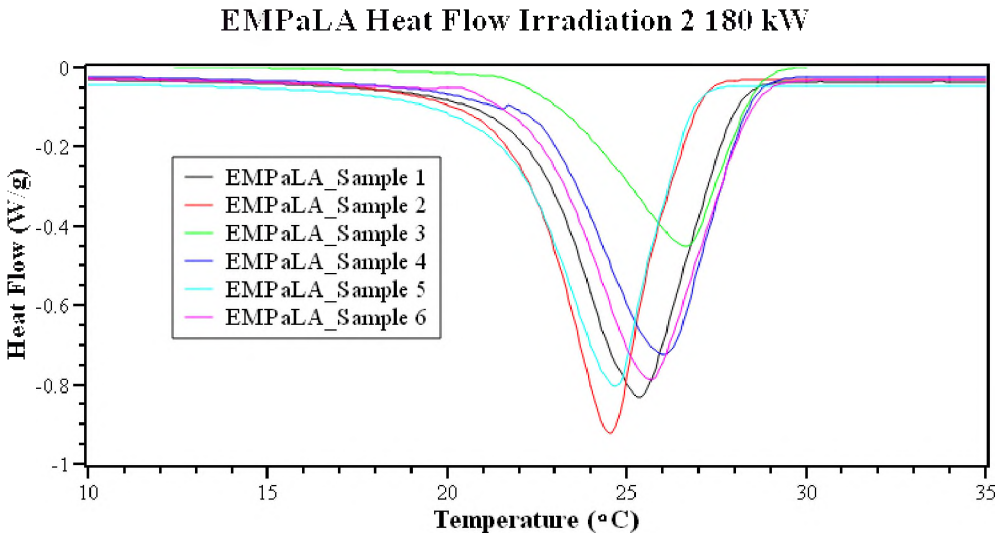
EMPaLA Heat Flow Irradiation 2 180 kW
Heat Flow (W/g)
Temperature (°C)
EMPaLA_Sample 1
EMPaLA_Sample 2
EMPaLA_Sample 3
EMPaLA_Sample 4
EMPaLA_Sample 5
EMPaLA_Sample 6

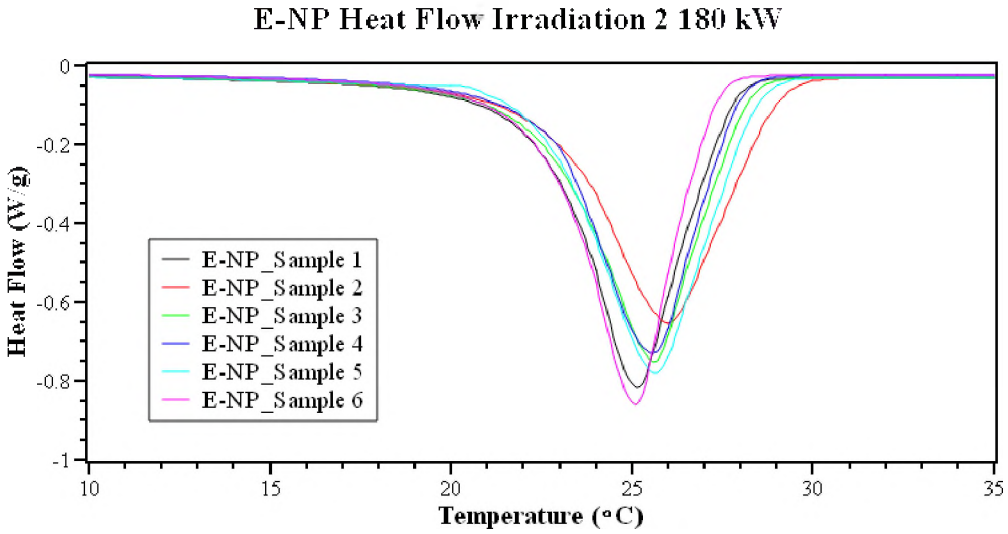
E-NP Heat Flow Irradiation 2 180 kW
Heat Flow (W/g)
Temperature (°C)
E-NP_Sample 1
E-NP_Sample 2
E-NP_Sample 3
E-NP_Sample 4
E-NP_Sample 5
E-NP_Sample 6

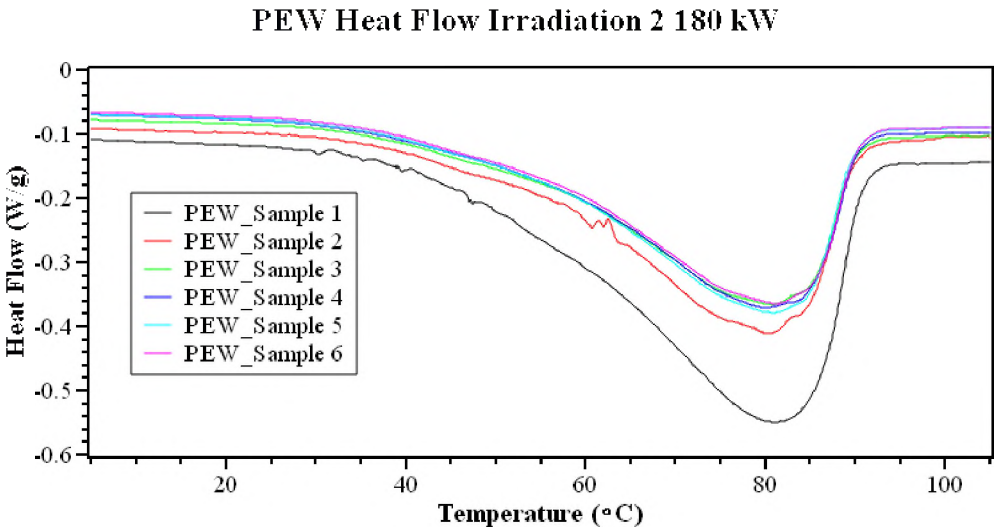
PEW Heat Flow Irradiation 2 180 kW
Heat Flow (W/g)
Temperature (°C)
PEW_Sample 1
PEW_Sample 2
PEW_Sample 3
PEW_Sample 4
PEW_Sample 5
PEW_Sample 6
0
-0.1
-0.2
-0.3
-0.4
-0.5
-0.6
20
40
60
80
100

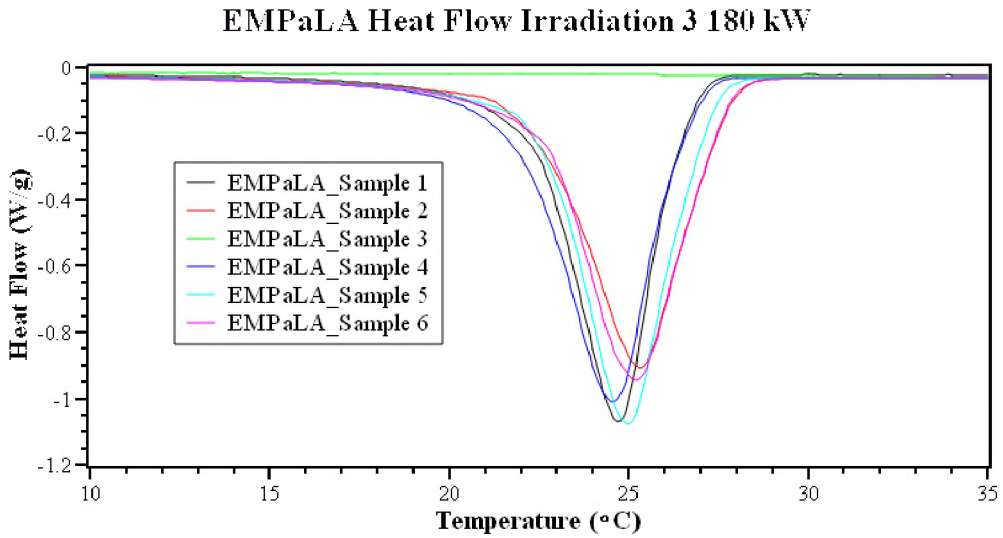
EMPaLA Heat Flow Irradiation 3 180 kW
Heat Flow (W/g)
Temperature (°C)
EMPaLA_Sample 1
EMPaLA_Sample 2
EMPaLA_Sample 3
EMPaLA_Sample 4
EMPaLA_Sample 5
EMPaLA_Sample 6
0
-0.2
-0.4
-0.6
-0.8
-1
-1.2
10
15
20
25
30
35

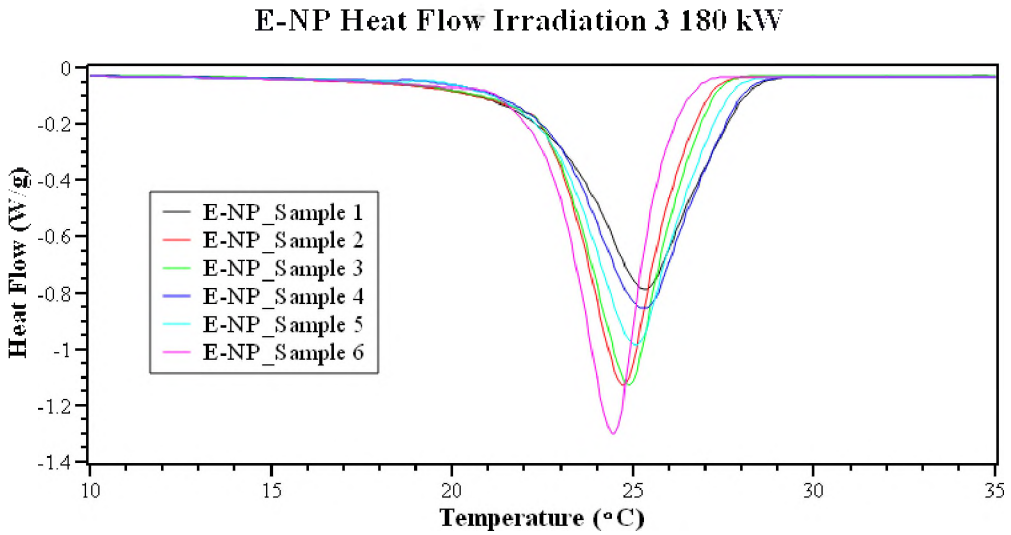
E-NP Heat Flow Irradiation 3 180 kW
Heat Flow (W/g)
Temperature (°C)
E-NP_Sample 1
E-NP_Sample 2
E-NP_Sample 3
E-NP_Sample 4
E-NP_Sample 5
E-NP_Sample 6

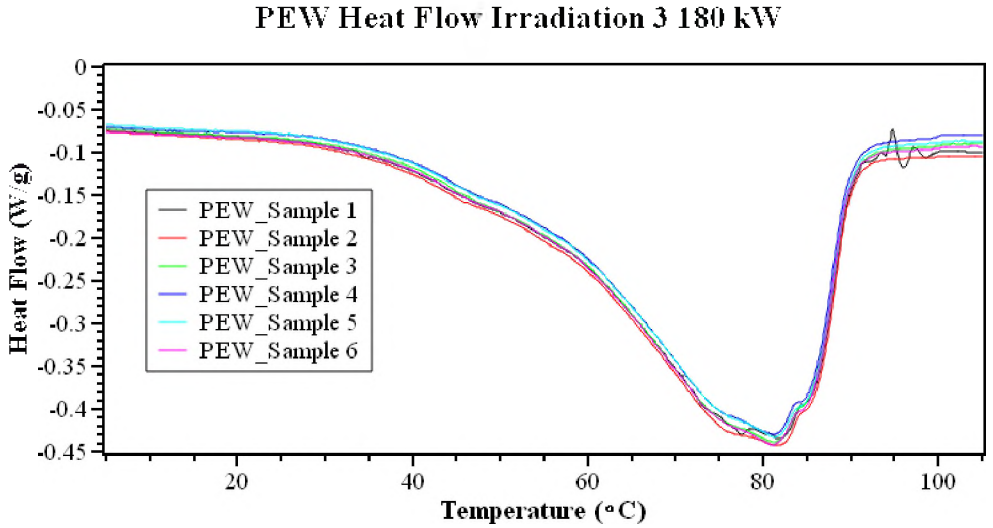
PEW Heat Flow Irradiation 3 180 kW
Heat Flow (W/g)
Temperature (°C)
PEW_Sample 1
PEW_Sample 2
PEW_Sample 3
PEW_Sample 4
PEW_Sample 5
PEW_Sample 6

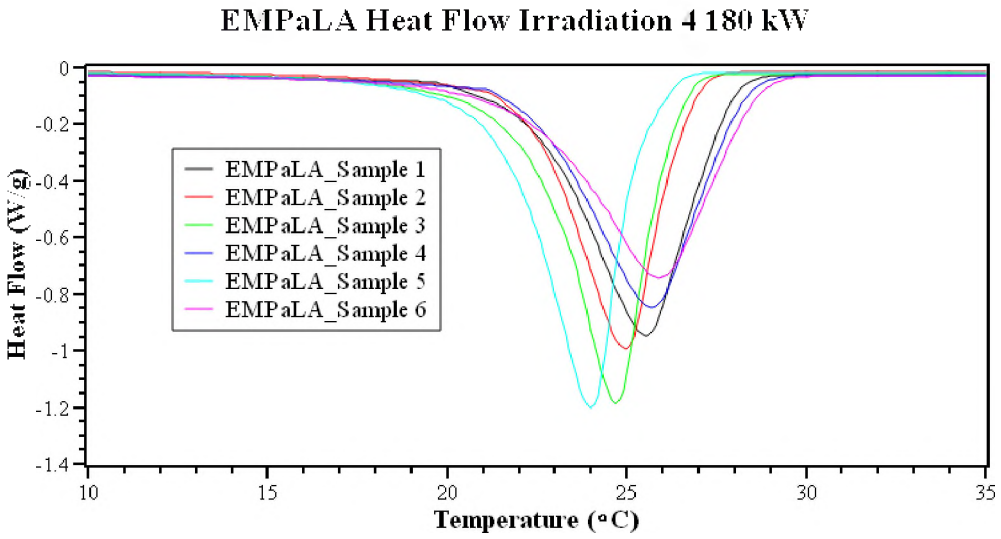
EMPaLA Heat Flow Irradiation 4 180 kW
Heat Flow (W/g)
Temperature (°C)
EMPaLA_Sample 1
EMPaLA_Sample 2
EMPaLA_Sample 3
EMPaLA_Sample 4
EMPaLA_Sample 5
EMPaLA_Sample 6

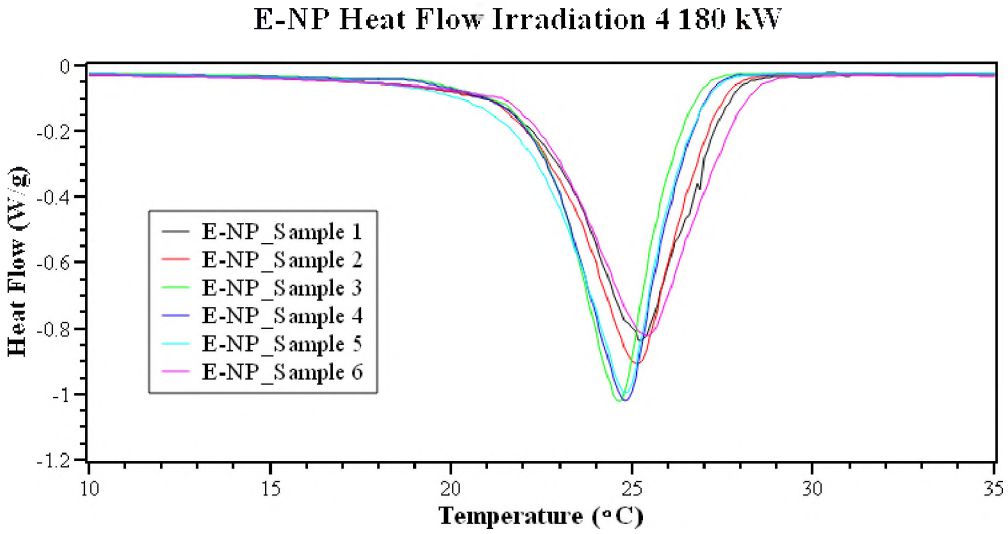
E-NP Heat Flow Irradiation 4 180 kW
Heat Flow (W/g)
Temperature (°C)
E-NP_Sample 1
E-NP_Sample 2
E-NP_Sample 3
E-NP_Sample 4
E-NP_Sample 5
E-NP_Sample 6

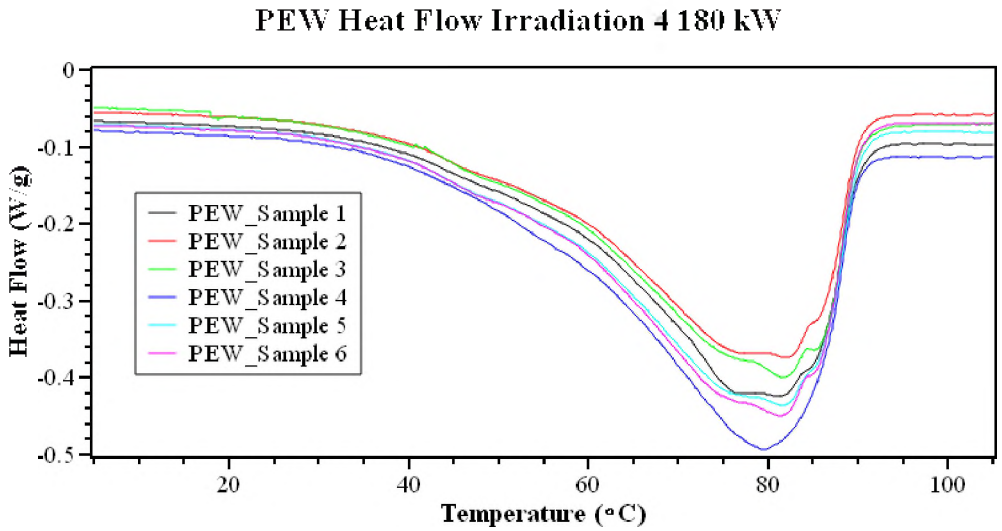
PEW Heat Flow Irradiation 4 180 kW
Heat Flow (W/g)
Temperature (°C)
PEW_Sample 1
PEW_Sample 2
PEW_Sample 3
PEW_Sample 4
PEW_Sample 5
PEW_Sample 6
0
-0.1
-0.2
-0.3
-0.4
-0.5
20
40
60
80
100

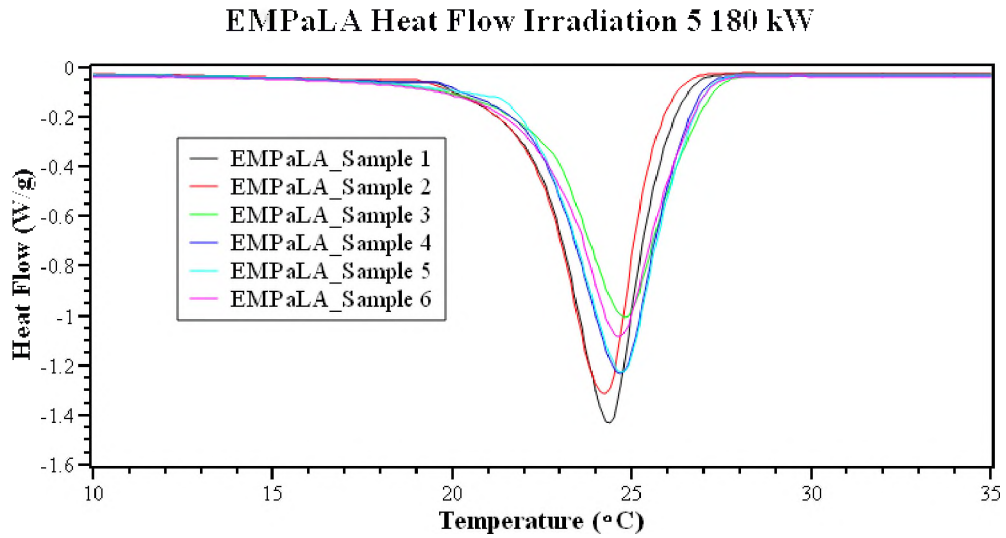
EMPaLA Heat Flow Irradiation 5 180 kW
Heat Flow (W/g)
Temperature (°C)
EMPaLA_Sample 1
EMPaLA_Sample 2
EMPaLA_Sample 3
EMPaLA_Sample 4
EMPaLA_Sample 5
EMPaLA_Sample 6
0
-0.2
-0.4
-0.6
-0.8
-1
-1.2
-1.4
-1.6
10
15
20
25
30
35

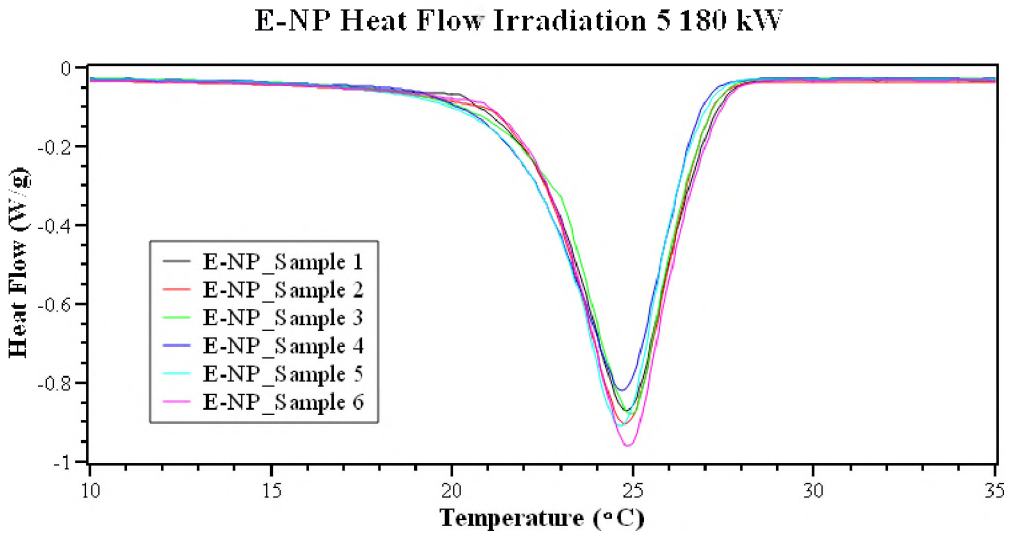
E-NP Heat Flow Irradiation 5 180 kW
Heat Flow (W/g)
Temperature (°C)
E-NP_Sample 1
E-NP_Sample 2
E-NP_Sample 3
E-NP_Sample 4
E-NP_Sample 5
E-NP_Sample 6

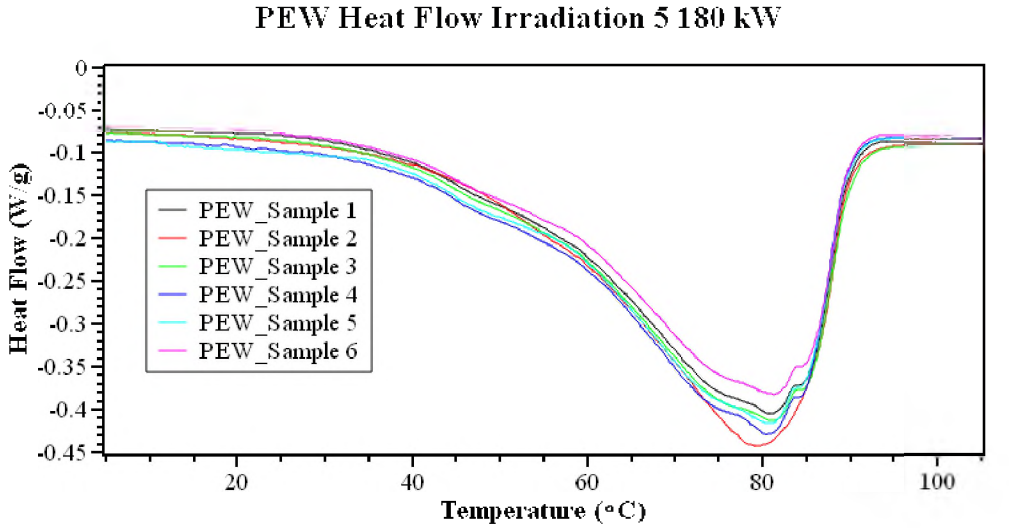
PEW Heat Flow Irradiation 5 180 kW
Heat Flow (W/g)
Temperature (°C)
PEW_Sample 1
PEW_Sample 2
PEW_Sample 3
PEW_Sample 4
PEW_Sample 5
PEW_Sample 6

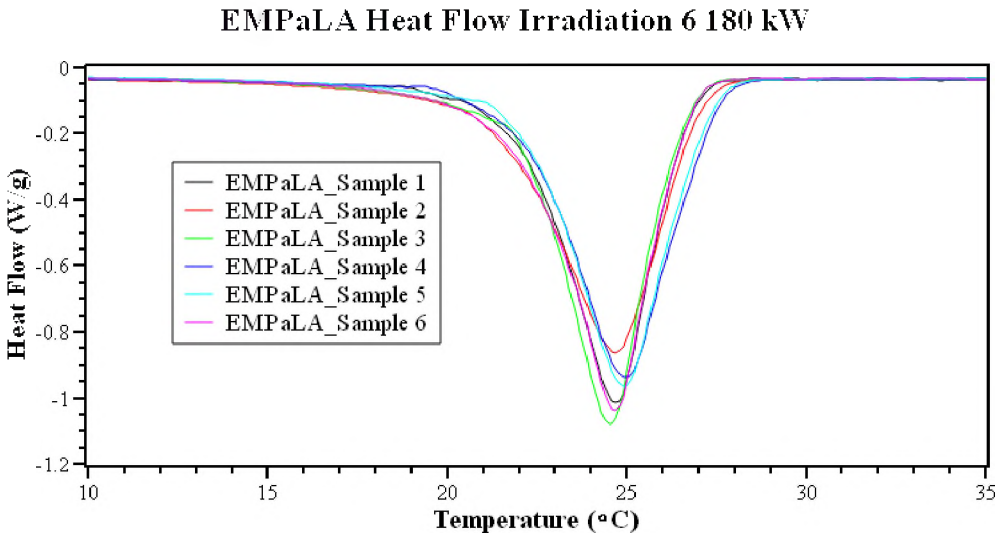
EMPaLA Heat Flow Irradiation 6 180 kW
Heat Flow (W/g)
Temperature (°C)
EMPaLA_Sample 1
EMPaLA_Sample 2
EMPaLA_Sample 3
EMPaLA_Sample 4
EMPaLA_Sample 5
EMPaLA_Sample 6

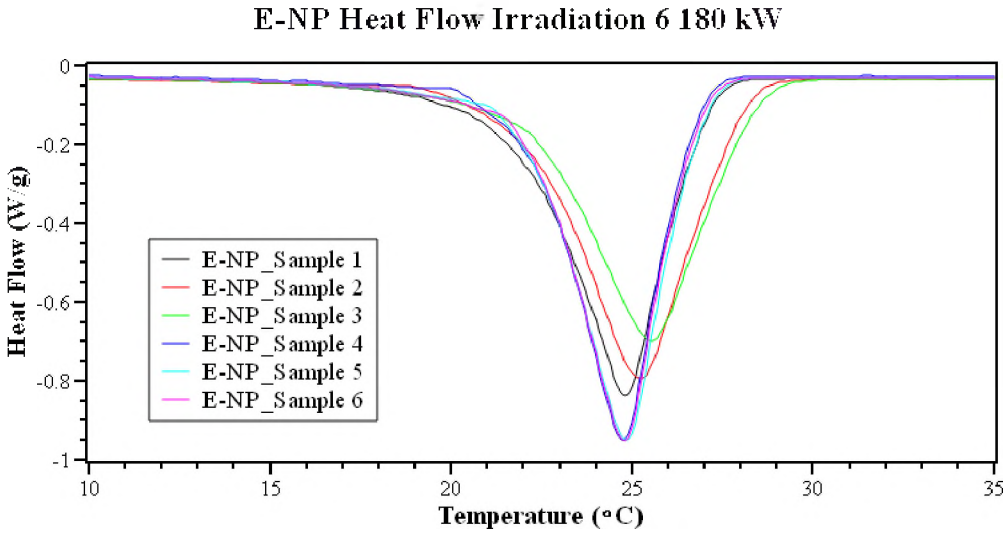
E-NP Heat Flow Irradiation 6 180 kW
Heat Flow (W/g)
Temperature (°C)
E-NP_Sample 1
E-NP_Sample 2
E-NP_Sample 3
E-NP_Sample 4
E-NP_Sample 5
E-NP_Sample 6

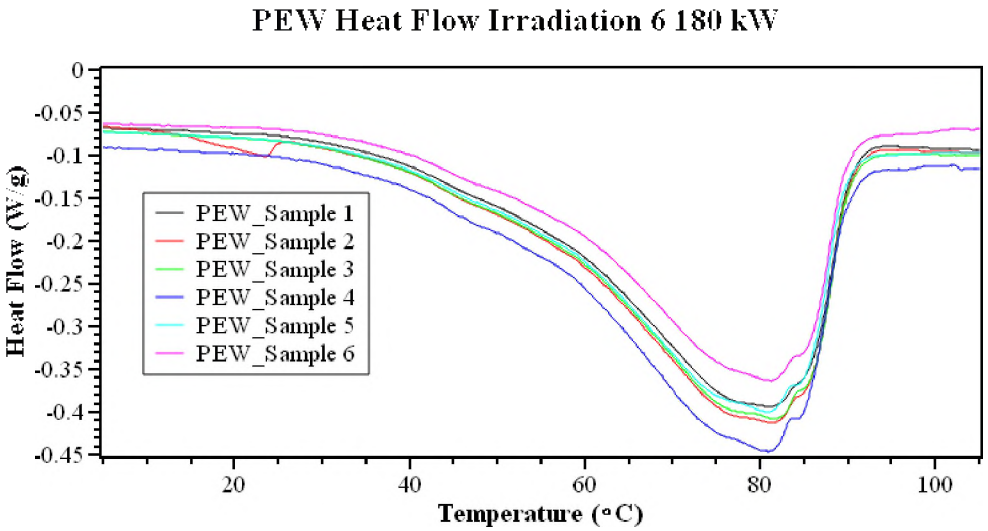
PEW Heat Flow Irradiation 6 180 kW
Heat Flow (W/g)
Temperature (°C)
PEW_Sample 1
PEW_Sample 2
PEW_Sample 3
PEW_Sample 4
PEW_Sample 5
PEW_Sample 6
0
-0.05
-0.1
-0.15
-0.2
-0.25
-0.3
-0.35
-0.4
-0.45
20
40
60
80
100

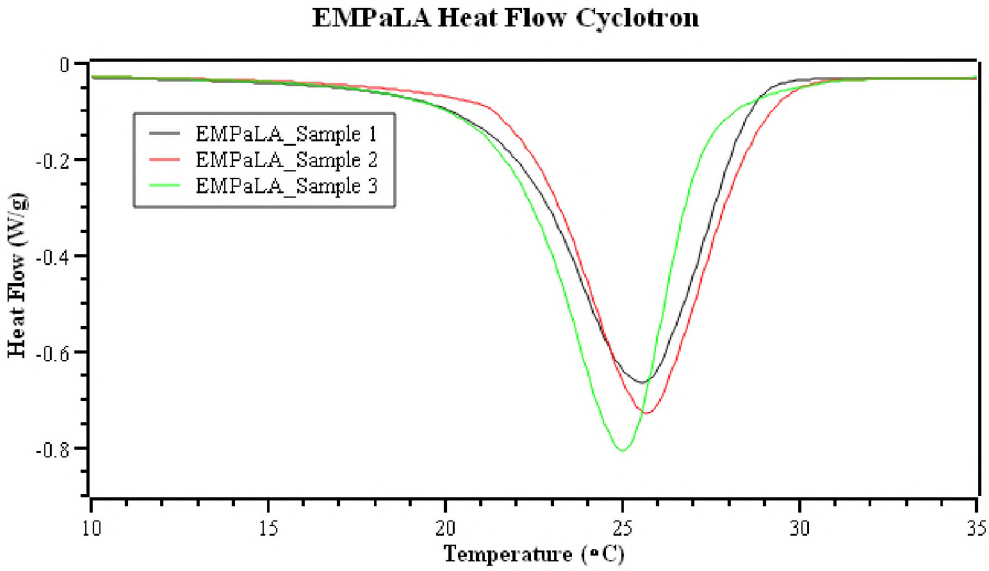
EMPaLA Heat Flow Cyclotron
Heat Flow (W/g)
Temperature (°C)
EMPaLA_Sample 1
EMPaLA_Sample 2
EMPaLA_Sample 3
0
-0.2
-0.4
-0.6
-0.8
10
15
20
25
30
35

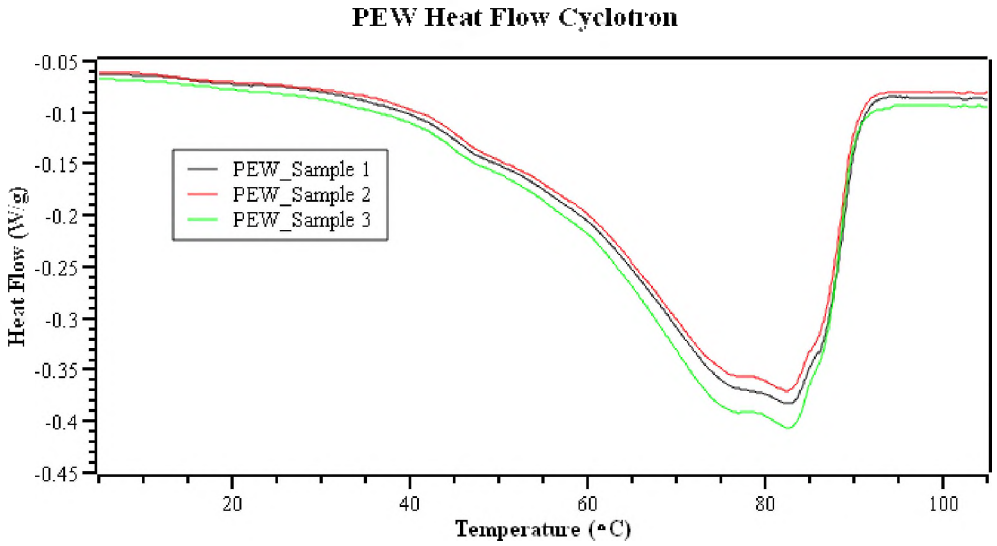
PEW Heat Flow Cyclotron
PEW_Sample 1
PEW_Sample 2
PEW_Sample 3
Heat Flow (W/g)
Temperature (°C)
-0.05
-0.1
-0.15
-0.2
-0.25
-0.3
-0.35
-0.4
-0.45
20
40
60
80
100

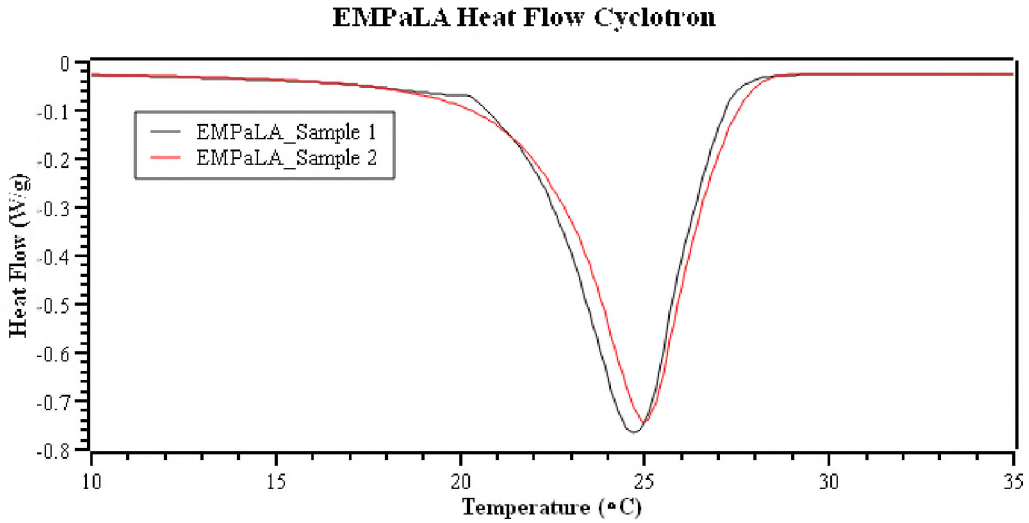
EMPaLA Heat Flow Cyclotron
EMPaLA_Sample 1
EMPaLA_Sample 2
Heat Flow (W/g)
Temperature (°C)
0
-0.1
-0.2
-0.3
-0.4
-0.5
-0.6
-0.7
-0.8
10
15
20
25
30
35

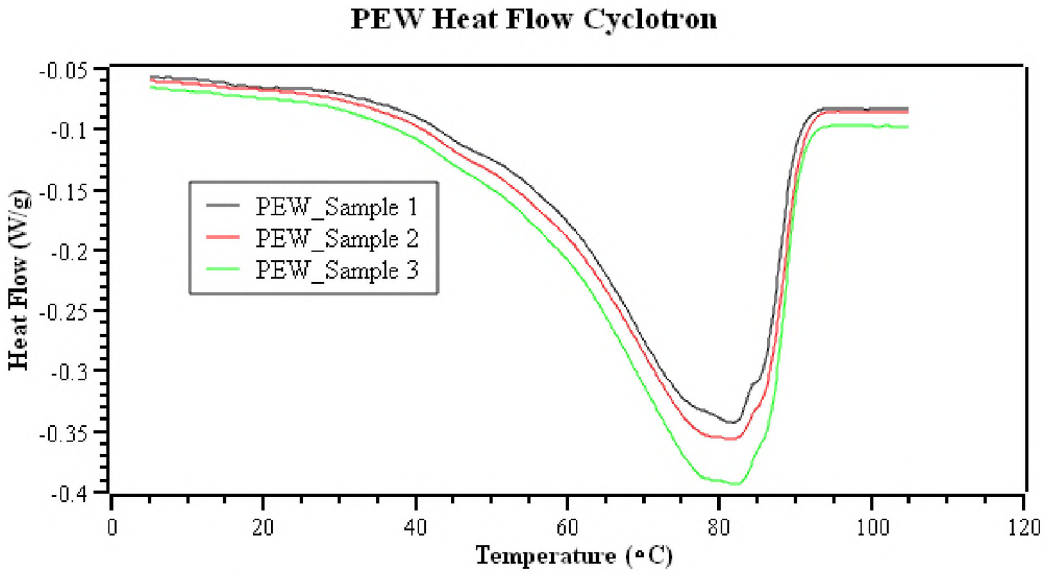

The following graphs are the Raman Spectra of EMPaLA and PEW from the various experiments. The naming convention for the legend is Sample type_Irradiation location/amount-sample number. For the Irradiation location/amount Cyc indicates Cyclotron at MUC, Irr0 indicates no irradiation, IRR6 indicates the 6th irradiation at MSTR, and MURR indicates the irradiation performed at MURR. All of the Spectra have been offset to better show the various peaks.

EMPaLA Raman Spectra

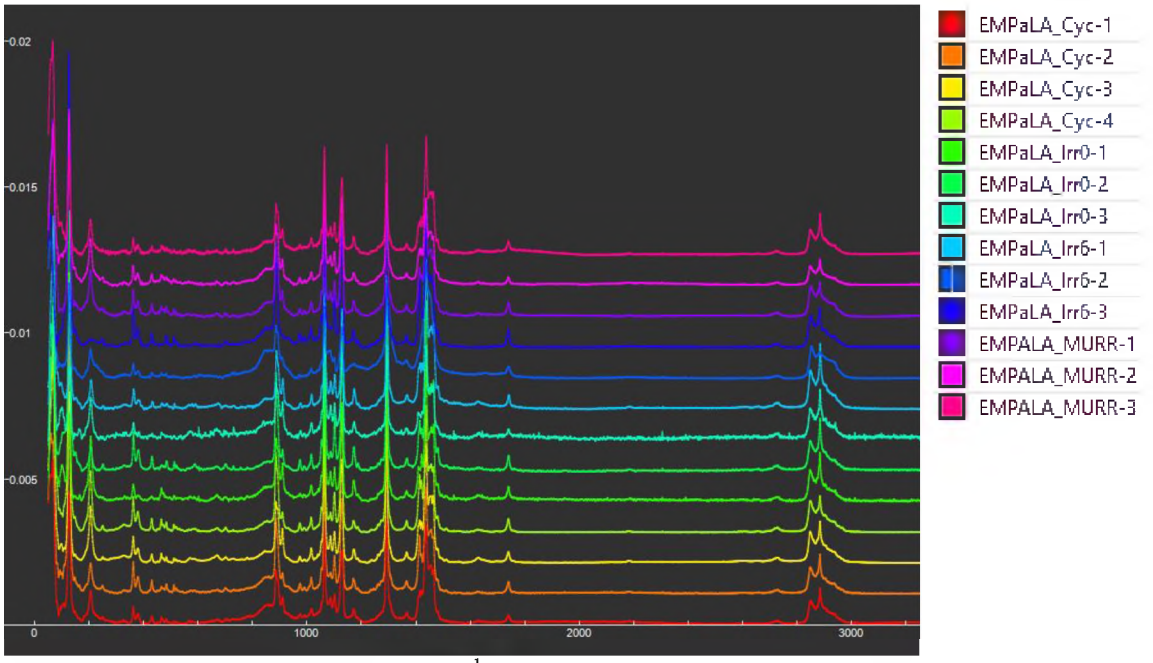

cm^{-1}

PEW Raman Spectra

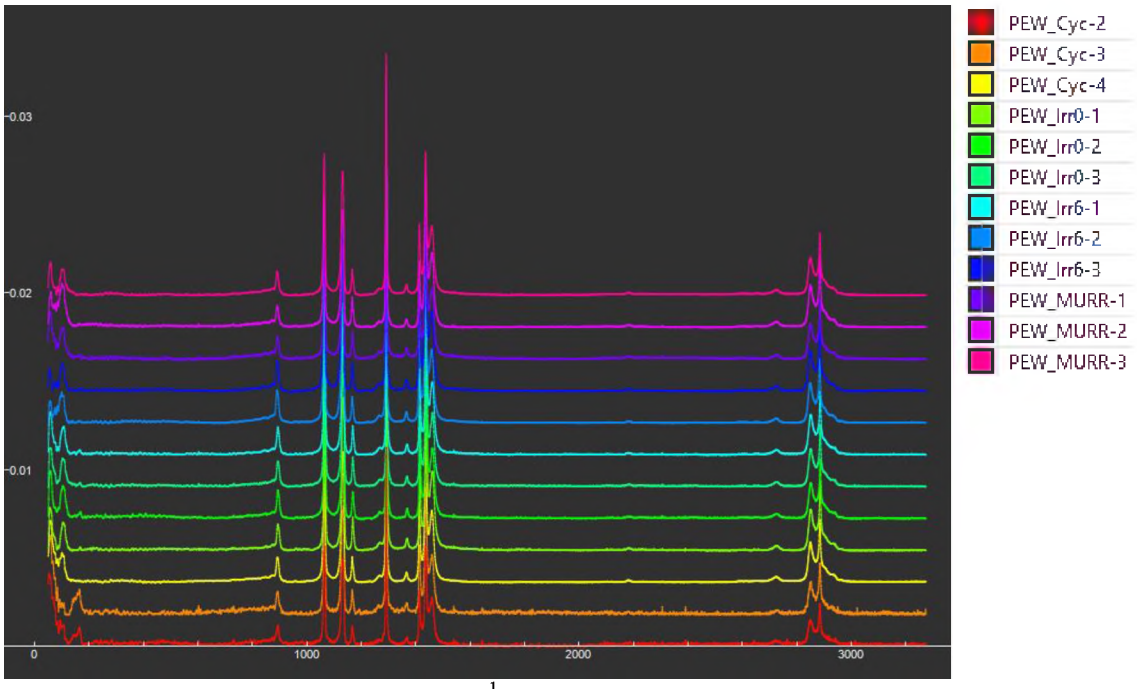

cm^{-1}

BIBLIOGRAPHY

[1] J. Kosny and D. Yarbrough, "Use of PCM-Enhanced Insulations in the Building Envelope (No. 5)", *Oak Ridge National Laboratory (ORNL); Building Technologies Research and Integration Center*, 2008.

[2] "Consulting Engineering Firm | Affiliated Engineers", *Affiliated Engineers*, 2020. [Online]. Available: http://www.aeieng.com/index.php/sustainability/phase_change_material.

[3] K. Pielichowska and K. Pielichowski, "Phase change materials for thermal energy storage", *Progress in Materials Science*, vol. 65, pp. 67-123, 2014. Available: https://doi.org/10.1016/j.pmatsci.2014.03.005

[4] M. Demirbas, "Thermal Energy Storage and Phase Change Materials: An Overview", *Energy Sources, Part B: Economics, Planning, and Policy*, vol. 1, no. 1, pp. 85-95, 2006. Available: 10.1080/009083190881481.

[5] "IBM scientists imitate the functionality of neurons with a phase-change device", *Phys.org*, 2016. [Online]. Available: http://phys.org/news/2016-08-ibm-scientists-imitate-functionality-neurons.html.

[6] Union of Concerned Scientists, "Donald C. Cook Unit 2: Bridgeman, MI", 2000.

[7] L. Trevino and E. Orndoff, "Advanced Space Suit Insulation Feasibility Study", *SAE Technical Paper Series*, 2000. Available: 10.4271/2000-01-2479

[8] "NASA to Begin Testing Next Generation of Spacecraft Heat Exchangers", *NASA*, 2016. [Online]. Available: https://www.nasa.gov/feature/nasa-to-begin-testing-next-generation-of-spacecraft-heat-exchangers.

[9] Georgia institute of Technology, "Radiation Effects on Organic Materials in Nuclear Plants", Electric Power Research Institute, 1981.

[10] A. Charlesby, "The cross-linking and degradation of paraffin chains by high-energy radiation", Proceedings of the Royal Society of London. Series A. Mathematical and Physical Sciences, vol. 222, no. 1148, pp. 60-74, 1954. Available: 10.1098/rspa.1954.0052.

[11] "Chemical Name Search", Webbook.nist.gov. [Online]. Available: https://webbook.nist.gov/chemistry/name-ser/.

[12] R. Saeed, J. Schlegel, C. Castano and R. Swafta, "Uncertainty of Thermal Characterization of Phase Change Material by Differential Scanning Calorimetry Analysis", International Journal of Engineering Research & Technology, vol. 5, no. 1, pp. 405-412, 2016.

[13] D. Lin-Vien, N. Colthup, W. Fateley and J. Grasselli, The Handbook of Infrared and Raman Characteristic Frequencies of Organic Molecules. San Diego: Academic Press, 1991.

[14] H. Abou Zeid, Z. Ali, T. Abdel Maksoud and R. Khafagy, "Structure-property behavior of polyethylene exposed to different types of radiation", Journal of Applied Polymer Science, vol. 75, no. 2, pp. 179-200, 2000. Available: 10.1002/(sici)1097-4628(20000110)75:2<179::aid-app1>3.0.co;2-b.

[15] C. Warren and D. Hooper, "Chain Length Determination of Fatty Acids by Raman Spectroscopy", Canadian Journal of Chemistry, vol. 51, no. 23, pp. 3901-3904, 1973. Available: 10.1139/v73-581

VITA

Ryan Phillip Steere was born in Pittsburgh Pennsylvania. He received his Bachelor of Science in Nuclear Engineering from Missouri University of Science and Technology in May 2016. In the summer of 2016, he worked at Lawrence Livermore National Lab attempting to optimize the energy resolution of silicon photomultipliers for use in detector systems. In August 2016 he started his Ph.D. in Nuclear Engineering with Dr. Joshua Schlegel.

The Ph.D. work was focused on thermal energy storage systems for several applications. These applications included passive safety systems in nuclear reactor containment, spacecraft environmental control systems, and structural temperature regulation in building envelopes. He was awarded a Doctor of Philosophy in Nuclear Engineering from Missouri University of Science and Technology in July 2021.